THE ICELAND MICROCONTINENT AND A CONTINENTAL GREENLAND-ICELAND-FAROE RIDGE

Gillian R. Foulger[1], Tony Doré[2], C. Henry Emeleus[1,§], Dieter Franke[3], Laurent Geoffroy[4], Laurent Gernigon[5], Richard Hey[6], Robert E. Holdsworth[1], Malcolm Hole[7], Ármann Höskuldsson[8], Bruce Julian[1], Nick Kusznir[9], Fernando Martinez[10], Ken J.W. McCaffrey[1], James H. Natland[11], Alex Peace[12], Kenni Petersen[13], Christian Schiffer[1], Randell Stephenson[14] & Martyn Stoker[15].

[1] Department of Earth Sciences, Durham University, Science Laboratories, South Rd. DH1 3LE, UK

[2] Statoil UK Ltd., Statoil House, 11a Regent Street, London SW1Y 4ST, UK

[3] Bundesanstalt für Geowissenschaften und Rohstoffe (Federal Institute for Geosciences and Natural Resources), Germany

[4] Université de Bretagne Occidentale, Brest, 29238 Brest, CNRS, UMR 6538, Laboratoire Domaines Océaniques, 29280 Plouzané, France

[5] Norges Geologiske Undersøkelse (NGU), Geological Survey of Norway, Leiv Erikssons vei 39, N-7491 Trondheim, Norway

[6] Hawaii Institute of Geophysics and Planetology, School of Ocean and Earth Science and Technology, University of Hawaii, Honolulu, HI 96822 USA

[7] Department of Geology & Petroleum Geology, University of Aberdeen, Aberdeen AB243UE, UK.

[8] Háskóli Íslands (University of Iceland), Sturlugötu 7, 101 Reykjavík, Iceland

[9] School of Environmental Sciences, University of Liverpool, Jane Herdman Building, Liverpool L69 3GP, UK

[10] Hawaii Institute of Geophysics and Planetology, School of Ocean and Earth Science and Technology, University of Hawaii, Honolulu, HI 96822 USA

[11] Rosenstiel School of Marine and Atmospheric Science, University of Miami, Miami FL 33149, USA

[12] Department of Earth Sciences, Memorial University of Newfoundland, St. Johns, Newfoundland, Canada, A1B 3X5; currently at School of Geography and Earth Sciences, McMaster University, 1280 Main Street West, Hamilton, Ontario, Canada L8S 4K1

[13] Department of Geoscience, Aarhus University, Høegh-Guldbergs Gade 2, DK-8000 Aarhus C., Denmark

[14] School of Geosciences, Geology and Petroleum Geology, Meston Building, King's College, University of Aberdeen, Aberdeen AB24 3UE, UK

[15] Australian School of Petroleum, University of Adelaide, Adelaide, South Australia 5005 Australia

[§] deceased

Abstract

The breakup of Laurasia to form the Northeast Atlantic Realm disintegrated an inhomogeneous collage of cratons sutured by cross-cutting orogens. Volcanic rifted margins formed that are underlain by magma-inflated, extended continental crust. North of the Greenland-Iceland-Faroe Ridge a new rift–the Aegir Ridge–propagated south along the Caledonian suture. South of the Greenland-Iceland-Faroe Ridge the proto-Reykjanes Ridge propagated north through the North Atlantic Craton along an axis displaced ~150 km to the west of the rift to the north. Both propagators stalled where the confluence of the Nagssugtoqidian and Caledonian orogens formed an ~300-km-wide transverse barrier. Thereafter, the ~150 x 300-km block of continental crust between the rift tips–the Iceland Microcontinent–extended in a distributed, unstable manner along multiple axes of extension. These axes repeatedly migrated or jumped laterally with shearing occurring between them in diffuse transfer zones. This style of deformation continues to the present day in Iceland. It is the surface expression of underlying magma-assisted stretching of ductile continental crust that has flowed from the Iceland Microplate and flanking continental areas to form the lower crust of the Greenland-Iceland-Faroe Ridge. Icelandic-type crust which underlies the Greenland-Iceland-Faroe Ridge is thus not anomalously thick oceanic crust as is often assumed. Upper Icelandic-type crust comprises magma flows and dykes. Lower Icelandic-type crust comprises magma-inflated continental mid- and lower crust. Contemporary magma production in Iceland, equivalent to oceanic layers 2-3, corresponds to Icelandic-type upper crust plus intrusions in the lower crust, and has a total thickness of only 10-15 km. This is much less than the total maximum thickness of 42 km for Icelandic-type crust measured seismically in Iceland. The feasibility of the structure we propose is confirmed by numerical modeling that shows extension of the continental crust can continue for many tens of millions of years by lower-crustal ductile flow. A composition of Icelandic-type lower crust that is largely continental can account for multiple seismic observations along with gravity, bathymetric, topographic, petrological and geochemical data that are inconsistent with a gabbroic composition for Icelandic-type lower crust. It also offers a solution to difficulties in numerical models for melt-production by downward-revising the amount of melt needed. Unstable tectonics on the Greenland-Iceland-Faroe Ridge can account for long-term tectonic disequilibrium on the adjacent rifted margins, the southerly migrating rift propagators that build diachronous chevron ridges of thick crust about the Reykjanes Ridge, and the tectonic decoupling of the oceans to the north and south. A model of complex, discontinuous continental breakup influenced by crustal inhomogeneity that distributes continental material in growing oceans fits other regions including the Davis Strait, the South Atlantic and the West Indian Ocean.

62

List of acronyms. See also Table 2.

GIFR	-	Greenland-Iceland-Faroe Ridge
JMMC	-	Jan Mayen Microplate Complex
SDR	-	Seaward-dipping reflector
NVZ	-	Northern Volcanic Zone
EVZ	-	Eastern Volcanic Zone
WVZ	-	Western Volcanic Zone
HVLC	-	High-velocity lower crust
T_P	-	potential temperature
V_P	-	compressional (*P*-) wave velocity
REE	-	rare-Earth element
SCLM	-	sub-continental lithospheric mantle

Keywords: Atlantic; Iceland; continental breakup; tectonics; Icelandic-type crust; SDRs; geochemistry; geophysics.

1 Introduction

The NE Atlantic Realm, the region north of the Charlie Gibbs Fracture Zone, including the seas and seaboards west of Greenland, has persistently resisted attempts to account for many of its features in terms of conventional plate tectonics. Although the region figured prominently in the development of the spectacularly successful continental drift and plate tectonic theories, *e.g.*, with the discovery of symmetrical magnetic anomalies across the Reykjanes Ridge, it has also defied predictions made by this theory that are successful in most other areas. This is particularly true along the Greenland-Iceland-Faroe Ridge (GIFR) where the crust is typically 30 km thick and the bathymetry a full kilometer shallower than is expected by cooling and subsidence models for oceanic-crust [Detrick *et al.*, 1977]. These observations cannot be satisfactorily explained simply as conventional sea-floor-spreading with a larger-than-typical magmatic rate at Iceland (Figure 1).

It is ironic that, despite the GIFR region not fitting the simple plate tectonic theory, it played an important role in development of that theory. In the early 20th century Iceland attracted the attention of Alfred Wegener who, as part of his theory of continental drift [Wegener, 1915], predicted that Greenland and Scandinavia were separating at 2.5 m/a. Although his estimate of rate was two orders of magnitude too large, his general theory was correct. Wegener was influenced by arguments that a land bridge, postulated on biogeographical grounds to have connected Europe and America, was inconsistent with isostasy. At the time, such land bridges were widely invoked to explain the similarity, at some times in geological history, between biota on opposite sides of wide oceans. Wegener recognized that biogeographical observations worldwide could be explained by continental drift without land bridges.

Following acceptance of continental drift, the land bridge theory was essentially dropped. Ironically, the NE Atlantic is perhaps the only place in the world where a long, ocean-spanning land bridge did actually exist [Ellis & Stoker, 2014] (Section 3). The reason why such a bridge existed, even when the ocean had attained a width of over 1000 km, is one feature of many of the NE Atlantic that has, to date, not been satisfactorily explained.

A model for development of the NE Atlantic Realm that can account for these and all other observations in a holistic way is required. Models that involve simple palinspastic reconstructions of Laurasian super-continent breakup, and assume a bimodal crustal composition (continental or oceanic) with sharp boundaries, are insufficient [Barnett-Moore *et al.*, 2018; Nirrengarten *et al.*, 2018]. Models that explain the quantity, distribution and petrology of igneous rocks in an *ad hoc* fashion are not forward-predictive and cannot account for observations such as the close juxtaposition of volcanic and non-volcanic margins, high-velocity lower crust (HVLC), frequent ridge jumps, and southward-propagating rifts on the Reykjanes Ridge [Hey *et al.*, 2010; Peron-Pinvidic & Manatschal, 2010]. Nor can such models, a century after Wegener's work, explain why a land bridge spanned the NE Atlantic Ocean until it had attained a width of ~1,000 km, and why 40% of its length remains subaerial to the present day as the island of Iceland.

In this paper we develop such a model. We propose that the currently ~1,200 km wide Greenland-Iceland-Faroe Ridge (GIFR) formed by magma-assisted continental extension facilitated by ductile crustal flow, in a similar fashion to magmatic passive margins. The extraordinary width of the GIFR was enabled by the inclusion of a ~45,000 km^2 block of continental crust which we term the Iceland Microcontinent. The lower part of the ~30 km thick GIFR crust is magma-dilated continental mid- and lower crust. Surface extension has been taken up on the GIFR by distributed, migrating rifts with shear between them accommodated diffusely. Continental material is dispersed throughout the GIFR and sea-floor spreading has not yet been established on a single, stable rift. Complete continental breakup has thus still not fully occurred at this latitude.

Our paper is structured in the following way. First, we describe the unusual setting and complex history of breakup of the NE Atlantic Realm that predicated the subsequent complexities (Section 2). We then summarize structural and tectonic observations from the GIFR and the adjacent Faroe-Shetland basin (Section 3). In Section 4 we present our new model for the structure and evolution of the GIFR. Section 5 presents a numerical thermo-mechanical simulation that illustrates the model is physically viable given reasonable geological assumptions and Section 6 shows that it is consistent with the petrology, geochemistry and source potential temperatures of NE Atlantic igneous rocks. Finally, in Section 7, we discuss wider implications and analogous regions elsewhere in the oceans.

2 Continental breakup forming the Northeast Atlantic Realm

Opening of the NE Atlantic Realm in the early Cenozoic was not a simple, abrupt, isolated event. It was the latest event in a >300 Myr period of episodic rifting and cooling that lasted from the Late Palaeozoic through the Mesozoic. It affected a region extending some half the circumference of the Earth and disassembled a heterogeneous patchwork of cratonic blocks and orogens [Bingen & Viola, 2018; Gasser, 2014; Gee *et al.*, 2008b; Peace *et al.*, this volume; Wilkinson *et al.*, 2017].

Final breakup occurred by magma-assisted continental extension [Gernigon *et al.*, this volume; Lundin & Doré, 2005; Peace *et al.*, this volume; Roberts, 2003; Roberts *et al.*, 1999; Skogseid *et al.*, 2000; Soper *et al.*, 1992]. The crust extended by tens or hundreds of kilometers from the Rockall Trough to the Barents Sea [Funck *et al.*, 2017; Gaina *et al.*, 2017; Skogseid *et al.*, 2000; Stoker *et al.*, 2017]. Pre-breakup magmatism occurred throughout the region including in Britain, the Rockall Trough, East Greenland, the Faroe Islands and small-volume, small-fraction, scattered fields found in west Greenland and Newfoundland [Larsen *et al.*, 2009; Peace *et al.*, 2016; Wilkinson *et al.*, 2017]. Final development of the axes of breakup in the NE Atlantic was influenced by both the direction of extensional stress, pre-existing structure, and magmatism [Peace *et al.*, 2018; Peace *et al.*, submitted; Schiffer *et al.*, this volume].

Greenland is cross-cut by several orogens that continue across formerly adjacent landmasses. Easterly orientated orogens include the Inglefield mobile belt in the north (Paleoproterozoic—ca. 1.96 - 1.91 Ga), the central Greenland Nagssugtoqidian orogen bounded to the north by the Disko Bugt suture and to the south by the Nagssugtoqidian front (Paleoproterozoic—ca. 1.86 - 1.84 Ga), and the south

Greenland Ketilidian orogen (Paleoproterozoic—ca. 1.89 - 1.80 Ga) (Figure 2) [Garde *et al.*, 2002; van Gool *et al.*, 2002]. On the Eurasian continent the Nagssugtoqidian orogen is represented in Scotland as the Lewisian gneiss (Laxfordian) and the Ketilidian orogen is represented in NW Ireland as the Rhinns Complex (Figure 3).

The much younger Caledonian suture formed in the Ordovician-Devonian and closed the Tornquist Sea and Iapetus Ocean to unite Laurentia, Baltica and Avalonia [Pharaoh, 1999; Schiffer *et al.*, this volume; Soper *et al.*, 1992]. The Scottish Caledonides lie orthogonal to the eastward continuation of the Nagssugtoqidian and Ketilidian orogens [Holdsworth *et al.*, 2018]. The western frontal thrust of this suture runs down east Greenland ~100 - 300 km from the coast [Gee *et al.*, 2008a; Haller, 1971; Henriksen, 1999; Henriksen & Higgins, 1976]. A dipping feature imaged seismically using receiver functions at ~40 - 100 km beneath east Greenland is interpreted as a subducted slab, trapped in the continental lithosphere, when the Caledonian suture finally closed (Figure 4) [Schiffer *et al.*, 2014]. Residual Caledonian slabs beneath the region were predicted earlier by plate models for the geochemistry of Icelandic volcanics [Foulger & Anderson, 2005; Foulger *et al.*, 2005]. A congruent structure—the Flannan reflector—has been imaged seismically beneath north Scotland [Schiffer *et al.*, 2015; Smythe *et al.*, 1982].

The breakup phases that formed the oceans west and east of Greenland are described in detail by Peace *et al.* [this volume], Gernigon *et al.* [this volume] and Martinez and Hey [this volume]. It is summarized here and a brief chronology of the most significant events is given in Table 1. The north-propagating mid-Atlantic Ridge reached the latitude of the future Charlie Gibbs Fracture Zone in the Late Cretaceous (~86.3 - 83.6 Ma) and the Rockall Trough formed (Figure 1). The rift then propagated west of present-day Greenland at ~63 Ma forming magma-poor margins and opening the Labrador Sea [Abdelmalak *et al.*, 2018; Keen *et al.*, 2018; Nirrengarten *et al.*, 2018; Oakey & Chalmers, 2012; Roest & Srivastava, 1989].

Propagation proceeded unhindered across the Grenville and Ketilidian orogens and the North Atlantic craton but stalled at the junction of the Nagssugtoqidian and Rinkian orogens [Connelly *et al.*, 2006; Grocott & McCaffrey, 2017; Peace *et al.*, 2018; Peace *et al.*, submitted]. There, the crust was locally thick [Clarke & Beutel, 2019; Funck *et al.*, 2007; Funck *et al.*, 2012; Peace *et al.*, 2017; St-Onge *et al.*, 2009] and pre-existing subducted slabs may also have been preserved in the lithosphere [Heron *et al.*, 2019]. Rift propagation stalled and the Davis Strait NNE-SSW sinistral, right-stepping transtensional accommodation zone formed. This subsequently opened by magma-assisted continental transtension and transpression. Further north Baffin Bay opened by a combination of continental extension and possibly some subsidiary sea-floor spreading [Chalmers & Laursen, 1995; Chauvet *et al.*, 2019; Oakey & Chalmers, 2012; Suckro *et al.*, 2012; Welford *et al.*, 2018]. The Davis Strait today is a 550-km wide shallow ridge of extended, magma-inflated, continental crust that spans the ocean from Baffin Island to West Greenland [Dalhoff *et al.*, 2006; Heron *et al.*, 2019; Schiffer *et al.*, 2017].

At ~56 - 52 Ma rifting began to propagate east of Greenland forming the proto-Reykjanes Ridge and a ridge-ridge-ridge triple junction at the location of the current Bight fracture zone (Figure 1). Shortly thereafter, at ~50 - 48 Ma, the pole of rotation for Labrador Sea/Baffin Bay opening migrated south by ~1000 km resulting in clockwise rotation of ~30 - 40˚ of the direction of motion of Greenland relative to Laurentia [Oakey & Chalmers, 2012; Srivastava, 1978]. As a consequence the Labrador Sea/Baffin Bay plate boundary west of Greenland became less favorable to extension [Gaina *et al.*, 2017] and motion was progressively transferred to the axis east of Greenland. From ~36 Ma, opening was taken up entirely in the NE Atlantic [Chalmers & Pulvertaft, 2001; Gaina *et al.*, 2017].

As was the case for breakup west of Greenland, development of the mid-Atlantic Ridge in the NE Atlantic was strongly influenced by pre-existing structure [Schiffer *et al.*, this volume]. The classic "Wilson Cycle" model suggests that continental breakup occurs along older sutures [Ady & Whittaker, 2018; Buiter & Torsvik, 2014; Chenin *et al.*, 2015; Krabbendam, 2001; Petersen &

Schiffer, 2016; Vauchez *et al.*, 1997]. The collage of cratons and cross-cutting orogens that comprised the disintegrating Laurasian supercontinent had several sutures that influenced breakup.

Development of the oceanic regions north and south of the GIFR described in more detail in Sections 2.2.1 and 2.2.2 is summarized here. North of the present GIFR, the axis of extension opened by southerly propagation within the Caledonian orogen. That orogen consists of overthrust stacks of nappes and sinistral shear zones including the Møre-Trøndelag Fault Zone (Norway) and the Walls Boundary-Great Glen Fault and Highland Boundary Fault (Scotland). These features may have controled the structures that opened [Dewey & Strachan, 2003; Doré *et al.*, 1997; Fossen, 2010; Peace *et al.*, this volume]. The new mid-Atlantic Ridge formed obliquely along the orogen, however, so the propagating rift tip eventually intersected its edge at the Caledonian Western Frontal Thrust [Schiffer *et al.*, this volume]. There, it stalled.

South of the present GIFR the proto-Reykjanes Ridge propagated north from the Bight Fracture Zone, cut unhindered across the Ketilidian orogen as did the Labrador Sea rift, and split the North Atlantic craton. It arrived at the confluence of the transverse Nagssugtoqidian and Caledonian orogens at ~C21 (50 - 48 Ma) [Elliott & Parson, 2008] and stopped at a location ~300 km to the south and ~150 km to the west of the stalled, south-propagating ridge tip to the north. It was between and around these two stalled ridge tips that the GIFR formed, by magma-assisted deformation of the continental region between them.

2.1 High-velocity lower crust

High velocity lower crust (HVLC) is widespread beneath the margins of the NE Atlantic and has very similar geophysical properties to the lower part of the Icelandic-type crust that underlies the GIFR [Bott, 1974; Foulger *et al.*, 2003]. Because of this, understanding the origin and composition of HVLC is key to unraveling the development and current structure of the NE Atlantic. In this section, we discuss in detail its geophysical characteristics and possible origins.

Before oceanic crust began to form in the NE Atlantic Realm, wide rifted margins of stretched continental crust developed and in some areas were blanketed by thick sequences of seaward-dipping basalt flows (seaward-dipping reflectors—SDRs) [Á Horni *et al.*, 2016; Talwani & Eldholm, 1977]. Lithospheric necking occurred by normal faulting in the upper crust and distributed magma inflation and ductile flow in the mid- and lower crust (Figure 5). Multiple changes in extension direction complicated the final structure [Barnett-Moore *et al.*, 2018].

The volcanic rifted margins may be divided into Inner-SDR and Outer-SDR regions [Planke *et al.*, 2000]. The Inner-SDRs comprise lavas up to 5 - 10 km thick that blanket heavily dyke-injected continental upper crust formed during the continental extensional necking phase [*e.g.*, Benson, 2003; Geoffroy, 2005; Geoffroy *et al.*, 2015]. Beneath this the sill-injected lower crust exhibits high seismic velocities. Outer-SDRs sometimes lie seaward of these and directly overlie thinner HVLC, with seismic properties identical to the HVLC beneath the necked continental crust [Geoffroy *et al.*, 2015]. HVLC may also extend for up to 100 km beneath both the adjacent oceanic and continental domains [Funck *et al.*, 2016 and references therein; Rudnick & Fountain, 1995; Thybo & Artemieva, 2013].

HVLC typically has seismic velocities intermediate between those expected for crust and mantle. Constraints on its density are poor because the densities of the SDRs and underlying lower crust are not well known. Geoffroy *et al.* [2015] define two kinds of HVLC – LC1 and LC2. Typical working values for velocity and density are, for LC1 V_P ~7.2 - 7.3 km/s and density 3000 - 3100 kg/m^3, and for LC2 V_P ~7.6 to 7.8 km/s and density 3200 - 3300 kg/m^3 (Figure 5) [Bauer *et al.*, 2000; Geoffroy *et al.*, 2015; Schiffer *et al.*, 2016].

These geophysical properties are ambiguous regarding the composition, origin, and tectonic significance of HVLC. Possible lithologies include:

- Ultra-high-pressure granulite/eclogite crystalline basement representing exhumed continental mid- and lower crust [Abdelmalak *et al.*, 2017; Ebbing *et al.*, 2006; Gernigon *et al.*, 2004; Gernigon *et al.*, this volume; Mjelde *et al.*, 2013]. Such material can have both high V_P (7.2 - 8.5 km/s) and high density [2.8-3.6 g/cm3; Fountain *et al.*, 1994]. It outcrops in the Norwegian Western Gneiss Region which continues beneath the North Sea and the platform east of the Møre basin. Its top surface may comprise old suture accommodation zones that controlled deformation prior to breakup;
- Syn-extension sill-intruded mid-to-lower continental crust. In wide-angle seismic lines most HVLC beneath Inner-SDRs present high-amplitude, folded reflectors disconnected from the deepest layered lower crust [Clerc *et al.*, 2015; Geoffroy, 2005; Geoffroy *et al.*, 2015]. Such deformation fits with seaward ductile flow of this layer;
- Exhumed and syn-rift serpentinized mantle. The HVLC beneath the mid-Norwegian early Cretaceous basins, the Labrador Sea, Baffin Bay, Rockall Trough and the Porcupine basin may be partially syn-rift serpentinized mantle exhumed beneath the axes of maximum extension [Keen *et al.*, 2018; Lundin & Doré, 2011; O'Reilly *et al.*, 1996; Peron-Pinvidic *et al.*, 2013; Reston *et al.*, 2001; Reynisson *et al.*, 2011]. It is directly observed at amagmatic margins, *e.g.*, the Iberian margin, where the serpentinization is thought to be caused by seawater infiltrating down crustal faults and reacting with exhumed mantle at shallow depths. The HVLC beneath the NE Atlantic SDRs lies under several kilometers of sediments and crust and it is unlikely that seawater can penetrate sufficiently deep to cause pervasive serpentinization beneath the basalt [Abdelmalak *et al.*, 2017; Gernigon *et al.*, 2004; Zastrozhnov *et al.*, 2018];
- Inherited serpentinized material. Water could have been sourced from inherited Caledonian or Sveconorwegian-Grenvillian mantle wedge material [Fichler *et al.*, 2011; Petersen & Schiffer, 2016; Schiffer *et al.*, 2016; Slagstad *et al.*, 2017]. The source of NE Atlantic basalts is known to be wet [Jamtveit *et al.*, 2001; Nichols *et al.*, 2002]. Pressure conditions corresponding to deep crust/shallow upper mantle depths and temperatures of 500 - 700˚C should not be exceeded for serpentinite to exist [*e.g.*, Petersen & Schiffer, 2016; Ulmer & Trommsdorff, 1995]. Numerical modeling confirms that such material can be preserved in rifted margins [Petersen & Schiffer, 2016] and that its strength would be less than half that of dry peridotite [Escartin *et al.*, 2001];
- Mantle infiltrated with gabbroic melt. Such material has been observed at magma-poor margins [Lundin & Doré, 2018; Müntener *et al.*, 2010] and would have an average seismic velocity midway between that of mantle and gabbro (V_P ~7 km/s);
- Hybrid material comprising a mixture of some or all of the above on various scales. For example, Schiffer *et al.* [2015] interpret HVLC bodies beneath east Greenland as Caledonian subduction material including eclogitized mafic crust. What appears geophysically to be a continuous layer might also vary laterally in composition—a classic example of geophysical ambiguity [Mjelde *et al.*, 2002].

An interpretation of HVLC as underplated material, i.e., high-temperature melt that accumulated during initial opening of the NE Atlantic [Eldholm & Grue, 1994b; Mjelde *et al.*, 1997; Mjelde *et al.*, 2002; Mjelde *et al.*, 1998; Thybo & Artemieva, 2013] is challenged by key geophysical and structural observations from the outer Vøring basin. There, Cretaceous deformation was partly controlled by the top of a HVLC dome before the main magmatic event in the Late Paleocene-Early Eocene, suggesting that the dome may predate breakup magmatism by at least 15 - 25 Myr [Abdelmalak *et al.*, 2017; Gernigon *et al.*, 2004; Gernigon *et al.*, 2006].

In summary, the provenance of the HVLC underlying the Outer SDRs is ambiguous but it likely includes a large proportion of continental crust. As a consequence the exact locations of the outer limits of continuous offshore continental material (the continent-ocean boundary) is poorly known in some areas [Bronner *et al.*, 2011; Eagles *et al.*, 2015; Gernigon *et al.*, 2015; Lundin & Doré, 2018;

Schiffer *et al.*, 2018]. Continental crust may grade into thick oceanic crust via a magmatic transition zone tens of kilometers wide of stretched, intruded continental crust—the continent-ocean transition [Eagles *et al.*, 2015; Eldholm *et al.*, 1989; Gernigon *et al.*, this volume; Meyer *et al.*, 2009]. The width of the continent-ocean transition may be partly controlled by the degree of stretching with narrow extensional zones forming where new rifts follow pre-existing fabric, and wide zones where rifts cross-cut tectonic fabric [Buck, 1991; Dunbar & Sawyer, 1988; Harry *et al.*, 1993; Schiffer *et al.*, this volume].

Full rupture of the crust leading to region-wide sea-floor spreading may be discontinuous, diachronous and segmented [Elliott & Parson, 2008; Guan *et al.*, 2019; Manton *et al.*, 2018; Schiffer *et al.*, this volume; Theissen-Krah *et al.*, 2017]. Continental fragments trapped between pairs of volcanic rifted margins and transported into the new ocean to form "C-blocks" may be widespread (Figure 5; Section 4) [Geoffroy *et al.*, 2015; Geoffroy *et al.*, submitted]. Continental crust may also be distributed by igneous mullioning as seen in the southern Jan Mayen Microplate Complex (JMMC; Section 2.2.1), and by small-scale lateral rift migrations [Bonatti, 1985; Gernigon *et al.*, 2012; Gillard *et al.*, 2017]. Continental fragments may range in size from the 100-km scale down. Geophysical ambiguity and blanketing of microcontinents with lavas hinder mapping the full distribution of continental crust in the oceans. The eastern margin of the JMMC, for example, is overlain by SDRs and the subaerial part of the GIFR (i.e. Iceland) is blanketed with lavas younger than ~17 Ma [Breivik *et al.*, 2012; Gudlaugsson *et al.*, 1988]. Geochemistry can be used to complement geophysics by testing the viability of proposed HVLC petrologies (Section 6).

2.2 Seafloor spreading north and south of the Greenland-Iceland-Faroe Ridge

Clear, well-mapped, linear magnetic anomalies reveal the contrasting histories of ocean opening north and south of the GIFR (Figure 6). Breakup did not occur simultaneously along the entire seaboard, as often assumed, but involved several isolated propagators and intermediate continental blocks [Elliott & Parson, 2008; Gernigon *et al.*, this volume].

2.2.1 North of the Greenland-Iceland-Faroe Ridge

The earliest anomalies are likely associated with magma injection into extended continental crust. True sea-floor spreading on the Aegir Ridge began at ~54 Ma (C24r). It started at its northern end and propagated south to reach its full extent by ~52 Ma (Chron C23). Tectonic reorganization and fan-shaped spreading occurred about this ridge C22-C21 (~48 Ma) with spreading slower in the south than in the north (Table 1) [Gernigon *et al.*, 2015].

Much if not all of the southern extension deficit was accommodated by diffuse, dyke-assisted crustal dilation in the continental crust immediately to the west. This region later became the southern JMMC [Brandsdóttir *et al.*, 2015]. Crustal extension of up to 500% occurred forming mullioned crust [Gernigon *et al.*, 2015; Schiffer *et al.*, 2018]. Extension ultimately concentrated on the most westerly axis of dilation which developed into the Kolbeinsey Ridge. The first unambiguous magnetic anomaly formed there at ~24 Ma [C6/7; Blischke *et al.*, 2017; Vogt *et al.*, 1980].

The Aegir Ridge dwindled and became extinct a little after ~31 - 28 Ma [C12-C10; Gernigon *et al.*, 2015] after which all spreading north of the GIFR was taken up on the proto-Kolbeinsey Ridge. This migration of the locus of extension likely occurred as a result of a tectonic reorganization that rotated the local direction of motion counter-clockwise [Gaina *et al.*, 2017]. This would have rendered the southern part of the Aegir Ridge less favorable for spreading and encouraged extension on the proto-Kolbeinsey Ridge. That extension progressively detached the continental block and adjacent mullioned crust between the proto-Kolbeinsey Ridge and the Aegir Ridge to form the JMMC [Schiffer *et al.*, 2018]. Opening of the Atlantic north of the GIFR (*e.g.* the Norwegian-Greenland Sea) thus occurred on a series of unconnected, sub-parallel, migrating, propagating rifts.

346 The northern part of the JMMC is a coherent microcontinent on the 100-km scale [Peron-Pinvidic *et*
347 *al.*, 2012]. SDRs formed on its eastern margin [Kodaira *et al.*, 1998]. The crust that makes up its
348 southern part is severely intruded continental crust with clear rift zones [Brandsdóttir *et al.*, 2015].
349 The nature of its transition into Iceland is, however, unknown.

350 Despite developing in the highly magmatically productive environment of the early NE Atlantic the
351 late Aegir Ridge was magma-starved and formed oceanic crust only 4 - 7 km thick [Breivik *et al.*,
352 2006; Greenhalgh & Kusznir, 2007]. This contrasts with both the Kolbeinsey Ridge and the
353 Reykjanes Ridge which are underlain by oceanic crust ~10 km thick. Extreme variations in magmatic
354 rate over short distances are inconsistent with mechanisms of melt production that envisage extensive,
355 coherent regions of influence and suggest, instead, local dependency on melt productivity [Lundin *et*
356 *al.*, 2018; Simon *et al.*, 2009].

357 2.2.2 South of the Greenland-Iceland-Faroe Ridge

358 South of the GIFR, on the European side, poorly constrained, complicated magnetic anomalies SW of
359 the Faroe Islands suggest early disaggregated sea-floor spreading. The first unambiguous and
360 continuous spreading anomaly south of the Faroe Plateau formed at ~47 Ma (C21) [Elliott & Parson,
361 2008; Ellis & Stoker, 2014; Stoker *et al.*, 2012]. On the Greenland side, the oldest linear magnetic
362 anomalies produced by the proto-Reykjanes Ridge date from C24-22 (56 - 52 Ma), but they may
363 represent rift-related basalt extrusion in the Outer-SDR region and not true oceanic spreading. Linear
364 magnetic anomalies terminate along the SE Greenland margin, unlike the European side where they
365 are continuous along the margin. This is consistent with early westward migration of the spreading
366 axis. It finally stabilized along a zone ~150 km west of the Aegir Ridge.

367 Extension proceeded normal to the strike of the Reykjanes Ridge and the continental edges until ~37 -
368 38 Ma (C17) when an abrupt counter-clockwise rotation of the direction of plate motion occurred.
369 Spreading in the Labrador Sea then rapidly ceased (Table 1) [Gaina *et al.*, 2017; Jones, 2003;
370 Martinez & Hey, this volume]. The Bight ridge-ridge-ridge triple junction ceased to exist and the
371 linear Reykjanes Ridge reconfigured to a right-stepping ridge-transform array such that the new ridge
372 segments were normal to the new direction of plate motion.

373 Subsequently, and up to the present day, the Reykjanes Ridge has been slowly migrated east by a
374 series of small-offset, right-stepping propagators within the plate boundary zone that have eliminated
375 the transforms [Benediktsdóttir *et al.*, 2012; Hey *et al.*, 2010; Martinez & Hey, this volume]. They
376 originate at the GIFR and migrate south at rates of 10 - 25 cm/a, each slicing a few kilometers off the
377 Eurasian plate and transferring it to the North American plate [Hey *et al.*, 2016]. At least five and
378 possibly as many as seven propagators [Jones *et al.*, 2002] have now transferred a swathe of the
379 Eurasian plate ~30 km wide to the North American plate between the GIFR and the Bight Fracture
380 Zone [Benediktsdóttir *et al.*, 2012].

381 Progression of each propagator tip is associated with transient changes in thickness of ~2 ± 1 km in
382 the oceanic crust formed. This has the curious consequence that the Reykjanes Ridge is flanked by
383 diachronous "chevrons" (also called "V-shaped ridges") of alternating thick and thin crust that are
384 most clearly seen in the gravity field (Figure 7) [Vogt, 1971].

385 **3 The Greenland-Iceland-Faroe Ridge**

386 The GIFR comprises a ~1,200-km-long, shallow, trans-oceanic aseismic ridge up to 450 km wide in
387 the northerly direction (Figure 1). At present, 40% of it is exposed above sea level in Iceland. It is
388 shallower than 600 m and 500 m deep offshore west and east Iceland respectively, ~1000 m shallower
389 than the ocean basins to the north and south (Figure 8).

The GIFR was subaerial along its entire length for most of the history of the NE Atlantic. Biogeographical evidence for plant and animal dispersal [Denk *et al.*, 2011] and dating of the onset of overflow of intermediate- and deep waters between the Norway and Iceland basins [Ellis & Stoker, 2014; Stoker *et al.*, 2005b] suggest that it formed a largely intact, trans-Atlantic land bridge (the Thulean land bridge) until ~10 - 15 Ma and that much survived above sea level longer than this. This leads to the surprising conclusion that the Thulean land bridge survived intact until the NE Atlantic Ocean had attained a width of ~1000 km.

Magnetic anomalies on the GIFR are poorly defined, broader than classical oceanic spreading anomalies, and resemble more closely anomalies on the outer SDRs (Figure 6) [*e.g.*, Gaina *et al.*, 2017]. Very few can be clearly traced across the GIFR so the detailed history of breakup in this region cannot be deduced reliably. Previous interpretations have relied largely on extrapolation of anomalies to the north and south that are clear, assuming simple oceanic crustal accretion in the region between.

Prior explanations for the poorly developed magnetic anomalies include repeated dyke intrusion into the same zone during more than one magnetic chron, re-magnetization by later intrusions, weathering, lateral migration of spreading centers and magmatism at multiple spreading centers [Bott, 1974]. Unclear anomalies are also expected because basalt extrusion was subaerial and flooded older lavas, and because the legacy magnetic data available are poor quality, limited, and poorly levelled.

We concur with these suggestions but go further and propose that distinct, oceanic-type linear magnetic anomalies do not exist on the GIFR because it does not comprise oceanic crust formed by classical sea-floor spreading. Instead, much of it may consist of magma-dilated, ductile continental crust. Upper Icelandic-type crust [Bott, 1974 ; Foulger *et al.*, 2003] corresponds to current basaltic production. Lower Icelandic-type crust corresponds to magma-inflated mid- and lower continental crust, the most likely lithology for the HVLC that is widespread beneath the NE Atlantic passive margins (Section 2.1).

3.1 Crustal structure

The GIFR has been the target of numerous refraction, wide-angle reflection, and passive seismic experiments [Foulger *et al.*, 2003] as well as gravity, magnetic and magnetotelluric work [Beblo & Bjornsson, 1978; 1980; Beblo *et al.*, 1983; Eysteinsson & Hermance, 1985; Hermance & Grillot, 1974; Thorbergsson *et al.*, 1990]. It was the anomalous seismic nature of its crust that led to it being termed “Icelandic-type” [Bott, 1974; Foulger *et al.*, 2003]. It features an upper crust with a thickness of ~3 - 10 km with high vertical velocity gradients, and a lower crust ~10 - 30 km thick with low vertical velocity gradients (Figure 9 and Figure 10) [Darbyshire *et al.*, 1998a; Foulger *et al.*, 2003; Holbrook *et al.*, 2001; Hopper *et al.*, 2003]. The lower crust has a V_P of 7.0 - 7.3 km/s. Icelandic-type crust has, in recent years, usually been assumed to be anomalously thick oceanic crust with the lower crust equivalent to oceanic layer 3. That model became the default assumption after Bjarnason *et al.* [1993] reported a deep reflecting horizon at ~ 20 - 24 km depth beneath SW Iceland. It replaced an earlier model that interpreted the layer beneath the upper crust as anomalously hot mantle [Angenheister *et al.*, 1980; Gebrande *et al.*, 1980; Palmason, 1971; Tryggvason, 1962].

The model that Icelandic-type lower crust is oceanic is inconsistent with other observations. Isostatic studies reveal the density of the lower crust to be ~3150 kg/m^3, which is too high for it to be oceanic [Gudmundsson, 2003; Menke, 1999]. At the same time, its seismic velocity is too low for normal mantle peridotite. Models involving partial melt are ruled out by the low attenuation of seismic shear waves which suggests that Icelandic-type lower crust is no hotter than 800 - 900˚C if it is peridotite [Sato *et al.*, 1989] and 875 - 950˚C if it is gabbroic [Menke & Levin, 1994; Menke *et al.*, 1995].

The theory that Icelandic lower crust is oceanic is largely based on interpreting deep seismic reflections as the Moho. However, such reflections can also be interpreted as sills intruded into continental lower crust. Refracted head waves are almost never observed in Iceland and the large amplitudes of reflections expected from a Moho are not observed in receiver functions [Du &

Foulger, 1999; Du *et al.*, 2002; Du & Foulger, 2001]. These properties are similar to those of HVLC beneath the Inner- and Outer SDRs of the continental margins [Mjelde *et al.*, 2001]. The possible compositions and provenances of that material, discussed in Section 2.1, thus provide candidates for Icelandic-type lower crust.

A serpentinized mantle origin for Icelandic-type lower crust is unlikely. If it were serpentinized mantle, ~20% of serpentinization of peridotite at ~1 GPa (~30 km depth) is required [Christensen, 2004]. Serpentinization in a rifting environment occurs from the top down and water is unlikely to be able to reach the mantle at the active rift zones of Iceland. If it did, it would only be stable at temperatures < 700 ˚C or possibly < 500 ˚C [Tuttle & Bowen, 1958] and the Icelandic lower crust is hotter than this [Menke & Levin, 1994; Menke *et al.*, 1995; Sato *et al.*, 1989]. The only other possible way of serpentinizing the mantle is via fluxing from beneath. In the NE Atlantic such serpentinization could have occurred in the Caledonian suture [Fichler *et al.*, 2011] and water is present in the source of basalts erupted in Iceland [Jamtveit *et al.*, 2001; Nichols *et al.*, 2002]. However, no peridotite xenoliths have been found in Iceland despite a century of extensive geological mapping and drilling, suggesting that, whereas serpentinite may exist beneath some rifted margins, it probably does not comprise lower Icelandic-type crust or HVLC beneath the adjacent volcanic margins.

Transitional crust comprising massively dyke- and sill-intruded, hyper-extended mid- and lower continental crust is the most likely composition for Icelandic-type lower crust, as it is for much of the HVLC beneath the volcanic margins. There is considerable support for this:

- The seismic velocity and density of continental lower crust match those of Icelandic-type lower crust. Continental lower crust is thought to comprise predominately mafic garnet-bearing granulites which have V_P ~7.1 - 7.3 km/s and densities of 3000 - 3150 kg/m^3 [Rudnick & Fountain, 1995]. It may also contain minor components of metapelite, intermediate and felsic granulites and mafic melts that would reduce V_P and density.
- The thickness of the brittle surface layer in Iceland and the viscosity of the underlying material have been constrained by geodetic studies of post-diking stress relaxation [Foulger *et al.*, 1992; Heki *et al.*, 1993; Hofton & Foulger, 1996a; b; Pollitz & Sacks, 1996] and post-glacial rebound [Sigmundsson, 1991]. The brittle surface layer is ~10 km thick, a value that is consistent with the maximum depth of earthquakes [Einarsson, 1991] and corresponds roughly to the upper crust from explosion seismology and receiver functions (Figure 9). The lower crust beneath has a viscosity of ~10^{19} Pa s and is thus ductile.
- The Faroe Islands are underlain by continental crust topped by > 6 km of basalt [Bott *et al.*, 1974; Ólavsdóttir *et al.*, 2017]. Seismic data from the eastern part of the Iceland-Faroe Ridge detect stretched continental crust similar to that underlying the Rockall Bank where HVLC has been interpreted as inherited continental crust of Palaeo-European affinity [Bohnhoff & Makris, 2004].
- Palinspastic reconstructions of Iceland require up to 150 km of crust older than the surface lavas to underlie the island—the extreme westerly and easterly ~15-Ma palaeo-rift products are separated by ~450 km whereas only ~300 km of widening could have occurred at the ambient rate of 1.8 cm/a. Reassembly of the NE Atlantic Ocean also requires up to 150 km of continental crust (original unstretched width) to lie in the ocean [Blischke *et al.*, 2017; Bott, 1985; Foulger, 2006; Gaina *et al.*, 2009; Gaina *et al.*, 2017; Gernigon *et al.*, 2015]. A similar width is required by the original lateral offset of the tips of the Aegir Ridge and proto-Reykjanes Ridge. A southerly continuation of the JMMC beneath the GIFR would be a simple source of this material [Bott, 1985; Foulger & Anderson, 2005; Schiffer *et al.*, 2018]. Icelandic-type crust also underlies the transitional region between the NE Icelandic shelf and the JMMC [Brandsdóttir *et al.*, 2015].

- Magma-assisted extension at the far western and eastern ends of the proto-GIFR, outside of the axes of breakup, is predicted by stress modeling and may have fed additional continental crust into the developing GIFR.
- There are multiple lines of petrological and geochemical evidence for a component of continental crust in Icelandic lavas, including Proterozoic and Mesozoic zircons [Amundsen *et al.*, 2002; Foulger, 2006; Paquette *et al.*, 2006; Schaltegger *et al.*, 2002] elevated $^{87}Sr/^{86}Sr$ and Pb isotope ratios [Prestvik *et al.*, 2001] and extensive silicic and intermediate rocks including rhyolite and icelandite—an Fe-rich form of andesite (Section 6).

3.2 The Faroe-Shetland basin—a bellwether of GIFR tectonic instability

The Faroe-Shetland basin comprises the eastern extension of the GIFR, is thus sensitive to tectonic activity in that zone, and has been unstable throughout the Palaeogene-early Neogene [Stoker *et al.*, 2018; Stoker *et al.*, 2005b]. Key phases are summarized in Figure 11 and include the following.

- Paleocene (~63 - 56 Ma): The pre-breakup rifting phase (late Danian—Thanetian) was characterized by formation of a series of sag and fault-controlled sub-basins [Dean *et al.*, 1999; Lamers & Carmichael, 1999], coeval borderland uplift events (rift pulses) [Ebdon *et al.*, 1995; Goodwin *et al.*, 2009; Mudge, 2015] and rifting and extension accompanied by volcanism [Mudge, 2015; Ólavsdóttir *et al.*, 2017].
- Latest Paleocene (~56 - 55 Ma): Uplift [Ebdon *et al.*, 1995] and extrusion of syn-breakup flood basalts and tuffs [Mudge, 2015] probably mark the onset of local, discontinuous sea-floor spreading [Passey & Jolley, 2009].
- Early-Mid-Eocene (~54 - 46 Ma): The syn-breakup rift-to-drift transition continued during the early/mid-Ypresian-early Lutetian [Stoker *et al.*, 2018]. Cyclical coastal plain, deltaic and shallow-marine deposits attest to tectonic instability linked to episodic uplift of the Munkagrunnur and Wyville Thomson ridges on the south flank of the basin [Ólavsdóttir *et al.*, 2010; Ólavsdóttir *et al.*, 2013b; Stoker *et al.*, 2013]. Onset of continuous sea-floor spreading in the Norway basin (chron C21) was accompanied by uplift events, continued growth of the Wyville Thomson and Munkagrunnur ridges, and formation of inversion domes in the basin [Ólavsdóttir *et al.*, 2010; Ólavsdóttir *et al.*, 2013b; Ritchie *et al.*, 2008; Stoker *et al.*, 2013; Stoker *et al.*, 2018].
- Late Paleogene-early Neogene (~35 - 15 Ma): The present-day basin physiography was initiated in the latest Eocene/Early Oligocene with sagging leading to basin-ward collapse of the margin west of Shetland [Stoker *et al.*, 2013]. Onlapping Oligocene and Lower Miocene basinal sequences were deformed by compressional stresses and widespread inversion and fold growth culminated in the early Mid-Miocene [Johnson *et al.*, 2005; Ritchie *et al.*, 2008; Stoker *et al.*, 2005c].
- Mid-Miocene—Pleistocene (16/15 Ma - present): Basinal sedimentation was dominated by deep-water deposits [Stoker *et al.*, 2005b] with Early Pliocene uplift and tilting of the West Shetland and East Faroe margins accompanied by basinal subsidence and reorganization of bottom current patterns [Andersen *et al.*, 2000; Ólavsdóttir *et al.*, 2013b; Stoker *et al.*, 2005a; Stoker *et al.*, 2005b]. Mid-and Late Pleistocene sedimentation was dominated by shelf-wide glaciations [Stoker *et al.*, 2005a].

In summary, the Faroe-Shetland basin has experienced persistent tectonic unrest from the Paleocene to the Early Miocene (~63 - 15 Ma). This is reflected onland in the Faroe Islands in Paleogene and younger faults and dykes that show progressive changes in the direction of extension prior to and following NE Atlantic break-up [Walker *et al.*, 2011]. This chronic unrest likely reflects both instability on the GIFR to the west and the protracted breakup of the wider NE Atlantic region.

4 A new model for the Greenland-Iceland-Faroe Ridge

In this section, we build on the background given above and propose a new working hypothesis for development of the GIFR and how this affected the rest of the NE Atlantic Realm. Numerical modeling of the processes we propose, and model fit with petrology and geochemistry, are discussed in Sections 5 and 6.

As described above, the NE Atlantic Realm formed in a disorderly way as a consequence of inherited strength anisotropy, coupled with frequent changes in the poles of rotation of sub-regions [Hansen *et al.*, 2009; Schiffer *et al.*, 2018]. North of the GIFR, the Aegir rift opened by southward propagation obliquely along the Caledonian orogen. It stalled at the western frontal thrust and hooked around to the west (Figure 1). The Reykjanes Ridge to the south stalled at the Nagssugtoqidian orogen, ~300 km south of the Caledonian frontal thrust and ~150 km west of the Aegir Ridge (Section 2.2). The Reykjanes Ridge and Aegir Ridge thus formed a pair of propagating, approaching, laterally offset rifts. The broad barrier formed by the Nagssugtoqidian and Caledonian orogens prevented them from propagating further and conceivably eventually forming a continuous, conventional oceanic plate boundary.

As a consequence, the continental region between their tips, the ~300 x 150 km Iceland Microcontinent, deformed by magma-assisted, distributed continental transtension and developed into the GIFR as the ocean widened (Figure 12). The crust beneath the Iceland Microcontinent and flanking areas thinned by ductile flow in its deeper parts. Extensive magmatism built SDRs of the kind observed on the eastern margin of the JMMC and the NE Atlantic rifted margins. Initially, the GIFR may have comprised an array of four passive margins–one on each of the east Greenland and west Faroe margins, and one on either side of the Iceland Microcontinent.

As the GIFR lengthened, and up to the present day, deformation persisted in a distributed style along a series of ephemeral extensional rifts and diffuse, intermediate, poorly developed shear transfer zones [Gerya, 2011]. The loci of extension repeatedly reorganized by migrating laterally to positions that were stress-optimal and likely also influenced by pre-existing structures in the underlying continental crust. Rifts that became extinct were transported laterally out of the actively extending, central part. As it formed the GIFR was blanketed by lavas in the style of volcanic-rifted-margins. Similar rift migrations also occurred in the eastern Norway basin where the oceanic crust is thickest [Gernigon *et al.*, 2012]. After ~48 Ma (C22) it seems that this style of extension persisted only on the GIFR. The permanent disconnect between the Aegir Ridge and the Reykjanes Ridge and the low spreading rate in the NE Atlantic (1 - 2 cm/a) would have further encouraged long-term diffuse deformation.

Figure 13 shows palinspastic reconstructions of the observed positions of active and extinct rifts in the NE Atlantic Realm at various times. Swathes of extinct, short, NE-orientated ridges similar to those that are currently active onland in Iceland are observed also in submarine parts of the GIFR [Hjartarson *et al.*, 2017]. There is insufficient observational data at present to fully reconstruct the sequence of deformation on the GIFR because of the blanketing lava flows and insufficient geophysical and geological research to date. Nevertheless, in Figure 14 we attempt such a reconstruction by extrapolating in time from known active and extinct rifts [Hjartarson *et al.*, 2017; Johannesson & Saemundsson, 1998].

A large block of crust older than the surface lavas is required by palinspastic reconstructions to lie beneath Iceland [Foulger, 2006]. Thus, much of the Iceland Microcontinent may still exist beneath Iceland and comprise a C-block [Geoffroy *et al.*, 2015; Geoffroy *et al.*, submitted]. C-blocks are expected to be flanked by Outer-SDRs and the geometry of some dykes and lava flows in Iceland resemble these [Bourgeois *et al.*, 2005; Hjartarson *et al.*, 2017]. It has long been speculated that the continental crust required by geochemistry to underlie Iceland (Section 6) comprises a southerly extension of the magma-dilated southern JMMC. Give the extent of continental crust that is required

579 to underlie the GIFR it may be more appropriate to view the JMMC as an offshore extension of the
580 Iceland Microcontinent.

581 Deformation on the GIFR cannot be described by traditional rigid plate tectonics and corresponding
582 reconstructions. It corresponds to the case of multiple overlapping ridges, the limit of an extensional
583 zone [Engeln *et al.*, 1988]. It may be likened to a lateral array of hyper-extended SDRs underlain by
584 HVLC comprising heavily intruded, stretched, ductile continental crust. Repeated rejuvenation of the
585 rift axes by lateral migration may have boosted volcanism. Westerly migrations may have induced
586 extension to the north to concentrate in the westernmost axis of extension in the southern JMMC,
587 leading to extinction of the Aegir Ridge and formation of the Kolbeinsey Ridge at ~24 Ma. That
588 migration switched the sense of the ridges north and south of the GIFR from right-stepping to left-
589 stepping.

590 Iceland is ~450 km wide in an EW direction and exposes ~40% of the GIFR (Figure 1). The oldest
591 rocks found there to date are 17 Ma. There is no evidence, or reason to think, that the tectonic style on
592 the GIFR was fundamentally different in the past from present-day Iceland. On the contrary, the
593 similarity of the submarine GIFR synclines to structure on land in Iceland suggests that it was the
594 same [Hjartarson *et al.*, 2017].

595 Onland in Iceland extension over the last ~15 Ma has occurred via multiple unstable, migrating,
596 overlapping spreading segments connected by complex, immature shear transfer zones that reorganize
597 every few Myr (Figure 15). These include the South Iceland Seismic Zone [Einarsson, 1988; 2008]
598 and the Tjörnes Fracture Zone [*e.g.*, Rognvaldsson *et al.*, 1998]. Both are broad, diffuse seismic zones
599 that deform in a bookshelf-faulting manner and have not developed the clear topographic expression
600 of faults that experience long-term repeated slip.

601 There is geological evidence in Iceland for at least 12 spreading zones (Table 2) of which seven are
602 currently active, two highly oblique to the direction of plate motion, one waning, one propagating,
603 two non-extensional and five extinct. At least five lateral rift jumps are known and a sixth is currently
604 underway via transfer of extension from the Western Volcanic Zone (WVZ) to the Eastern Volcanic
605 Zone (EVZ). Extension has always been concentrated in a small number of active, ephemeral rift
606 zones at any one time (Figure 15).

607 There is no evidence that mature sea-floor spreading has yet begun anywhere along the GIFR. If such
608 were the case it would be expected that all extension would be rapidly transferred to that zone and
609 normal-thickness oceanic crust (i.e., ~6 - 7 km) would begin to form. Indeed, the fact that rift-zone
610 migrations are still ongoing in Iceland suggest that this is not the case. There may be some narrow
611 zones where embryonic sea-floor spreading began but was abandoned due to subsequent lateral rift
612 jumps, *e.g.*, immediately east of the east Icelandic shelf, and in the deep channel in the Denmark
613 Strait. Until this can be confirmed, however, it remains a possibility that full continental breakup has
614 not yet occurred in the latitude band of the GIFR. This fundamentally challenges the concept that
615 continental breakup has yet occurred in this part of the NE Atlantic.

616 *4.1 Mass balance*

617 The GIFR today is 1,200 km long with a lower crust generally ~20 km thick and maximally ~30 km
618 beneath central Iceland (Figure 9). If a substantial part of this is continental, a large volume thus
619 needs to be accounted for. Taking a present-day average breadth for the GIFR of ~200 km, the surface
620 area is ~0.24 x 10^6 km^2. If an average thickness of 15 km of continental material lies beneath, a
621 volume of ~3.6 x 10^6 km^3 is required.

622 We propose that this material was sourced from the Iceland Microcontinent and flanking continental
623 regions by ductile flow of mid- and lower crust. Ductile flow can stretch such crust to many times its
624 original length (necking), draw in material from great distances, and maintain large crustal

thicknesses. Numerical thermo-mechanical modeling (Section 5) confirms that these processes can account for the lower-crustal thicknesses proposed and even increase crustal thickness as material rises to fill the void created by rupture of the upper crust.

Flow is enabled by the low viscosity of the lower crust beneath Iceland. This has been shown to be 10^{18} - 10^{19} Pa s by GPS measurements of post-diking stress relaxation following a regional, 10-m-wide dyke injection episode in the Northern Volcanic Zone (NVZ) 1975 - 1995 [Bjornsson *et al.*, 1979; Foulger *et al.*, 1992; Heki *et al.*, 1993; Hofton & Foulger, 1996a; b]. Numerical modeling of those data also showed that the surface, brittle layer was approximately 10 km thick. The low viscosity found for the lower crust was confirmed by measurements and modeling of the rapid isostatic rebound from retreat of the Weichselian ice cap in Iceland and melting of the Vatnajökull glacier in south Iceland [Sigmundsson, 1991]. [Sigmundsson, 1991].

As a prelude to numerical thermo-mechanical modeling we present here a simple mass-balance calculation. Inland in Greenland, receiver function studies indicate a Moho depth of ~40 km [Kumar *et al.*, 2007]. The Caledonian crust of east Greenland is currently up to ~50 km thick [Darbyshire *et al.*, 2018; Schiffer *et al.*, 2016; Schmidt-Aursch & Jokat, 2005; Steffen *et al.*, 2017]. A pre-breakup Caledonian crustal thickness of about 60 km and a post-breakup thickness of 30 km [Holbrook *et al.*, 2001] is not unrealistic.

Beneath the Faroe-Shetland basin, crustal thinning left only a 10-km-thick crust while below the Faroe shelf and islands seismic data indicate basement modified by weathering, igneous intrusions and tuffs with a thickness of about 25 - 35 km [Richard *et al.*, 1999]. Beneath the banks to the SW of the Faroe Islands the thickness of the subvolcanic crust is up to 25 km but it is as little as 8 km beneath the channels between them [Funck *et al.*, 2008]. In the Faroe Bank Channel and the channel between George Bligh and Lousy Bank, in prolongation of the GIFR, the continental middle crust is almost completely gone and the lower crust is dramatically thinned. Initial and final thicknesses of 60 km and 15 km are reasonable.

Thinning of the mid- and lower crust of 30 km (Greenland) and 45 km (Faroe region) extending ~200 km along the margins and ~100 km inland could provide ~1.5 x 10^6 km^3 of material. Assuming original northerly and easterly dimensions for the Iceland Microcontinent of 300 km and 150 km respectively, and thinning from an original 60 km to 15 km, an additional ~2 x 10^6 km^3 of material is accounted for. Together, this totals ~3.5 x 10^6 km^3 of material, very close to the ~3.6 x 10^3 km^3 required.

This mass balance calculation illustrates simply that our model is reasonable. It also shows that the Iceland Microcontinent can provide over half of the continental material required. This suggests that the formation of such an unusually large microcontinent was likely a key element in the development of this unique region.

4.2 Problems and paradoxes solved

The model we propose can account naturally for many hitherto unexplained observations from the GIFR and surrounding regions, and it is supported by multiple lines of evidence. In particular, it offers a solution to the decades-old problems of why the Thulean land bridge existed, and the nature of Icelandic-type crust. Thus:

- A composition of Icelandic-type crust comprising magma-inflated continental crust blanketed with lavas can explain the high topography and bathymetry of the GIFR and its prolonged persistence above sea level.
- The assumption that the full thickness of Icelandic-type crust corresponds to melt has been widely accepted ever since Bjarnason *et al.* [1993] reported a reflective horizon at ~20 - 24 km depth beneath south Iceland which they interpreted as the Moho. That model cannot,

671 however, account for the absence of refracted seismic phases (Section 3.1) which is
672 inconsistent with gabbroic crust overlying mantle with a step-like interface velocity increase.
673 The lack of such refractions is, however, consistent with the reflective horizon being a sill-
674 like structure within or near the base of magma-inflated continental crust.

675 • Icelandic-type lower crust has a seismic velocity V_P of 7.0 - 7.3 km/s and a density of ~3150
676 kg/m^3. No reasonable basaltic petrology is consistent with this [Gudmundsson, 2003; Menke,
677 1999], but these values fit a composition of magma-inflated continental crust.

678 • A lower crust containing significant continental material solves the paradox of magmatic
679 production on the GIFR. Icelandic-type lower crust cannot be gabbroic because a melt layer
680 up to 40 km thick cannot be explained with any reasonable petrology and temperatures
681 (Section 6) [Hole & Natland, this volume]. If the melt layer corresponds only to Icelandic-
682 type upper crust plus magma inflating the lower crust—possibly a total thickness of up to ~15
683 km—much less melt needs to be explained.

684 • A substantial volume of continental material in the lower crust can explain why the
685 thicknesses of the upper and lower crustal layers on the GIFR are de-correlated (Figure 9)
686 [Foulger *et al.*, 2003; Korenaga *et al.*, 2002]. In particular, the lower crust is thick throughout
687 a NW-SE swathe across central Iceland where the upper crust is of average thickness. In the
688 far south, the upper crust has its maximum thickness but the lower crust is unusually thin
689 (Figure 9).

690 • MORB melt formed in the mantle below the crust passes through the latter, melting fusible
691 components to a high degree, boosting melt volume, and acquiring the continental signature
692 observed in Icelandic rocks including the geochemistry, Proterozoic and Mesozoic zircons,
693 and voluminous felsic and intermediate petrologies (Section 6).

694 • The numerous, northerly trending synclines detected by seismology throughout submarine
695 parts of the GIFR are readily explained as volcanically active extensional zones that were
696 abandoned by lateral jumps and subsequently became extinct [Hjartarson *et al.*, 2017] (Figure
697 8).

698 • If the JMMC is a northerly extension of the Iceland Microcontinent, the former may have
699 shared the tectonic instability of the GIFR, providing an explanation for why the JMMC
700 broke off east Greenland.

701 Our new model for the GIFR can account for the many unusual extensional, transtensional and shear
702 tectonic elements in the region. These include the curious distributed, bookshelf mode in which shear
703 deformation is taken up in Iceland in the South Iceland Seismic Zone and the Tjörnes Fracture Zone
704 [Bergerat & Angelier, 2000; Einarsson, 1988; Taylor *et al.*, 1994].

705 It can also account for the widespread hook-like tectonic morphology that resembles the tips of
706 overlapping propagating cracks (Figure 16). These suggest that short extensional elements are
707 abundant. The southernmost Aegir Ridge is hooked westward, mirroring the shape of the Blosseville
708 coast of Greenland and curving into the transverse Caledonian frontal thrust [Brooks, 2011]. The
709 extensional NVZ of Iceland curves westward at its northern end where it links with the Kolbeinsey
710 Ridge via the Tjörnes Fracture Zone. At its north end, the Reykjanes Ridge hooks to the east where it
711 runs onshore to form the Reykjanes Peninsula extensional transform zone [Taylor *et al.*, 1994]. The
712 direction of extension in the EVZ is rotated ~35˚ clockwise compared with the NVZ as shown by both
713 the strike of dyke- and fissure swarms and current measurements of surface deformation made using
714 GPS [*e.g.*, Perlt *et al.*, 2008]. The southernmost tip of this propagating rift, the Vestmannaeyjar
715 archipelago, hooks to the west, complementing the east-hooking northern Reykjanes Ridge and
716 Reykjanes Peninsula Zone (Figure 16).

717 The contrasting tectonic morphology and behavior north and south of the GIFR are naturally
718 explained by tectonic decoupling by the GIFR that separates them. North of the GIFR the boundary is
719 dominated by spreading ridges orthogonal to the direction of extension, separated by classic transform

faults. To the south, the Reykjanes Ridge as a whole is oblique to the spreading direction and devoid of transform faults. Numerous tectonic events occurred north or south of the GIFR but not in both regions simultaneously [Gernigon *et al.*, this volume; Martinez & Hey, this volume]. In Iceland, tectonic decoupling can explain the north-south contrast in geometry, morphology and history of the rift zones and the north-south asymmetry in geochemistry [*e.g.*, Shorttle *et al.*, 2013]. The latter may be important in mapping the distribution of continental material beneath Iceland.

Unstable tectonics on the GIFR can further explain the diachronous chevrons of alternating thick and thin crust that form at the tips of propagators within the Reykjanes Ridge plate boundary zone (Figure 7; Sections 2.2.2 and 7.3.3). The onset times of several of the most recent of these propagators at the GIFR coincide with major ridge jumps in Iceland (Table 1). These observations are consistent with the propagators being triggered by major tectonic reorganizations on the GIFR. Several similar ridges are observed in the oceanic crust east of the Kolbeinsey Ridge [Jones *et al.*, 2002]. The chronic instability of the mid-Norwegian shelf and the adjacent Faroe-Shetland basin throughout the Palaeogene-earliest Neogene is also accounted for [Ellis & Stoker, 2014; Gernigon *et al.*, 2012; Stoker *et al.*, 2018] (Figure 11) (Section 3.2).

5 Thermo-mechanical modeling

We tested the plausibility of unusually prolonged survival of intact continental crust beneath the GIFR by modeling numerically the behavior under extension of structures characteristic of an ancient orogen such as the Caledonian and surrounding regions. The crust is required to have stretched to over twice its original width, retained a typical thickness of ~20 km, and persistently extended along more than one axis even up to the present day i.e. it underwent long-term, diffuse extension.

We used a two-dimensional thermo-mechanical modeling approach [Petersen & Schiffer, 2016] to calculate the visco-elastic-plastic response of an ancient orogen under simple extension. Full details of our methodological approach along with petrologic, thermodynamic, rheological, thermal conductivity, radiogenic heat productivity, initial model state, boundary conditions and melt productivity are described in detail by Petersen *et al.* [2018]. The initial state for the model we use here differs from that used by Petersen *et al.* [2018] only in that a) a uniform adiabatic temperature with potential temperature T_P =1325˚C is assumed for the entire mantle, and b) there is no MORB layer at the upper/lower mantle boundary.

Prior to continental breakup, crustal thickness and structure likely varied throughout the region, but precise details of the pre-rift conditions are not well known. Insights may be gained from well-studied, currently intact orogens. The Himalaya orogen, a heterogeneous stack of multiple terranes, entrained subduction zones, and continental material, is underlain by one or more fossil slabs trapped in the lithosphere. These locally thicken the crust and their lower parts are in the dense eclogite facies (Figure 17) [Tapponnier *et al.*, 2001]. The Palaeozoic Ural Mountains preserve a crustal thickness of 50 - 55 km [Berzin *et al.*, 1996]. The Caledonian crust is up to ~50 km thick under east Greenland [Darbyshire *et al.*, 2018; Schiffer *et al.*, 2016; Schmidt-Aursch & Jokat, 2005; Steffen *et al.*, 2017] and ~45 km thick beneath Scandinavia [Artemieva & Thybo, 2013; Ebbing *et al.*, 2012].

The pre-breakup crust in the region of the future NE Atlantic comprised the south-dipping Ketilidian and Nagssugtoqidian orogens and the bivergent Caledonian orogen with east-dipping subduction of Laurentia (Greenland) and west-dipping subduction of Baltica (Scandinavia) (Figure 4). The GIFR thus formed over fossil forearc/volcanic front lithosphere that may initially have had a structure similar to that of the Zangbo Suture of the Himalaya orogen (Figure 17). North of the GIFR the supercontinent broke up longitudinally along the Caledonian suture where the crust was thinner.

We modeled the Caledonian frontal thrust as an orogenic belt where the lithosphere contrasts with that of the flanking Greenland and Scandinavia areas in a) increased crustal thickness, and b) eclogite from fossil subducted slabs embedded in the lithospheric mantle (Figure 4) [Schiffer *et al.*, 2014]. The

767 eclogite is relatatively dense, potentially driving delamination, but is rheologically similar to dry
768 peridotite [Petersen & Schiffer, 2016 and references therein]. Additional weakening of the hydrated
769 mantle wedge preserved under the suture would enhance the model behavior we describe below
770 [Petersen & Schiffer, 2016]. For the mantle, we assume a pyrolite composition that is subject to melt
771 depletion during model evolution.

772 Figure 18 shows our initial, simplified model setup [Petersen *et al.*, 2018]. Pre-rift continental crustal
773 thickness is 40 km for the lithosphere adjacent to the orogen. The crust beneath the 200-km-wide
774 orogen is 50 km thick and underlain by an additional 20-km-thick slab of HVLC with an assumed
775 mafic composition. Phase transitions and density are self-consistently calculated from
776 pressure/temperature conditions throughout the model such that the topmost part of the body is above
777 eclogite facies and the lower part is in the eclogite facies and thus negatively buoyant.

778 Densities and entropy changes are pressure- and temperature-dependent and calculated using
779 Perple_X-generated lookup tables [Connolly, 2005] based on the database of Stixrude and Lithogow-
780 Bertelloni [2011]. We use a wide box (2000 km x 1000 km) to enable simulation of considerable
781 extension distributed over a broad region, a grid resolution of 2 km, and a run time of 100 Myr at a
782 full extension rate of 1 cm/a. Rifting of the lithosphere is kinematically forced by imposing plate
783 separation at a rate of 0.5 cm/a via outwards perpendicular velocities at both left and right boundaries
784 throughout the depth range of 0 - 240 km.

785 A multigrid approach is employed to solve the coupled equations for conservation of mass, energy
786 and momentum as described by Petersen *et al.* [2015; 2018]. For the continental crust, we assume
787 plagioclase-like viscous behavior [Ranalli, 1995]. The HVLC is assumed to follow an eclogite flow
788 law [Zhang & Green, 2007]. The upper mantle is assumed to follow a combined diffusion/dislocation
789 creep flow law [Karato & Wu, 1993]. The lower mantle, here defined as the region where the
790 pressure/temperature-dependent density exceeds 4300 kg/m^3, approximately corresponding to
791 Ringwoodite-out conditions, is assumed to follow the linear flow law inferred by Čížková *et al.*
792 [2012].

793 As the structure extends, rifting develops in the broad region where the crust is thickest. The Moho
794 temperature is highest there (i.e. ~800˚C; Figure 18 central panels) due to greater burial and
795 radiogenic heat production. During the first 10 Myr of widening, extensional strain within the crust is
796 laterally distributed due to the delocalizing effect of flow in the lower crust [*e.g.*, Buck, 1991].
797 Thinning of the mantle lithosphere is not counteracted by this effect and within 10 Myr it has been
798 thinned by a factor of up ~2. This results in onset of decompression melting after ~12 Myr. At this
799 point, the crust in the stretched orogen retains a large thickness of 30 - 40 km. This contrasts with the
800 sequence of events where the crust is thin and brittle under which conditions decompression melting
801 only onsets after breakup i.e. when complete thinning of the continental crust occurs [Petersen *et al.*,
802 2018].

803 Thinning of the mantle lithosphere leads to lateral density gradients between the asthenosphere and
804 displaced colder lithospheric mantle that destabilize the lithospheric mantle [Buck, 1986; Keen &
805 Boutilier, 1995; Meissner, 1999]. Consequently, the mantle lithosphere, including the already
806 negatively buoyant HVLC, starts to delaminate at ~12 Myr (Figure 18). As a result, asthenosphere at
807 a potential temperature (T_P) of ~1325˚C and crust at an initial temperature of ~600 - 800˚C are rapidly
808 juxtaposed. This leads to increased heat flow into the crust which therefore remains ductile enough to
809 flow and continues to extend in the delocalized, "wide rift mode" of Buck [1991]. The loci of
810 extension repeatedly migrate laterally and this mode of deformation continues as long as lower crust
811 is available. The loci of extension only stabilize after ~70 Myr.

812 Figure 18 shows the predicted structure after 51 Myr, approximately the present day, and a
813 magnification of the 51-Myr lithology panel is shown in Fig. 19. The continental crust is still intact
814 across the now 1,200-km-wide ocean and extending diffusely. Decompression melting is occurring

beneath two zones. The HVLC body has disintegrated and the largest pair of fragments are 200 - 300 km in diameter. These, along with carapaces of lithospheric mantle, have subsided to a depth near the base of the transition zone. Between them, a narrow arm of mantle upwells and flattens at the base of the crust to form a broad sill-like body ~200 km thick that underlies the entire ocean. Upwelling includes some material from just below the transition zone as a consequence of the sinking HVLC displacing uppermost lower-mantle material.

Full lithosphere breakup has not occurred by 51 Myr. It is imminent at 71 Myr (Figure 18). The lower crust beneath distal areas flows into the thinning extending zone and only when the supply of ductile lower crust is depleted does extension localize, leading to full lithosphere rupture and sea-floor spreading. This may take several tens of millions of years. In the case where the crust is thinner and/or HVLC is lacking modeling predicts transition to sea-floor spreading after only a few million years.

The generic model presented here shows that it is possible for extending lithosphere to remain for as long as 70 Myr in a delocalized 'wide' stretching mode [senso Buck, 1991] with lower crust from distal areas flowing into the extending zone. Since the delamination, the mantle lithosphere has effectively been removed and decompression melting occurs where the mantle wells up beneath the rift system. Together, these interdependent processes provide a physical mechanism for how continental crust could be preserved beneath the GIFR despite more than 50 Myr of extension (Figure 20). At the same time, the model accounts for the magmatism observed on the GIFR in that it predicts decompression melting in the mantle. These melts rise, intrude and erupt, covering the continental crust as it stretches, and would produce crust similar to the "embryonic" crust proposed to occur in the Norway Basin [Geoffroy, 2005; Gernigon *et al.*, 2012].

The predictions of our model for present-day structure compare well with seismic tomography images (Figure 21). For example, a cross section through the full-waveform inversion tomographic model of Rickers *et al.* [2013] shows several features that are in close correspondence to those we predict. These include the flanking high-wave-speed bodies at the bottom of the transition zone, a narrow, weak, vertical, low-wave-speed body between them and a broader, stronger, low-wave-speed body in the top ~200 km underlying the entire ocean. The high-wave-speed bodies correspond to the delaminated lithospheric mantle and the low-wave-speed anomalies correspond to the temperature anomalies predicted by the modeling (Figure 19). A mantle temperature anomaly of ~ 30˚C is predicted beneath the entire ocean down to ~ 200 km depth as a result of upper mantle upwelling. The seismic anomaly could then be explained by this temperature anomaly and a resulting increase in the degree of partial melt by up to 0.5% [Foulger, 2012]. Such a temperature anomaly is consistent with the low values predicted by Ribe et al. [1995] who modeled the topography of the region, and the petrological estimates of Hole and Natland [this volume]. Seismic tomography images are notoriously variable in detail, in particular anomaly amplitudes [Foulger et al., 2013], and we thus place most significance on the correspondence between the shape of the predicted (Figure 19) and observed (Figure 21) anomalies.

Our results differ from those of existing mechanical models in that breakup of the continental crust is more protracted [*e.g.*, Brune *et al.*, 2014]. For example, Huismans and Beaumont [2011] showed that extension of lithosphere with relatively weak crust results in pre-breakup wide-rift-mode extension for ~35 Myr. Our model differs from theirs by having dense HVLC that delaminates as a consequence of rifting thereby increasing heat flow into the crust. This enables wide rifting to persist for much longer than where no HVLC is present, even in the absence of an especially weak lower crustal rheology.

The amount and detailed history of wide-mode extension is controlled by the thickness of the initial crust and rheology-governing parameters such as initial thermal state, heat flow, radiogenic heat production and crustal flow laws. We examined models that varied some of these parameters to investigate the sensitivity of our results to the assumed initial conditions. We modeled crustal thicknesses of 35 km for the region and 40 km for the orogen, and lithosphere thickness of 100 km with quartzite-like crustal rheology. Similar results to those described above were obtained. Factors

we do not incorporate in our simple model that would further encourage crustal stretching and delay breakup include increased basal heat flow and/or internal heat production and inclusion of 3D effects that would permit ductile mid- and lower crust to flow along the strike of the Caledonides towards the GIFR during extension.

6 Geochemistry

All aspects of the petrology and geochemistry of igneous rocks in the NE Atlantic Realm are consistent with a model where Icelandic lower crust contains a substantial amount of continental crust. The geochemical and petrological work most powerful to test this model is that which addresses the composition and potential temperature (T_P) of the melt source.

6.1 Composition of the melt source

The source of Icelandic lavas cannot be explained by mantle peridotite alone [*e.g.*, Presnall & Gudfinnsson, 2011]. A component of continental material is required and some studies have presented evidence that this could be of Caledonian age [Breddam, 2002; Chauvel & Hemond, 2000; Korenaga & Kelemen, 2000]. It could come from subducted slabs still remaining in the shallow mantle, as has been proposed earlier [Foulger & Anderson, 2005; Foulger *et al.*, 2005]. The observations could also be explained by the upward flow of mantle melt through a substrate of stretched, magma-inflated continental crust similar to some HVLC beneath the passive margins.

Titanium: The petrology and geochemistry of igneous rocks along the mid-Atlantic ridge change radically at the Icelandic margin. Low-TiO_2 basalts are found on the Reykjanes and Kolbeinsey Ridges and in the rift zones of Iceland. These rocks do not follow the MORB array of Klein and Langmuir [1987] but have the least Na_8 and Ti_8 of the entire global array. These lavas are probably derived mostly from a peridotitic MORB source.

Basalts with high-TiO_2 and FeO(T) signatures occur in Iceland, Scotland, east and west Greenland, but not on the Reykjanes or Kolbeinsey Ridges. These basalts cannot come from MORB-source mantle—the source is required to have distinct Fe-Ti-rich material and other important geochemical indicators such as REE that are not found in MORB-source mantle. The extent of differentiation beneath Icelandic central volcanoes is also high enough to produce abundant silicic lavas—icelandite and rhyolite—in association with the FeO(T)-TiO_2-rich basalts. These rocks comprise 10% of the surface volcanics of Iceland but are not present on the adjacent submarine ridges and are uncommon on all other oceanic spreading plate boundaries.

A candidate for the source of such lavas is lower continental crust, possibly pyroxenite/eclogite arising from gabbro with elevated TiO_2 and FeO(T) at pressures in the eclogite facies, along with refractory sub-continental lithospheric mantle (SCLM), originally from the Greenland and European margins and still present in the central North Atlantic. A hybrid source of this sort can explain the diversity of Icelandic magmas [Foulger & Anderson, 2005; Foulger *et al.*, 2005; Korenaga, 2004; Korenaga & Kelemen, 2000]. Because there is no major isotopic anomaly, the source cannot be very old. Candidate material is common in continental lithosphere. For example, xenolith suites of lower crustal cumulates from Permian lamprophyres in Scotland have the required characteristics [Downes *et al.*, 2007; Hole *et al.*, 2015].

The close proximity of the low- and high-Ti, high-FeO(T) basalts suggests that their different sources are physically close together. It is clear that these sources have been tapped since the opening of the NE Atlantic as they are also seen in the same successions in the Skaergaard intrusion in east Greenland [Larsen *et al.*, 1999]. The high-TiO_2 and FeO(T) lavas found in Iceland are typical of lavas derived from sub-continental lithospheric mantle and pyroxenite. No more than 20 - 30% of pyroxenite in a hybrid source is required to explain the observations.

Isotope ratios: Elevated $^{87}Sr/^{86}Sr$ and Pb isotope ratios are found in basalts from east and southeast Iceland [Prestvik *et al.*, 2001]. This has been interpreted as requiring a component of continental material in the source beneath Iceland. That component could come from crust or detached SCLM buried beneath surface lavas [Foulger *et al.*, 2003].

Zircons: Archaean and Jurassic zircons with Lewisian (1.8 Ga) and Mesozoic (~126 - 242 Ma) inheritance ages have been reported from lavas in NE Iceland. This has been interpreted as indicating ancient continental lithosphere beneath Iceland [Paquette *et al.*, 2006; Schaltegger *et al.*, 2002]. A continental composition for Icelandic-type lower crust can explain these results.

Water: Water in basalt glass from the mid-Atlantic Ridge indicates elevated contents in the source from ~61˚N across Iceland [Nichols *et al.*, 2002]. The water contents are estimated to be ~165 ppm at the southern end of the Reykjanes Ridge, rising to 620 - 920 ppm beneath Iceland. Such a component, and other volatiles such as CO_2 [Hole & Natland, this volume] decrease the solidus of a source rock and increase the volume of melt produced for a given T_P (Section 6.2).

6.2 Temperature of the melt source

The temperature of the melt source of Icelandic rocks is too low to be able to account for a 30-40-km-thick basaltic crust using any reasonable lithology [Hole & Natland, this volume]. It is therefore an inevitable conclusion that much of the lower crust beneath the GIFR must arise from a process other than high-temperature partial melting of mantle peridotite.

Geochemical work aimed at determining the potential temperature of NE Atlantic source rocks has used basalts from Iceland and high-MgO picrites from the Davis Strait [Clarke & Beutel, 2019; Hole & Natland, this volume]. The T_P for the source of MORB is generally used as the standard against which other calculated mantle temperatures are compared. The currently accepted value of this is 1350±40˚C (Table 3) [Hole & Natland, this volume].

A large range of temperatures, T_P = 1400 - 1583˚C, has been suggested for the mantle beneath Iceland [Hole & Millett, 2016; Putirka, 2008]. The breadth of this range in itself indicates how difficult it is to derive a repeatable, reliable T_P using geochemistry and petrology. Difficulties include the lack of surface samples that correspond to an original mantle melt—crystalline rocks essentially always contain xenocrysts, and no picritic glass has been found in the NE Atlantic Realm [Presnall & Gudfinnsson, 2007]. The unknown source composition also introduces uncertainty. The geochemistry of Icelandic lavas requires there to be a component of recycled surface materials in the source and variable volatile contents including water [Nichols *et al.*, 2002]. Ignoring any of these unknowns causes estimates of T_P to be erroneously high.

Crystallization temperatures estimated from olivine-spinel melt equilibration, the so-called "aluminum-in-olivine" method, are independent of whole-rock composition. The temperatures yielded by this method are T_P ~1375˚C and ~100˚C higher for the Davis Strait picrites (Table 3) [Hole & Natland, this volume]. A summary of global maximum petrological estimates of T_P and ranges of olivine-spinel equilibrium crystallization temperatures for magnesian olivine are shown in Figure 22.

Petrological estimates of the potential temperature T_P of the source of basalts in the NE Atlantic Realm suggest upper-bound T_P of ~1450˚C for Iceland and ~1500˚C for the picrites of Baffin Island, Disko Island and west Greenland [Hole & Natland, this volume]. There may thus have been a short-lived, localized burst of magma from a relatively hot source lasting ~2 - 3 Myr when propagation of the Labrador Sea spreading center was blocked at the Nagssugtoqidian orogen, but there is no compelling evidence for a T_P anomaly > ~100˚C before or after this anywhere in the NE Atlantic Realm.

The melt volume produced at Iceland has also been used as a constraint in models for T_P. That work has assumed that the full thickness of the 30-40-km-thick seismic crustal layer is melt produced by steady state fractional melting of a peridotite mantle source. Production of just 20 km of igneous crust would require a T_P of ~1450 - 1550°C assuming a damp or dry peridotite source [Sarafian *et al.*, 2017]. No credible lithology or temperature can explain the crustal thickness of ~40 km that has been measured for central Iceland [Darbyshire *et al.*, 1998a; Foulger *et al.*, 2003].

Crustal thickness beneath the active volcanic zones of Iceland varies from ~40 km (beneath Vatnajökull) to ~15 - 20 km (beneath the Reykjanes Peninsula extensional transform zone) [Foulger *et al.*, 2003]. If the full thickness of crust everywhere is formed from melting in the mantle, unrealistically large lateral variations in temperature of the source of ~150˚C over distances of ~125 km would be required [Hole & Natland, this volume].

6.3 $^3He/^4He$

Elevated $^3He/^4He$ values are commonly assumed to indicate a core-mantle boundary provenance for the melt source. This association was originally suggested when it was found that some lavas from Hawaii contain high-$^3He/^4He$ [Craig & Lupton, 1976]. It was reasoned that, over the lifetime of Earth, the $^3He/^4He$ of the mantle has progressively decreased from an original value of ~200 times the present-day atmospheric ratio (Ra) to ~8 ± 2 Ra—the value most commonly observed in MORB. It was subsequently assumed that a lava with $^3He/^4He$ much larger than 8 Ra must have arisen from a primordial source, isolated for Earth's 4.6 Ga lifetime, deep in the mantle near the core-mantle boundary.

This theory has long been contested and it has been counter-proposed that the helium instead resided for a long time in depleted, unradiogenic materials such as olivine in the sub-continental lithospheric mantle [Anderson, 2000a; b; 2001; Anderson *et al.*, 2006; Foulger & Pearson, 2001; Natland, 2003; Parman *et al.*, 2005]. That theory would fit the high-$^3He/^4He$ values reported from Iceland and the Davis Strait [Starkey *et al.*, 2009; Stuart *et al.*, 2003] if the deeper parts of the crust beneath these regions contain ancient material, as we propose in this paper.

7 Discussion

7.1 The Greenland-Iceland-Faroe Ridge

The model presented here proposes that in general Icelandic-type upper crust is mafic in nature, equivalent to Layers 2 - 3 of oceanic crust, whilst Icelandic-type lower crust is magma-dilated continental crust. The pre-existing SCLM mostly delaminated during the stretching process (Section 5) (Figure 18). The melt layer thus comprises Icelandic-type upper crust plus the melt that intruded into the continental crust below as plutons, dykes and sills. The location of Iceland with respect to the east Greenland and Faroe Volcanic margins fits the model of Geoffroy *et al.* [2015; submitted] of a dislocated C-block (Figure 5).

This new model contributes to the > 40-year controversy regarding whether the crust beneath Iceland is thick or thin. A "thin crust" model, generally assumed in the 1970s and 1980s, attributed Icelandic-type upper crust to the melt layer—the subaerial equivalent of oceanic crust—and the layer currently termed "Icelandic-type lower crust" to hot, partially molten mantle [Björnsson *et al.*, 2005]. From the 1990s, long seismic explosion profiles using modern digital recording were shot and deep reflecting horizons were discovered. A "thick crust" model was then introduced that interpreted the layer previously thought to be hot, partially molten mantle as Icelandic-type lower crust, the equivalent of oceanic layer 3, and part of the melt layer.

Our findings support the thin-crust model with the caveat that Icelandic-type lower crust is indeed crust, and not hot mantle as previously proposed, but it is magma-inflated continental crust. This

model agrees with long-sidelined magnetotelluric work in Iceland which detects a high-conductivity layer at ~10 - 20 km depth. This layer was proposed to mark the base of the crust [Beblo & Bjornsson, 1978; 1980; Beblo *et al.*, 1983; Eysteinsson & Hermance, 1985; Hermance & Grillot, 1974]. High-conductivity layers are common in continental mid- and lower crust [*e.g.*, Muñoz *et al.*, 2008]. Explosion seismology and receiver functions find the thickness of Icelandic-type upper crust to be ~3 - 10 km (Figure 9; Figure 10) [Darbyshire *et al.*, 1998b; Foulger *et al.*, 2003] which is comparable with the crustal thicknesses beneath the Reykjanes Ridge and the Kolbeinsey Ridge if additional magma dilating the Icelandic-type lower crust is taken into consideration. This is nevertheless up to ~40% thicker than the global average of 6 - 7 km. Mantle fusibility enhanced by pyroxenite and water (Section 6), a moderate elevation in temperature (Section 6.2), and bursts of volcanism accompanying frequent rift jumps (Section 4) can account for the enhanced melt volumes.

The plate boundary traversing the GIFR cannot be likened to a conventional spreading ridge with segments connected by linear transform faults as is commonly depicted in simplified illustrations. Historically, motion in the GIFR region was postulated to have been taken up on a classic ~150-km-long sinistral transform fault named the Faroe Transform Fault or the Iceland Faroe Fracture Zone [Bott, 1985; Voppel *et al.*, 1979] and this idea was reiterated in subsequent work [*e.g.*, Blischke *et al.*, 2017; Guarnieri, 2015]. Locations proposed for this feature include the north edge of the Iceland shelf, central Iceland, and the South Iceland Seismic Zone [Bott, 1974].

There is, however, no observational evidence for such a structure [Gernigon *et al.*, 2015; Schiffer *et al.*, 2018] and it does not, even to a first order, fit the observations on the ground. Only a GIFR that deforms as a broad zone of distributed extension and shear can account for the reality of the geology of Iceland and adjacent regions [Schiffer *et al.*, 2018].

Our model may provide a long-awaited explanation for why the JMMC broke off east Greenland. Westerly migration of axes of extension on the GIFR may have changed the stress field in the diffusely extending continental area to the north and encouraged extension there to coalesce on the single most westerly zone which thereafter developed into the Kolbeinsey Ridge.

7.2 Crustal flow

Ductile crustal flow has been incorporated into earlier numerical models of continental breakup. A ductile, low-viscosity layer that decouples the upper lithosphere from the lower was incorporated in models of extending continental lithosphere by Huismans and Beaumont [2011; 2014]. Such a layer enables ultrawide regions of thinned, unruptured continental crust to develop along with distal extensional (sag) basins. Crustal thicknesses are maintained by widespread lateral flow of mid- and lower-crustal material from beneath surrounding regions. Lower crust may well up, further delaying full crustal breakup.

In our model, subsidence resulting from progressive thinning or delamination of the mantle lithosphere is mitigated by hot asthenosphere rising to the base of the crust. This abruptly raises temperatures, increasing heat flow and further encourages ductile flow. Low extension rates, such as have characterized the NE Atlantic, tend to prolong the time to breakup and encourage diffuse extension because ductile flow and cooling can continue for longer. The crust may stretch unruptured for tens of millions of years and widen by 100s of kilometers with axes of extension migrating diachronously and laterally across the extending zone. Only after eventual rupture of the continental lithosphere can sea-floor spreading begin. Until that occurs, geochemical signatures of continental crust and mantle lithosphere are expected in overlying magmas that have risen through the continental material.

Depth-dependent stretching, in particular involving the lower-crustal ductile flow that we model in Section 5, is both predicted by theory [McKenzie & Jackson, 2002] and required by observations from many regions. These include amagmatic margins, the Basin Range province, western USA

1045 [Gans, 1987] and deformation at collision zones, *e.g.*, the Himalaya and Zagros mountain chains [*e.g.*,
1046 Kusznir & Karner, 2007; Royden, 1996; Shen *et al.*, 2001]. Lower-crustal flow is actually observed
1047 where such crust is exhumed to the surface, *e.g.*, at Ivrea in the Italian Alps, where lower-crustal
1048 granulite intruded by mafic plutons is exposed [*e.g.*, Quick *et al.*, 1995; Rutter *et al.*, 1993].

1049 *7.3 Magmatism*

1050 7.3.1 The concept of the North Atlantic Igneous Province

1051 The issues laid out in this paper bring into question the concept that the magmas popularly grouped
1052 into the North Atlantic Igneous Province (NAIP) can be viewed as a single magmatic entity [Peace *et*
1053 *al.*, this volume]. The NAIP is generally considered to include the volcanic rocks in the region of the
1054 Davis Strait, the volcanic margins of east Greenland and Scandinavia, and the magmatism of the
1055 GIFR. These magmas are, however, only a subset of those in the region and many others are not
1056 typically included [Peace *et al.*, this volume]. These include melt embedded in the "amagmatic"
1057 margins of SW Greenland and Labrador, current volcanism at Jan Mayen, the Vestbakken Volcanic
1058 Province ~300 km south of Svalbard, conjugates in NE Greenland [Á Horni *et al.*, 2016], magmatism
1059 at the west end of the CGFZ [Keen *et al.*, 2014] and basaltic sills offshore Newfoundland detected in
1060 ODP site 210-1276 that are thought to extend throughout an area of ~20,000 km^2 [Deemer *et al.*,
1061 2010]. It is illogical to exclude these, especially since the Cretaceous(?) Anton Dohrn and Rockall
1062 seamounts are included in the NAIP [Jones *et al.*, 1994].

1063 The grouping of a select subset of magmas in the NE Atlantic Realm into a single province is
1064 predicated on and reinforces, the concept that they all arise from a single, generic source. A model of
1065 such simplicity that fits all observations has been elusive for over half a century. The obvious
1066 solution, and one that can readily account for the observations, is a model whereby each magmatic
1067 event occurs in response to local lithospheric tectonics and melts are locally sourced.

1068 The same reasoning may well apply to other volcanic provinces, *e.g.*, the South Atlantic Volcanic
1069 Province. Generally included in this are the Paraná and Etendeka flood basalts, the volcanic rocks of
1070 the Rio Grande Rise and the Walvis Ridge, the currently active Tristan da Cunha archipelago and
1071 even kimberlites and carbonatites in Angola and the Democratic Republic of the Congo [see Foulger,
1072 2018 for a review]. These volcanic elements contrast with one another in the extreme and each most
1073 likely erupted in reaction to local tectonic responses to global events and processes, with magmas
1074 locally sourced.

1075 7.3.2 Magma volume

1076 Estimates for the total volume of the magma generally lumped together as the NAIP are 2 - 10 x 10^6
1077 km^3 with a value of ~6.6 x 10^6 km^3 for the north Atlantic volcanic margins [Eldholm & Grue, 1994a].
1078 Assuming these margins formed in ~3 Myr, Eldholm and Grue [1994a] calculate a magmatic rate of
1079 2.2 km^3/a and suggest the NAIP is one of the most voluminous igneous provinces in the world. That
1080 calculation assumes that the HVLC beneath the *Inner* SDRs is all igneous and formed
1081 contemporaneously with the volcanic margins. If this is not the case, the volume and magmatic rate
1082 for the north Atlantic volcanic margins must be downward-revised by up to 30%, i.e. to ~4.4 x 10^6
1083 km^3 for volume and 1.5 km^3/a for magmatic rate. Eldholm and Grue [1994a] furthermore estimate a
1084 magmatic rate of ~ 0.2 km^3/a for Iceland. If the igneous crust on the GIFR is only 10 - 15 km thick,
1085 this rate must be downward-revised to 0.12 - 0.08 km^3/a. The magmatic rate per rift kilometer would
1086 then be 2 - 3 x 10^{-4} km^3/a compared with ~4.8 x 10^{-4} km^3/a per rift kilometer for the global plate
1087 boundary.
1088
1089 These changes reconcile geological estimates with those derived from numerical modeling.
1090 Magmatism at the NE Atlantic rifted margins has been simulated using models of decompression
1091 melting in a convectively destabilized thermal boundary layer coupled with upper-mantle ("small-

scale") convection [Geoffroy *et al.*, 2007; Mutter & Zehnder, 1988; Simon *et al.*, 2009]. These models explore whether the volumes and volume rates can be accounted for simply by breakup of the 100-200-km-thick lithosphere without additional *ad hoc* processes. Current numerical models slightly under-predict traditional geological estimates but could be reconciled with estimates lowered to take into account a wholly or partially continental affinity of HVLC.

More accurate estimates of volume could also explain the extreme variations in magmatic thickness over short distances required by assumptions of HVLC igneous affinity. For example, the radical contrast between the unusually thin (4 - 7 km) oceanic crust beneath the Aegir Ridge [Greenhalgh & Kusznir, 2007] and a ~30 km igneous thickness beneath the adjacent GIFR defies reasonable explanation but the problem vanishes if the latter assumption is dropped.

7.3.3 The chevron ridges

Lithosphere- and asthenosphere-related mechanisms compete to explain the chevron ridges that flank the Reykjanes Ridge [Hey *et al.*, 2008; Jones *et al.*, 2002]. Martinez and Hey [this volume] suggest that the required oscillatory changes in magmatic production result from axially propagating mantle upwelling instabilities that travel with ridge-propagator tips along the Reykjanes Ridge. These originate in Iceland and the gradient in mantle properties along the Reykjanes Ridge results in the convective instabilities migrating systematically south along the Ridge. Upwelling is purely passive and the propagators behave in a wave-like manner without the flow of actual mantle material along the Ridge. In this model, the transition from linear to ridge/transform staircase plate boundary geometry at ~37 - 38 Ma failed to eliminate the structure of the deeper asthenospheric melting zone and the Reykjanes Ridge is restructuring itself to realign over that zone.

Several of the propagators onset at the GIFR in concert with tectonic reorganizations there (Table 1) [Benediktsdóttir *et al.*, 2012] inviting consideration of lithospheric triggers. The Reykjanes Ridge as a whole is oblique to the direction of plate motion but its axis comprises an array of right-stepping *en echelon* spreading segments, each of which strikes perpendicular to the direction of motion. Such fabric resembles a left-lateral transtension zone.

The diachronous chevron crustal fabric began to form at ~37 - 38 Ma when the Reykjanes Ridge changed from a linear to a ridge-transform configuration with a ~30˚ counter-clockwise rotation in the direction of plate motion (Section 2.2.2) [Gaina *et al.*, 2017]. From 25-15 Ma slow, counter-clockwise rotation of the extension direction continued and from 15 Ma - present it rotated back [Gaina *et al.*, 2017]. Slow counter-clockwise migration of the spreading direction would gradually hinder strike-slip motion on the transform segments and encourage evolution toward extension with a minor left-lateral shear overprint. Very slow changes in the direction of extension might be insufficient to trigger a sudden and major reorganization but enough to bring about the slow plate-boundary evolution observed.

Regardless of whether a lithosphere- or asthenosphere-related mechanism is responsible for the chevron ridges, it is clear that shallow processes control them as their southerly propagation was temporarily blocked by several previously existing transform faults north of the present reorganization tip near the Bight transform fault. Furthermore, if their inception is related to tectonic reorganizations on the GIFR, then conversely the time at which the propagators set off from the GIFR could indicate the times of first-order tectonic reorganizations on the GIFR.

The transform-eliminating rift propagators of the Reykjanes Ridge are unique in their degree of development but not entirely unknown elsewhere. Examples outside the NE Atlantic include a southward propagator eliminating a transform formerly at 21˚40'N on the mid-Atlantic Ridge [Dannowski *et al.*, 2011] and propagators on the faster-spreading (~100 km/Myr) NE Pacific plate boundary that eliminated the Surveyor, Sila, Sedna and Pau transforms [Atwater & Severinghaus, 1989; Hey & Wilson, 1982; Shih & Molnar, 1975]. Propagating small-scale convective instabilities

have also been postulated to form volcanic ridges and seamount chains that flank parts of the East Pacific Rise in a direction parallel to plate motion [e.g, Forsyth *et al.*, 2006].

7.3.4 The North Atlantic geoid high

The GIFR sits at the apex of a ~3000-km-long bathymetric and geoid high (up to ~4000 m and 80 m respectively) that stretches from the Azores to the Jan Mayen Fracture Zone [Carminati & Doglioni, 2010; King, 2005; Marquart, 1991]. Without this high the Thulean land bridge and Iceland would not have been subaerial. Globally, the only other comparable geoid high extends through Indonesia and Melanesia and to the Tonga Trench. Major geoid highs with lower amplitudes or smaller spatial extents are associated with the SW Indian Ocean and the Andean mountain chain.

The geoid highs associated with Indonesia, Melanesia and Tonga, and the Andean mountain chain are a consequence of accumulations of dense subducted slabs. The geoid high of the north Atlantic corresponds closely to the pre-breakup Caledonian orogen plus the south European/North African Hercynian orogen (Figure 23). A possible explanation for part of the geoid anomaly is thus residual, dense, subducted Caledonian and Hercynian slabs along with continental lower crust and mantle lithosphere distributed in the shallow mantle. Henry Dick and colleagues have long argued that the petrology and geochemistry of magmas on the SW Indian ridge require SCLM in the melt source [Cheng *et al.*, 2016; Dick, 2015; Gao *et al.*, 2016; Zhou & Dick, 2013]. That ridge is the current locus of extension between Africa and Antarctica which separated as part of Pangaea breakup beginning in the Jurassic. By analogy with the NE Atlantic, continental material might also remain in the mantle beneath the ocean there and the SW Indian geoid high might thus be explained in a similar way to that of the north Atlantic.

7.3.5 Regions analogous to the GIFR

There are clear parallels between the GIFR and the Davis Strait. The structure and tectonic development of the latter show similar characteristics to the GIFR but to a less extreme degree (Figure 24). The Davis Strait is colinear with the GIFR and both function as transtensional shear zones. Its primary feature is the long Ungava Fault Complex [Peace *et al.*, 2017]. This is underlain by ~8 km of oceanic crust beneath which is ~8 km of HVLC with V_P up to 7.4 - 7.5 km/s [Chalmers & Pulvertaft, 2001; Funck *et al.*, 2006; Funck *et al.*, 2007; Srivastava *et al.*, 1982] and density of 2850 - 3050 kg/m^3 [Suckro *et al.*, 2013]. These values are similar to those of Icelandic-type lower crust.

Like the GIFR, the bathymetric high that contains the 550-km-long Davis Strait is elongated in the direction approximately perpendicular to plate motion. It has water depths of < 700 m, contrasting with the adjacent > 2000-m-deep Labrador Sea and Baffin Bay. At the Davis Strait north-propagating rifting stalled at the confluence of the Nagssugtoqidian and Rinkian orogens and continued displaced by several hundred kilometers in a right-stepping sense. In the case of the GIFR, both north- and south-propagating oceanic rifting stalled at the confluence of the Nagssugtoqidian and Caledonian orogens.

The Jan Mayen Fracture Zone formed where a major, pre-existing transverse structure formed a barrier to the south-propagating Mohns Ridge. It was also an episodic transtensional structure, has a history of migration of the locus of deformation, bathymetric highs and unusual volcanism, *e.g.*, on the island of Jan Mayen and in the submarine Traill Ø and Vøring Spur igneous complexes [Gernigon *et al.*, 2009; Kandilarov *et al.*, 2015]. Continental crust is possibly trapped between parallel segments of the Zone.

7.3.6 Regions analogous to the NE Atlantic Realm

The history, structure, tectonics and petrology of the NE Atlantic Realm are unusually complex but it represents an extreme example and not a unique case. Other regions that show similar features suggest

1184 that the style of breakup it exemplifies is generic. The NE Atlantic Realm may owe its extremity to
1185 the facts that the NE Atlantic was formed by two opposing propagators that stalled at a barrier, an
1186 unusually large microcontinent was captured, and the spreading rate was and is exceptionally slow.

1187 The South Atlantic Igneous Province also includes regions of shallow sea-floor, anomalously thick
1188 crust, anomalous volcanism and continental crust distributed in the ocean. It has a history of stalled
1189 spreading-ridge propagation, coincidence with a major pre-existing transverse structure and both
1190 shear and extensional deformation in a zone several hundred kilometers broad in the direction
1191 perpendicular to plate motion [Foulger, 2018; Kusznir & al., 2018]. Graça *et al.* [2019] recently
1192 presented evidence that the Rio Grande Rise, which contains continental material [Santos Ventura *et*
1193 *al.*, 2019], and parts of the Walvis Ridge were once joined, but split apart by at least four ridge jumps.
1194 Such a process is very similar to that which we propose for the GIFR.

1195 The Lomonosov Ridge in the Arctic ocean can be viewed as an incipient microcontinent. West of
1196 India, the Laxmi basin comprises a pair of aborted conjugate volcanic passive margins with Outer
1197 SDRs that appear to be underlain by HVLC and flank an intra-oceanic microcontinent—a C-block
1198 [Geoffroy *et al.*, submitted; Guan *et al.*, 2019; Nemčok & Rybár, 2017]. The Seychelles region in the
1199 West Indian Ocean, the Galapagos Islands region in the east Pacific [Foulger, 2010, p 100-101] and
1200 the Shatsky Rise [Korenaga & Sager, 2012; Sallares & Charvis, 2003] all display analogous features.
1201 Regions currently in the process of breaking up in a similar mode include the Afar area [Acton *et al.*,
1202 1991], the Imperial and Mexicali Valleys and Baja California (California and Mexico). The
1203 abundance of continental crustal fragments in the oceans is becoming increasingly clear, with much
1204 originating at locations where continental breakup was complicated by lithospheric heterogeneities.

1205 Despite the very different structure and context, tectonics comparable to those observed on the GIFR
1206 and in Iceland are also observed on the East Pacific Rise (EPR). There, "dueling" overlapping
1207 propagating ridge pairs with intermediate bookshelf shearing build ridge-perpendicular and ridge-
1208 oblique zones of crustal complexity (Figure 25) [Perram *et al.*, 1993]. In oceanic settings overlapping
1209 ridge tips tend to form where lithosphere is weak and to migrate along-strike. Overlapping spreading
1210 centers are kinematically unstable and the tips inevitably fail episodically and are replaced by new
1211 ones. An unusual facet of the development of the GIFR that is not reported from the East Pacific Rise
1212 is the switching of the sense of overlap when the Aegir Ridge was replaced by the Kolbeinsey Ridge.

1213 Comparable styles of deformation are also observed in the Japan-, Manus-, Lau- and Mariana Trench
1214 back-arc basins [Kurashimo *et al.*, 1996; Martinez *et al.*, 2018; Taylor *et al.*, 1994]. Beneath back-arc
1215 basins the hydrous mantle environment above the dewatering slab does not become dehydrated and
1216 the attendant increase in viscosity tends to localize upwelling melt. As a result, extension does not
1217 become focused in a single rift zone but remains distributed between multiple, parallel rifts. Magnetic
1218 anomalies are disorganized and water also reduces the solidus, increasing melt production [Dunn &
1219 Martinez, 2011; Martinez *et al.*, 2018].

1220 On land, similar petrologies, including high-TiO_2 basalts, association with abundant rhyolite, and
1221 likely provenance of the source in subcontinental material are observed in flood basalts that erupted
1222 through continental lithosphere. These include the Central Atlantic Magmatic Province [Peace *et al.*,
1223 this volume], the Deccan traps and the Columbia River Basalts.

1224 **8 Conclusions**

1225 Our main conclusions may be summarized:

1226 1. Disintegration of the Laurasian collage of cratons and orogens to form the Labrador Sea, Baffin
1227 Bay and the NE Atlantic Ocean lasted several tens of millions of years and occurred piecewise
1228 and diachronously via rift propagation.

2. The GIFR formed where the south-propagating Aegir Ridge and the north-propagating, Reykjanes Ridge stalled at the junction of the Nagssugtoqidian and Caledonian orogens. The intervening ~300-km wide (northerly) and ~150-km long (easterly) continental block, the Iceland Microcontinent, along with flanking areas, extended by distributed, magma-assisted continental extension via multiple parallel migrating rifts with diffuse shear zones between them. The continental crust was capped by surface lavas. It stretched to form the 1000-km long Thulean continental land bridge which was not overrun by oceanic waters until ~10 -15 Ma.
3. Magma-assisted continental extension was enabled by ductile flow of low-viscosity mid- and lower crust.
4. Icelandic-type crust comprises the 3 - 10 km thick upper crust, equivalent to oceanic layers 2 - 3, underlain by lower crust up to ~ 30 km thick comprising magma-inflated continental crust.
5. The melt layer that caps the GIFR comprises the Icelandic-type upper crust plus magma injected into the Icelandic-type lower crust, and has a total thickness of ~10 - 15 km.
6. The petrology and geochemistry of Icelandic lavas is consistent with inclusion of a component from underlying continental crust.
7. A largely continental Icelandic-type lower crust is consistent with the fact that no reasonable models of temperature or mantle petrology can generate the ~40 km of melt necessary to explain its entire thickness as wholly oceanic.
8. The chevron ridges that flank the Reykjanes Ridge form in association with small-offset propagators initiated by tectonic reorganizations on the unstable GIFR.
9. The GIFR tectonically decouples the oceanic regions to the north and south.
10. The continuity of continental crust beneath the GIFR means that, at this latitude, Laurasia still has not yet entirely broken up. An implication of this is that the GIFR could be considered to be a new kind of plate boundary.
11. A model whereby continental breakup is characterized by diachronous rifting, strong influence from pre-existing structures, distributed continental material in the new oceans, and anomalous volcanism matches many other oceanic regions.

Acknowledgments

Erin K. Beutel and D. Barrie Clarke made valuable contributions to the discussions that led to this manuscript. CS's postdoctoral fellowship at Durham University was financed by the Carlsberg Foundation. F. Martinez and R. Hey are supported by US NSF grants OCE-1154071 and OCE-1756760. A. Peace's postdoctoral fellowship at Memorial University of Newfoundland was funded by the Hibernia project geophysics support fund. M. Stoker acknowledges the award of Visiting Research Fellow at the Australian School of Petroleum.

1265 Table 1: Chronology of major tectonic events in the NE Atlantic. Timescale after Gradstein *et al.*
1266 [2012]. Chevron ridge # after Jones *et al.* [2002].
1267

Date (Ma)	Chevron ridge #	Magnetic chron	Event
58-57		C26	Beginning of opening of the Labrador Sea.
56-52		C24-22	First magnetic anomaly on the proto-Reykjanes Ridge.
54		C24r	Beginning of opening of the North Atlantic Ocean on the Aegir Ridge and west of the Lofoten margin.
54-ca 46		C24-21	Rift to drift transition, Faroe-Shetland and Hatton margins.
54.2-50			Spreading propagated from the Greenland Fracture Zone south to the Jan Mayen Fracture Zone.
52		C23	Aegir Ridge reaches its maximum southerly extent.
50-48		C21	~30-40˚ clockwise rotation of direction of plate motion .
48		C22-21	Onset of fan-shaped spreading about the Aegir Ridge. Pulse of extension in the southern JMMC. No major change south of the GIFR.
40		C18	Counter-clockwise rotation of direction of plate motion.
38-37	7	C17	Reykjanes Ridge becomes stair-step. First chevron ridge begins to form.
36		C13	Cessation of spreading in the Labrador Sea.
33-29		C12-10	Counter-clockwise rotation of direction of plate motion.
31-28	6	C12-10	Extinction of the ultra-slow Aegir Ridge. Second chevron ridge begins to form about the Reykjanes Ridge
24		C6/7	First unambiguous magnetic anomaly about the Kolbeinsey Ridge.
15-10		C5A/C5	Breaching of the Thulean land bridge.
14	5		Rift jump in Iceland from North West Syncline to Snæfellsnes Zone and Húnaflói Volcanic Zone, propagator "Loki" starts to travel south down Reykjanes Ridge forming third chevron ridge.
9	4		Propagator "Fenrir" starts to travel south down Reykjanes Ridge forming fourth chevron ridge.
7	3		Extinction of Snæfellsnes Zone, propagator "Sleipnir" starts to travel south down Reykjanes Ridge forming fifth chevron ridge.
5	2		Propagator "Hel" starts to travel south down Reykjanes Ridge forming sixth chevron ridge.
2	1		EVZ in Iceland forms, propagator "Frigg" starts to travel south down Reykjanes Ridge forming seventh chevron ridge.

1268

1269 Table 2: Rift zones indicated by geological observations on land in Iceland.

1270

Name	Acronym	Tectonic status
North West Syncline	NWS	Extinct
Austurbrún Syncline	AS	Extinct
East Iceland Zone	EIZ	Extinct
Snæfellsnes Zone	SZ	Oblique, non extensional
Húnaflói Volcanic Zone	HVZ	Extinct
Mödrudalsfjallgardar Zone	MZ	Extinct
Reykjanes Peninsula Zone	RPZ	Oblique, extensional
Western Volcanic Zone	WVZ	Active, waning
Hofsjökull Zone	HZ	Active, very short
Northern Volcanic Zone	NVZ	Active
Öræfajökull-Snæfell Zone	ÖVZ	Active, non extensional
Eastern Volcanic Zone	EVZ	Active, propagating

1271
1272

1273 Table 3: Potential temperatures required to produce 20 km of melt for various source compositions
1274 [from Hole & Natland, this volume].

1275

Source composition	T_P ˚C
dry peridotite	1550
dry peridotite + 10% pyroxenite	1540
dry peridotite + 40% pyroxenite	1470
damp peridotite + pyroxenite	1450
damp peridotite	1450
pyroxenite	1325-1450
Baffin Island picrites ($T_{Ol\text{-}Sp}$)	1500

1276

1277
1278

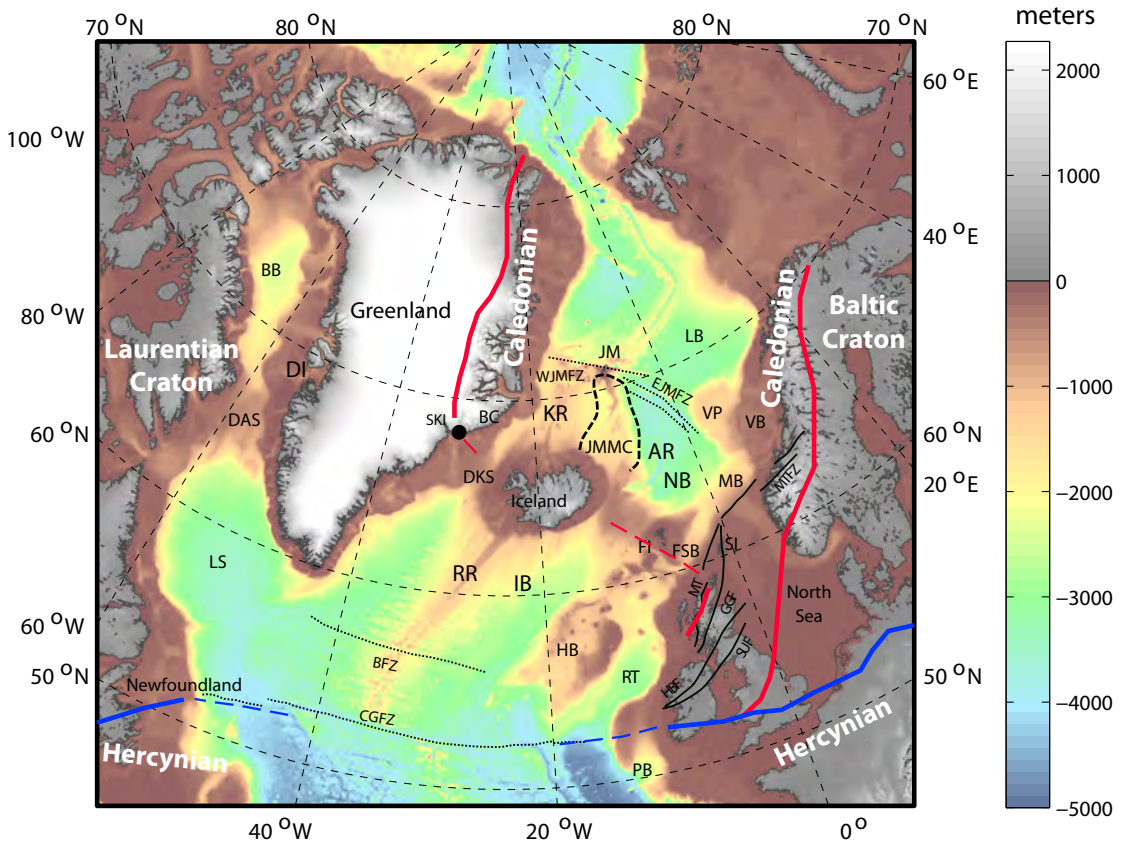

Figure 1: Regional map of the North East Atlantic Realm showing features and places mentioned in the text. Bathymetry is shown in color and topography in land areas in gray. BB: Baffin Bay, DAS: Davis Strait, DI: Disko Island, LS: Labrador Sea, CGFZ: Charlie-Gibbs Fracture Zone, BFZ: Bight Fracture Zone, RR: Reykjanes Ridge, IB: Iceland basin, DKS: Denmark Strait, SKI: Skaergaard intrusion, BC: Blosseville coast, KR: Kolbeinsey Ridge, JMMC: Jan Mayen Microcontinent Complex, AR: Aegir Ridge, NB: Norway basin, WJMFZ, EJMFZ: West and East Jan Mayen Fracture Zones, JM: Jan Mayen, LB: Lofoten basin, VP: Vøring Plateau, VB: Vøring basin, MB: Møre basin, FI: Faroe Islands, SI: Shetland Islands, FSB: Faroe-Shetland basin, MT: Moine Thrust, GGF: Great Glen Fault, HBF: Highland Boundary Fault, SUF: Southern Upland Fault, MTFZ: Møre-Trøndelag Fault Zone, HB: Hatton basin, RT: Rockall Trough, PB: Porcupine basin. Red lines: boundaries of the Caledonian orogen and associated thrusts, blue lines: northern boundary of the Hercynian orogen, both dashed where extrapolated into the younger Atlantic Ocean.

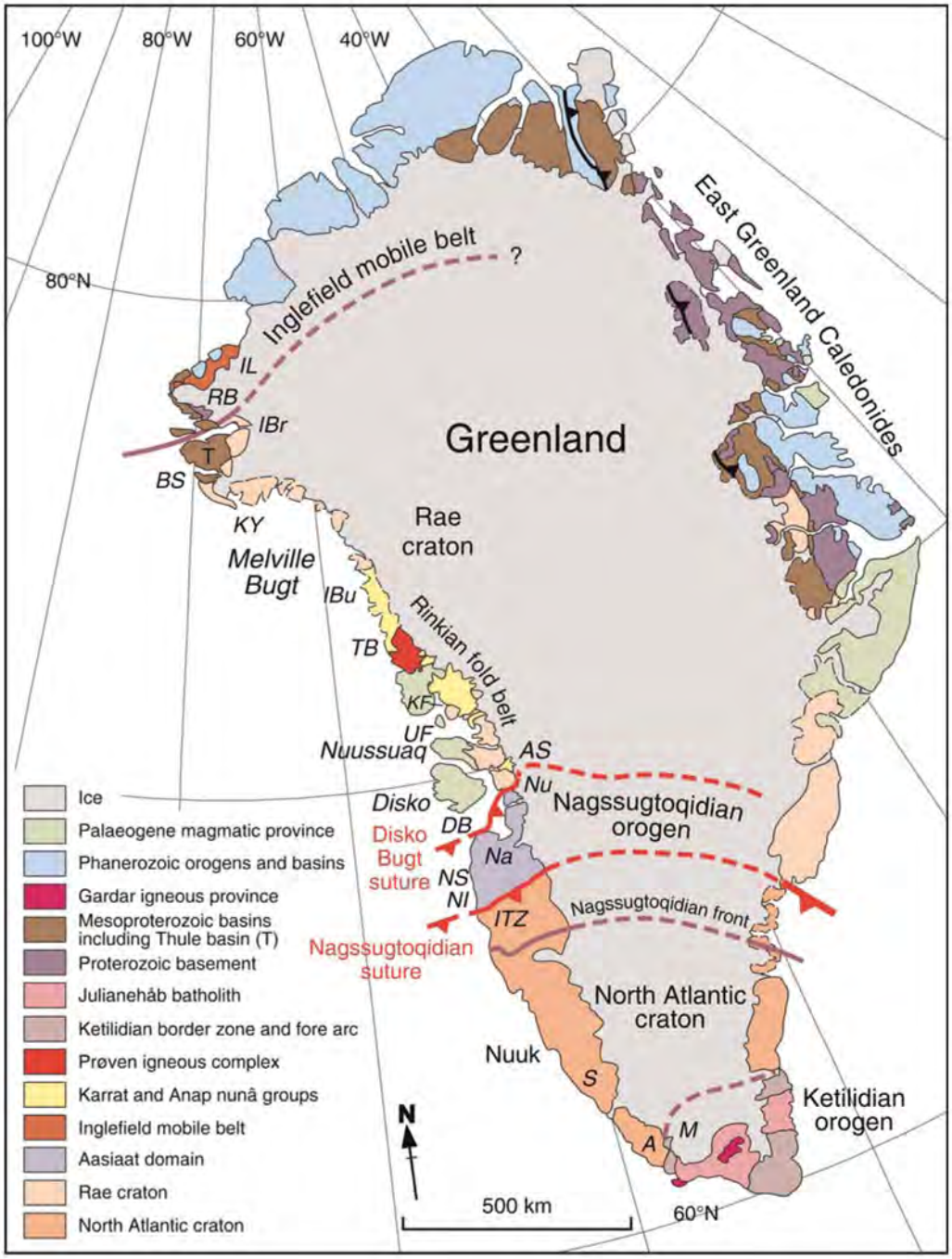

Figure 2: Schematic map of Greenland showing features referred to in the text. A: Arsuk, AS: Ataa Sund, BS: Bylot Sund, DB: Disko Bugt, IBr: Inglefield Bredning, IBu: Inussulik Bugt, IL: Inglefield Land, ITZ: Ikertoq thrust zone, KF: Karrat Fjord, KY: Kap York, M: Midternæs, Na: Naternaq, NI: Nordre Isortoq, NS: Nordre Strømfjord, Nu: Nunatarsuaq, RB: Rensselaer Bugt, S: Sermilik, T: Thule basin, TB: Tasiussaq Bugt, UF: Uummannaq Fjord [from St-Onge *et al.*, 2009].

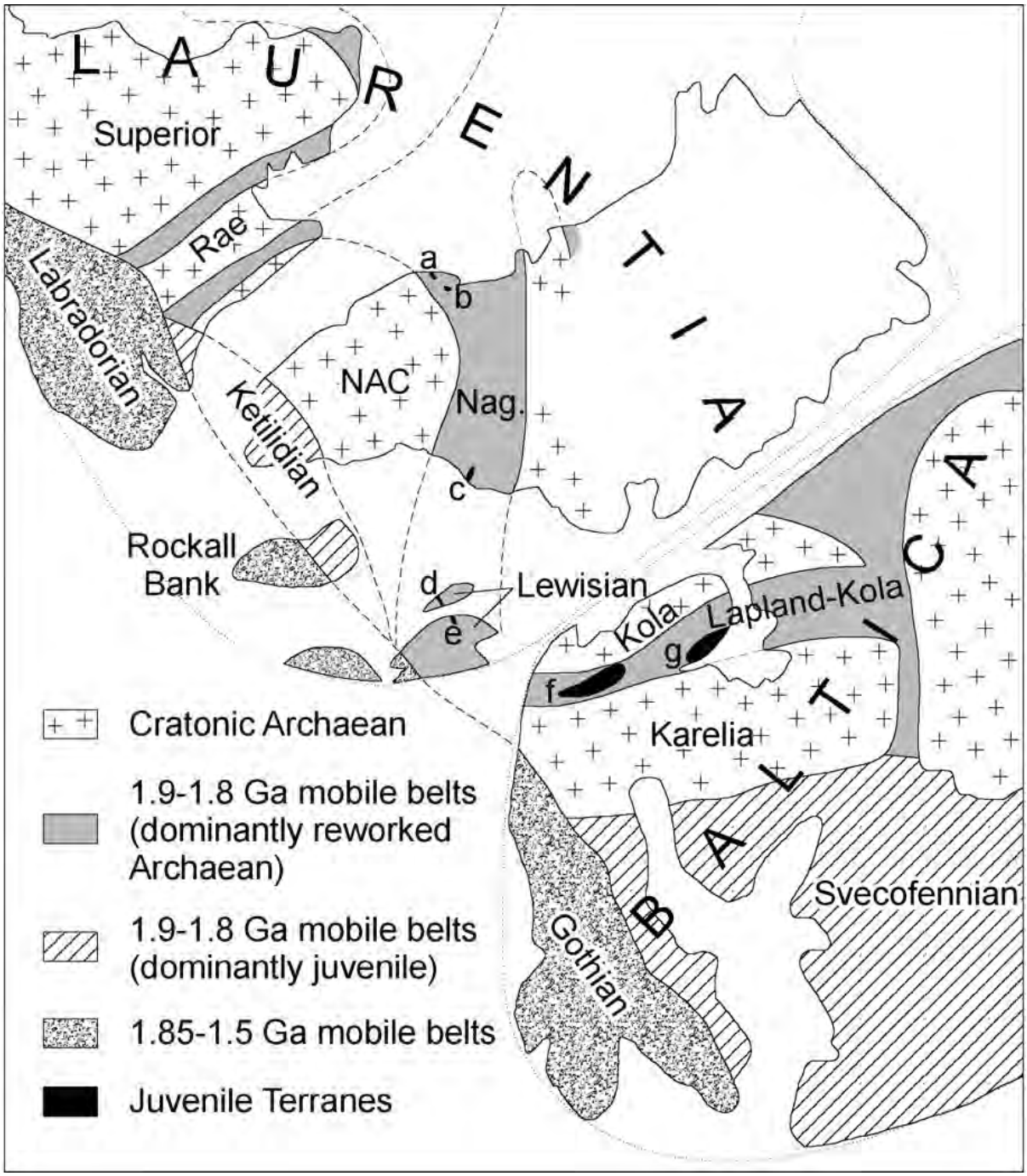

1306

1307

1308 Figure 3: Reconstruction of the North Atlantic Realm at 1265 Ma. NAC: North Atlantic Craton, Nag:
1309 Nagssugtoqidian. Juvenile terranes: a: Sissimuit Charnockite, b: Arfersiorfic diorite, c: Ammassalik
1310 Intrusive Complex, d: South Harris Complex, e: Loch Maree Group, f: Lapland-Kola Granulite Belt,
1311 g: Tersk and Umba terranes [from Mason *et al.*, 2004].
1312

1313

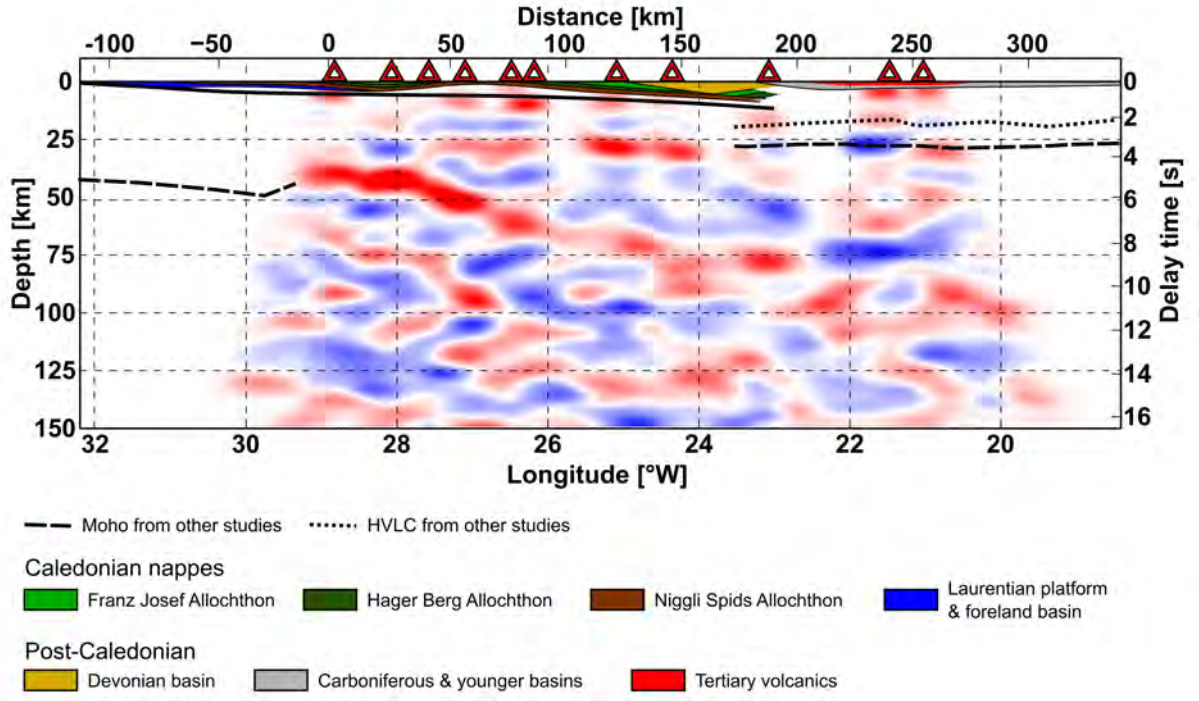

Figure 4: Receiver function image of the crust and upper mantle under central east Greenland from Schiffer *et al.* [2014] showing the Central Fjord structure. A geological cross-section based on Gee [2015] is overlain showing the Caledonian nappes and foreland basin, and the Devonian basin. Younger sedimentary basins are from Schlindwein & Jokat [2000]. Extrapolated Moho depths are from Schiffer *et al.* [2016].

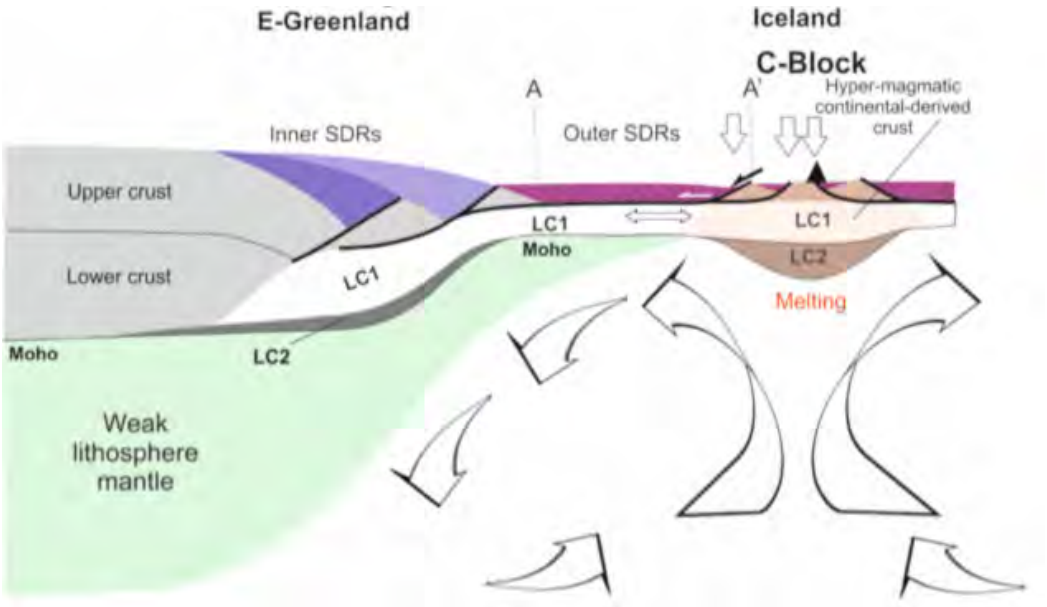

Figure 5: Schematic diagram illustrating the generalized structure of Inner- and Outer-SDRs and a possible "C-Block" under Iceland. Outer-SDRs comprise thick subaerial eruptive layers underlain by hyper-extended middle crust and high-V_P mafic material of uncertain affinity but similar in structure to massively sill-intruded lower crust. Ductile flow and magma-assisted inflation can extend such crust to many times its original length. Material eroded from the underlying lithospheric mantle may be distributed in the direction of extension and incorporated in the underlying asthenosphere. LC1: sill-injected continent-derived ductile crust. LC2: highly reflective, undeformed layer, tectonically disconnected from LC1, and with much higher V_P (7.6-7.8 km/s) [adapted from Geoffroy *et al.*, submitted].

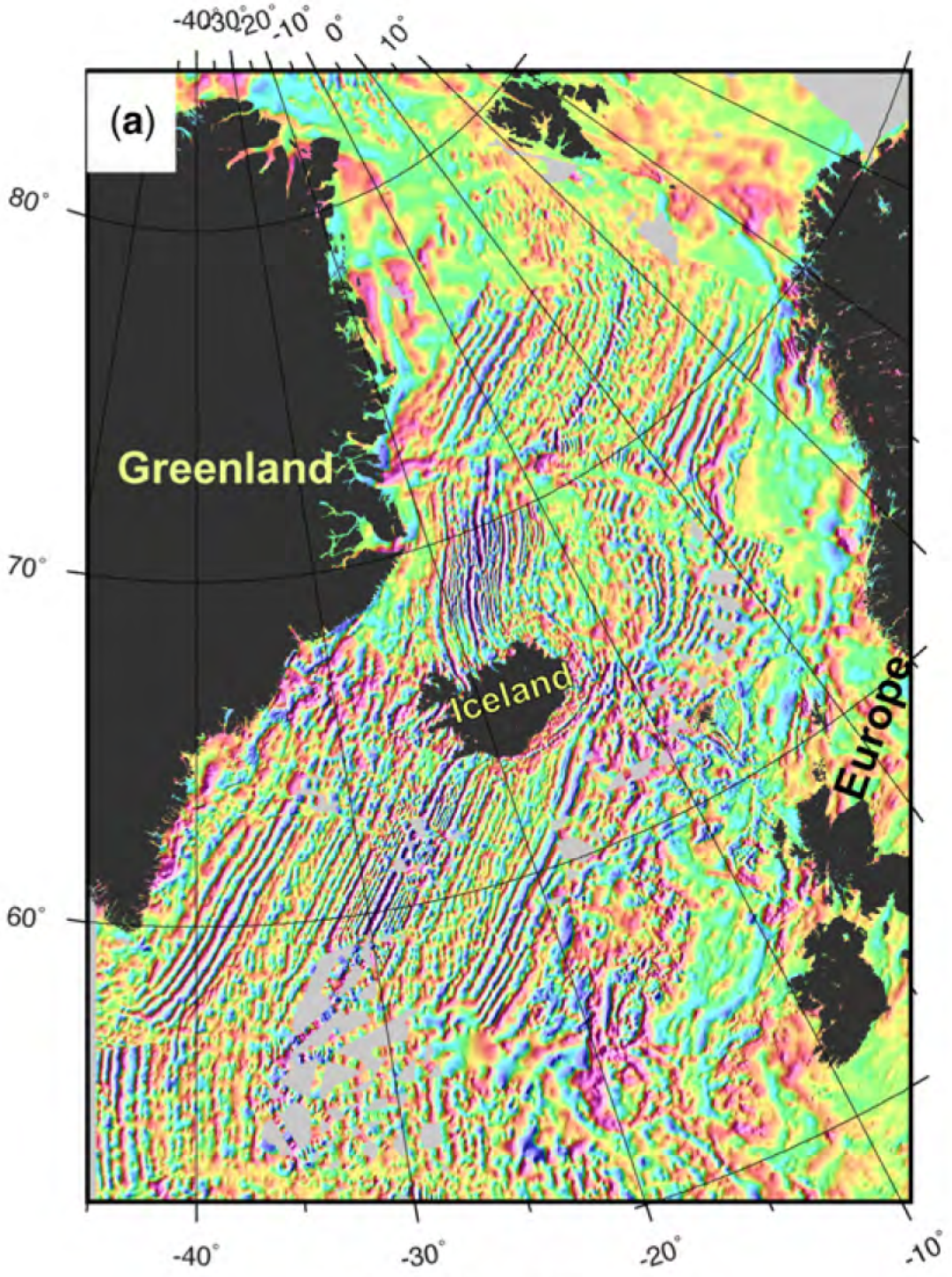

Figure 6: Magnetic anomalies in the North Atlantic Ocean [from Gaina *et al.*, 2017].

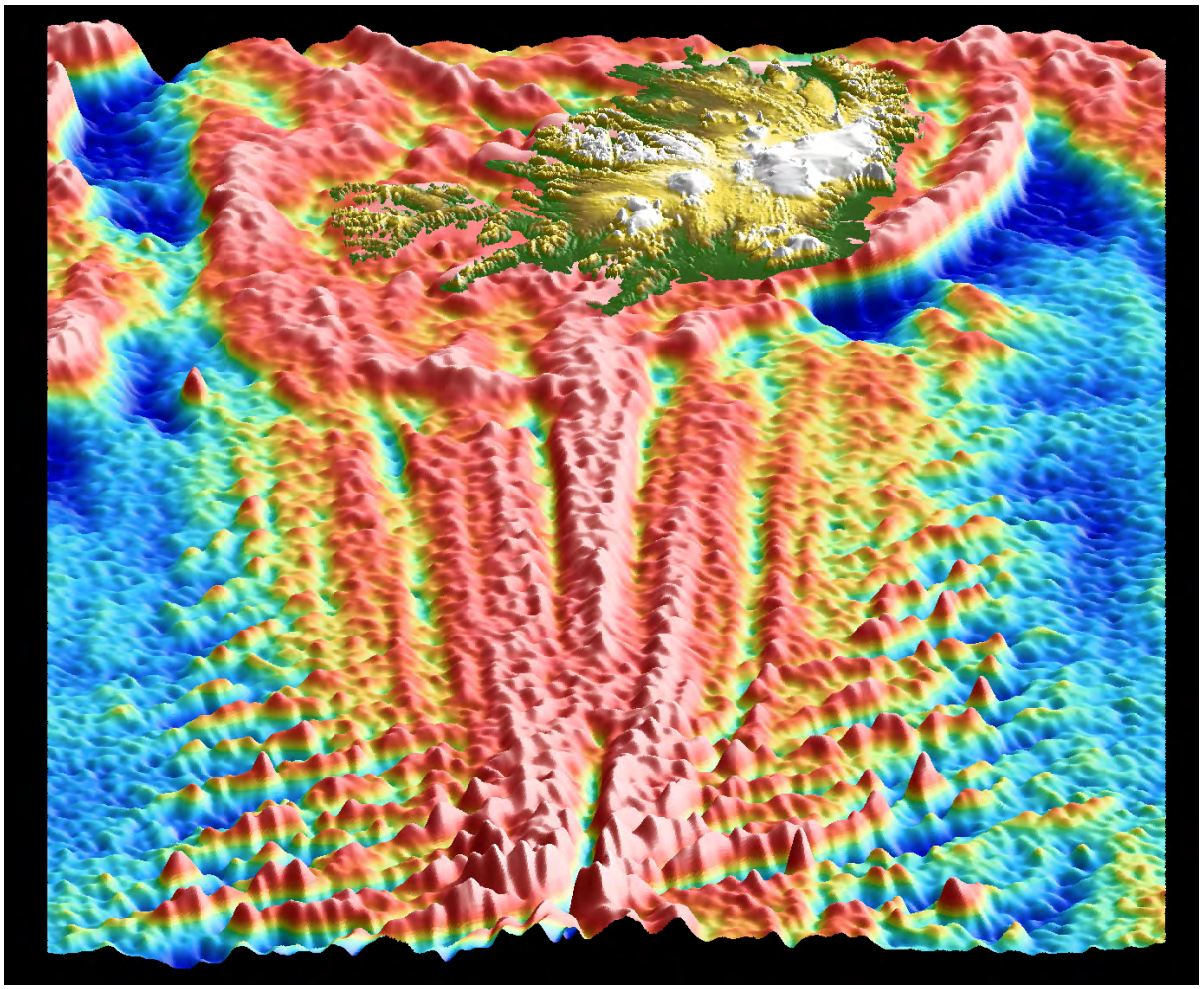

Figure 7: Perspective view along the Reykjanes Ridge looking towards Iceland showing the flanking chevron ridges converging with the spreading axis. Fracture-zone traces delineating former transform faults that have been eliminated can be seen as oblique cross-cutting structures in the lower part of the figure. Submarine areas show satellite-derived Free Air gravity anomalies from Sandwell *et al.* [2014] with the land topography of Iceland superimposed.

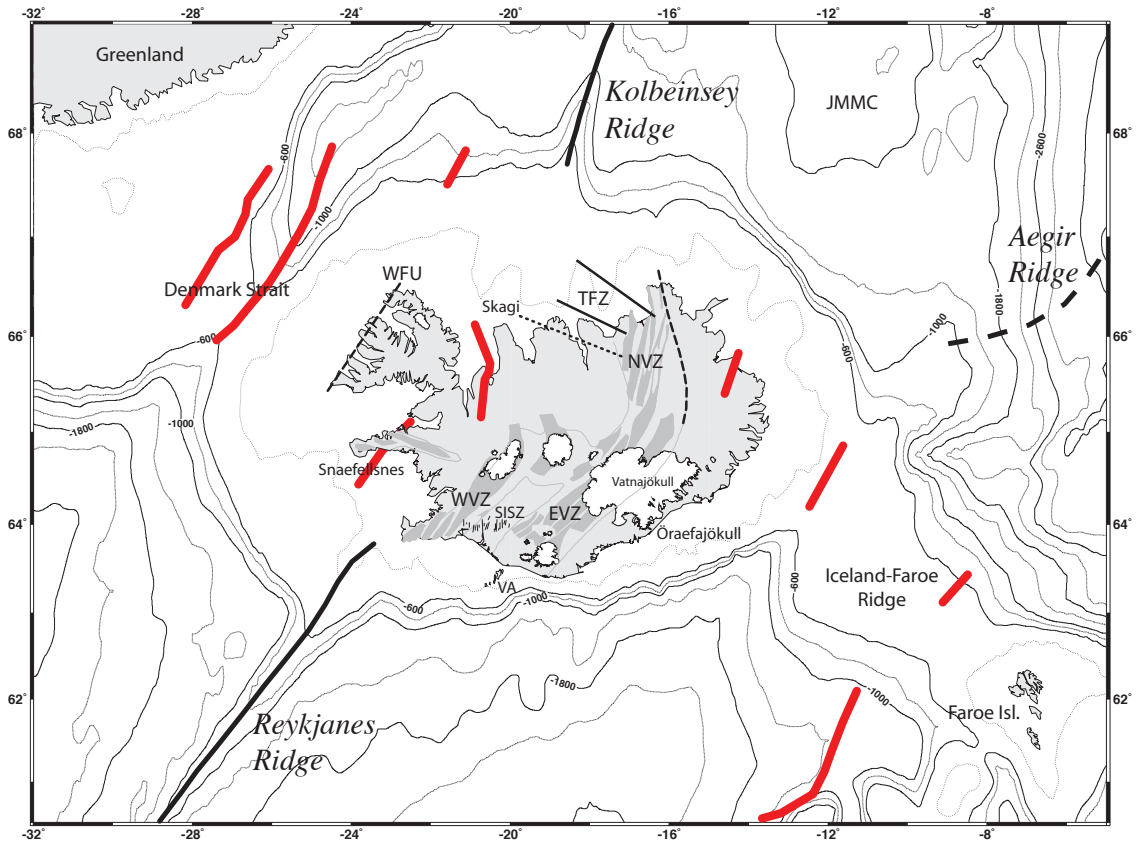

Figure 8: The Greenland-Iceland-Faroe Ridge and surrounding areas showing bathymetry and tectonic features. JMMC: Jan Mayen Microcontinent Complex. Thick black lines: axes of Reykjanes and Kolbeinsey Ridges, thin gray lines on land: outlines of neovolcanic zones, dark grey: currently active extensional volcanic systems, dashed black lines: extinct rifts on land, thin black lines: individual faults of the South Iceland Seismic Zone (SISZ), white: glaciers. WVZ, EVZ, NVZ: Western, Eastern, Northern Volcanic Zones, TFZ: Tjörnes Fracture Zone comprising two main shear zones and one (dotted) known only from earthquake epicenters (see also Figure 15). Thick red lines: extinct rift zones from Hjartarson *et al.* [2017].

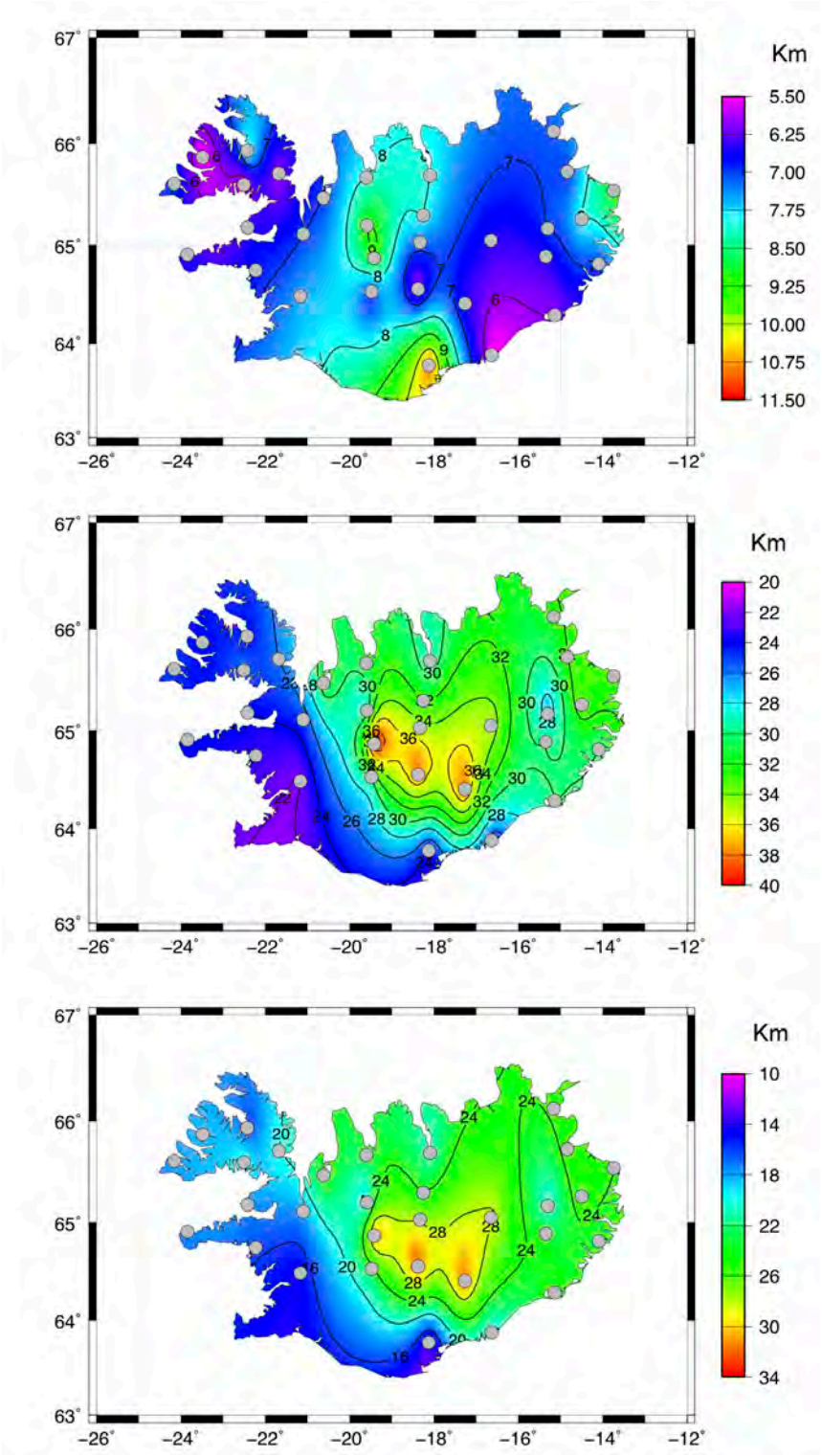

Figure 9: Compilation of results from receiver function analysis in Iceland. Top: Depth to the base of the upper crust, middle: depth to the base of the lower crust, bottom: thickness of the lower crust [data from Foulger *et al.*, 2003].

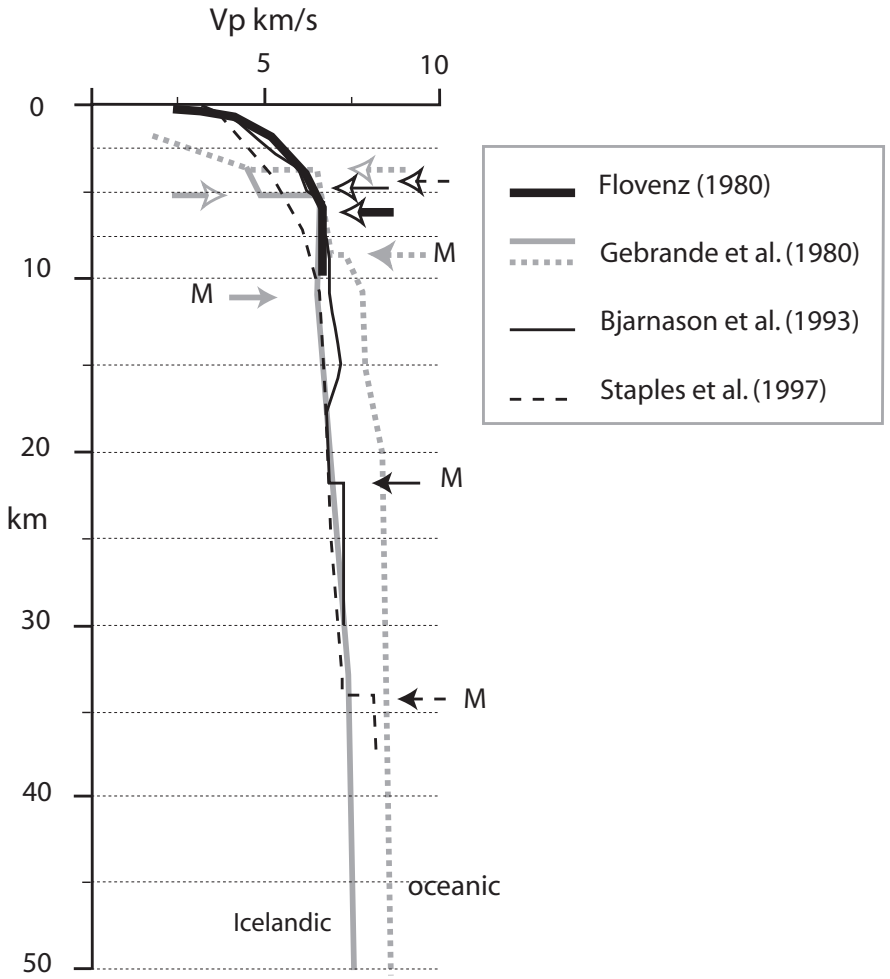

Figure 10: Velocity-depth profiles showing the average one-dimensional seismic structure of Icelandic-type crust from explosion profiles shot in Iceland and in 10-Ma oceanic crust south of Iceland [Gebrande *et al.*, 1980]. Open-headed arrows, estimates of the base of the upper crust from various studies; solid-headed arrows, estimates of the base of the lower crust; M, proposed Moho identifications [from Bjarnason *et al.*, 1993; Flovenz, 1980; Foulger *et al.*, 2003; Staples *et al.*, 1997].

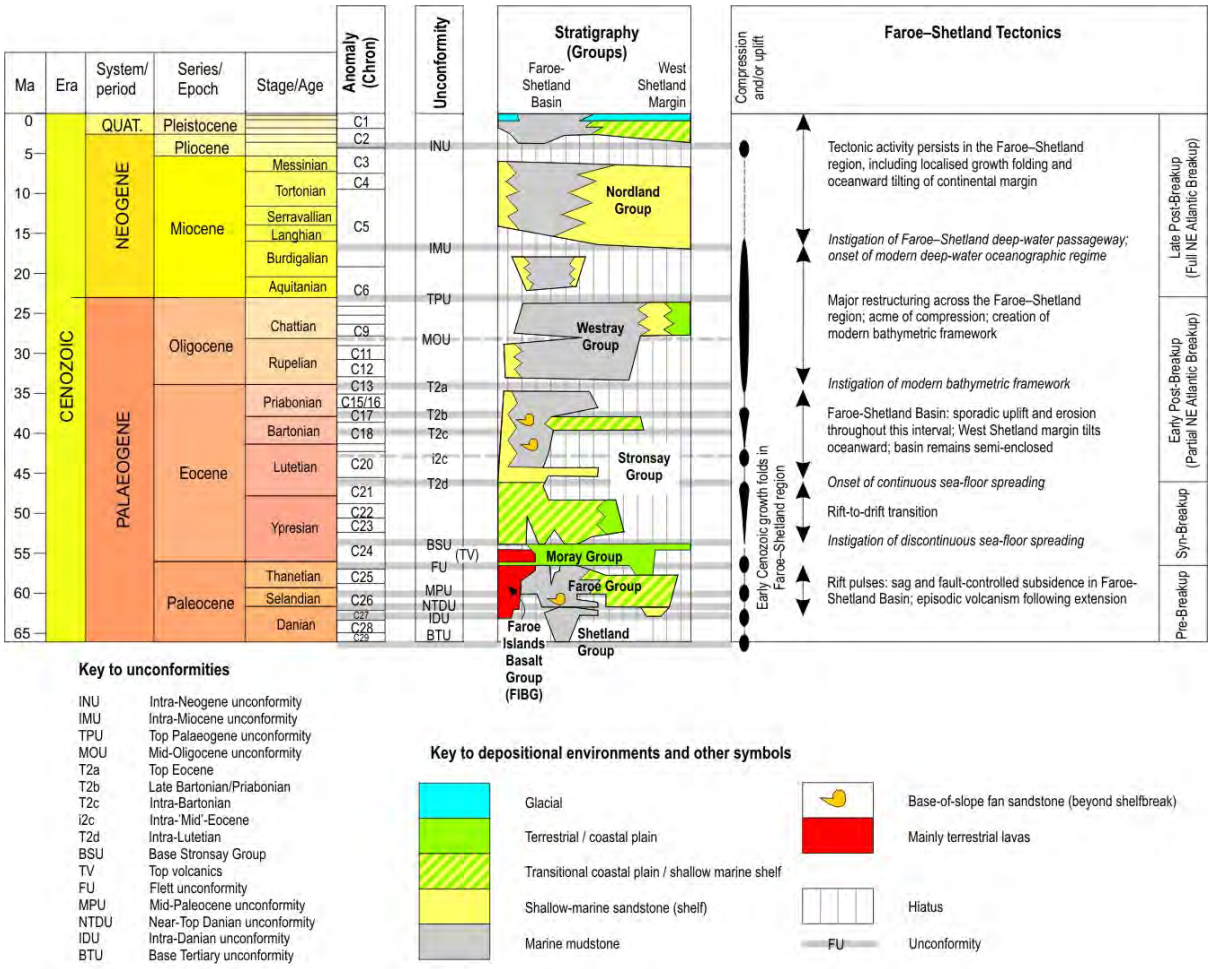

Figure 11: Cenozoic tectonostratigraphy for the Faroe-Shetland basin. The compilation of the stratigraphy and Faroe-Shetland tectonics is based mainly on Stoker *et al.* [2013; 2018; 2005b]. Additional information: 'Stratigraphy' and 'Unconformity' columns [Mudge, 2015], 'Faroe-Shetland Tectonics' column [Blischke *et al.*, 2017; Dean *et al.*, 1999; Ellis & Stoker, 2014; Johnson *et al.*, 2005; Ólavsdóttir *et al.*, 2013a; Stoker *et al.*, 2012; Stoker *et al.*, 2005a], timescale [Gradstein *et al.*, 2012].

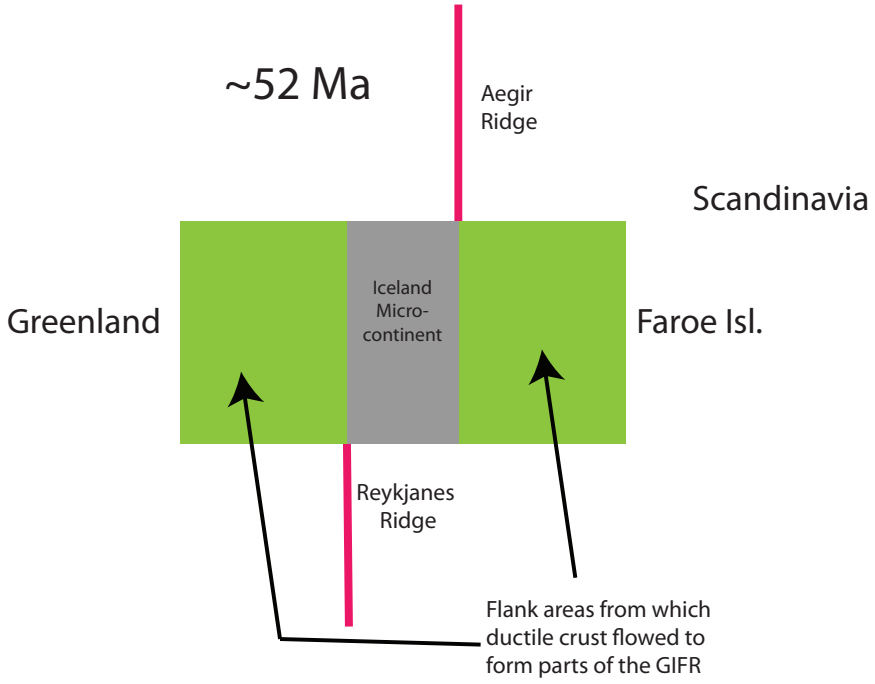

1390
1391

1392 Figure 12: Schematic diagram illustrating the Iceland Microcontinent.

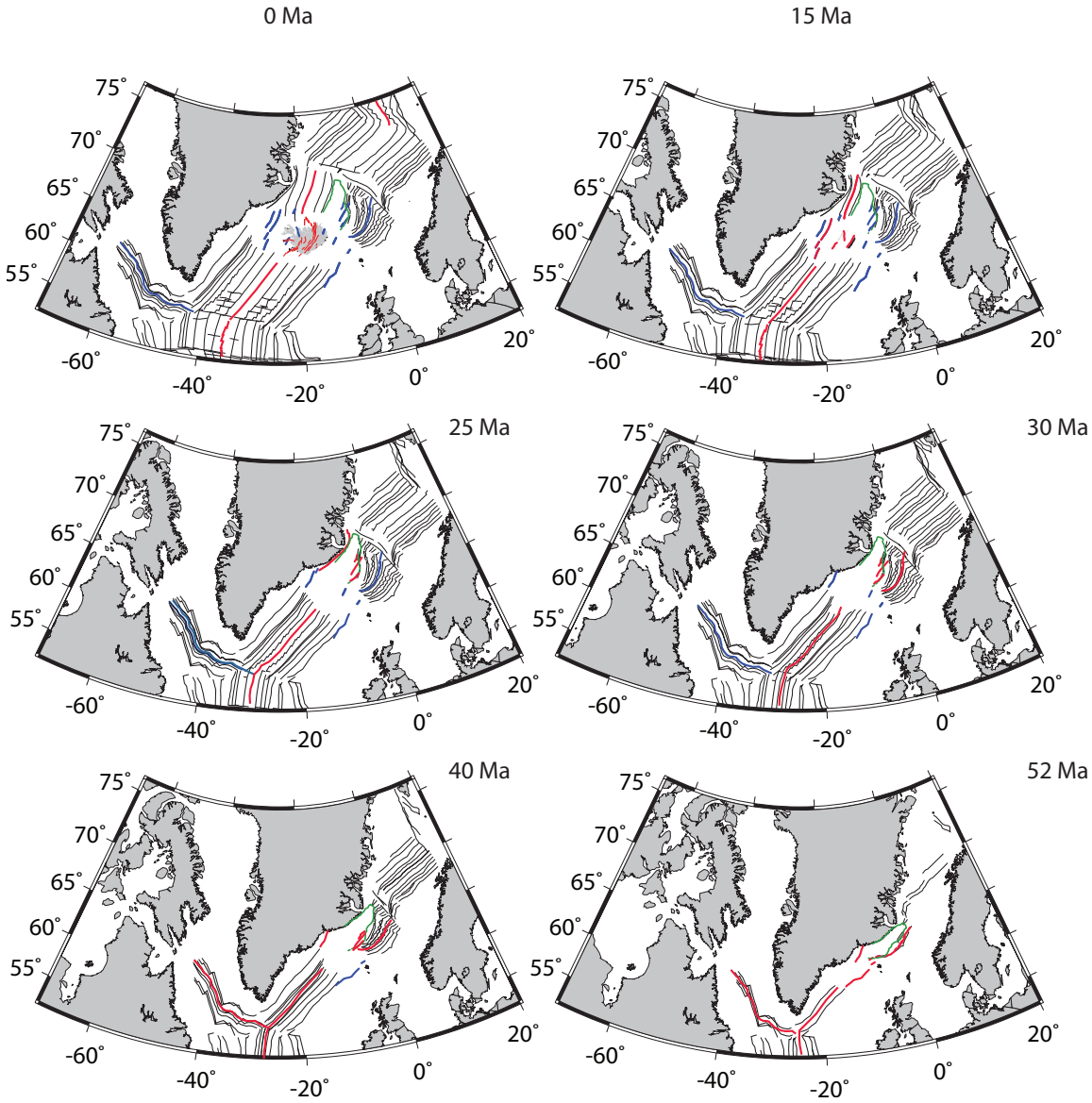

Figure 13: Locations of known extensional axes during opening of the NE Atlantic Ocean. Basemap and magnetic chrons (black lines) from GPlates using a Lambert Conformal Conic projection. Isochrons are from Müller *et al.* [2016]. Spreading ridges: Red—active, blue—extinct. Locations of some extinct offshore spreading axes are from Hjartarson *et al.* [2017] and Brandsdóttir *et al.* [2015]. Green: approximate boundary of Jan Mayen Microplate Complex. Areas where there is no direct evidence for rifts or spreading axes are left white.

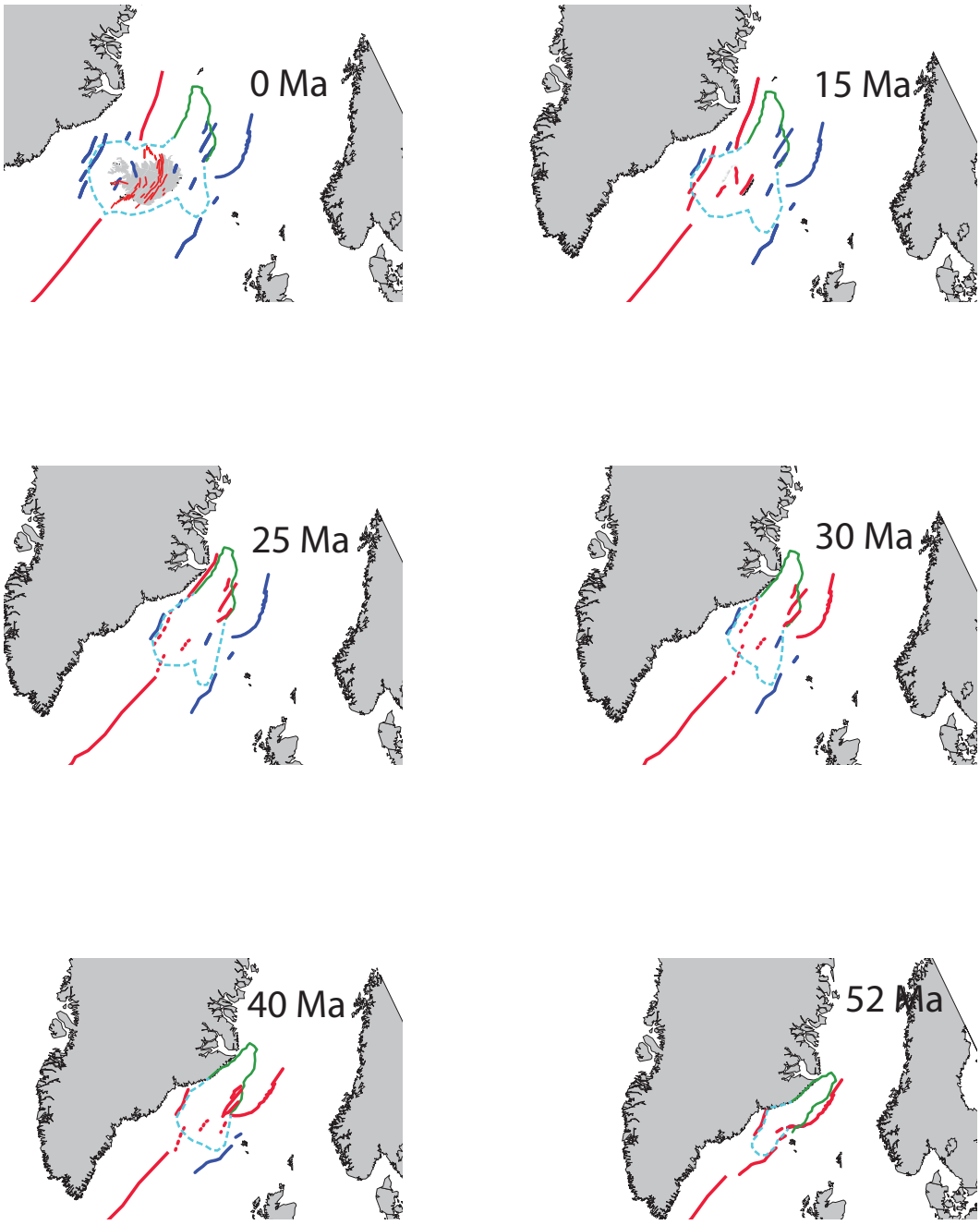

Figure 14: Speculative reconstruction of the sequence of extensional deformation on the GIFR and surroundings. Outline of land areas and locations of known extensional axes are from Figure 13 with the latter shown as solid lines. Red: active, blue: extinct. Dashed lines show speculative positions of ridges at times when observational data are lacking. Green solid line: approximate boundary of Jan Mayen Microplate Complex. Pale blue dashed line: approximate boundary of Iceland Microcontinent. This, and the Jan Mayen Microplate Complex expand with time as a result of magma inflation and ductile flow.

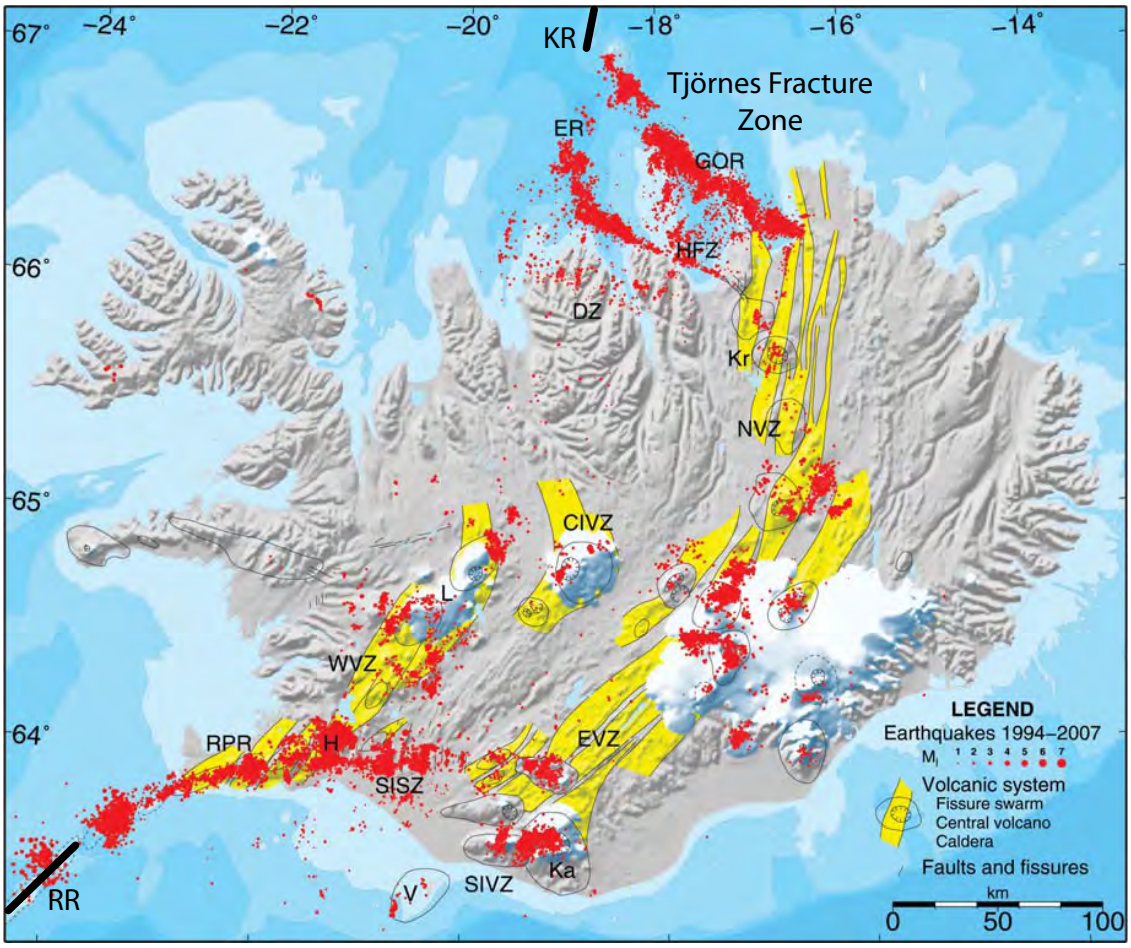

1414

1415

1416 Figure 15: Map of Iceland from Einarsson [2008] showing earthquakes 1994-2007 from the database
1417 of the Icelandic Meteorological Office. Yellow: volcanic systems. The Tjörnes Fracture Zone
1418 comprises GOR: the Grímsey Oblique Rift, HFZ: the Húsavík-Flatey Zone, ER: the Eyjafjardaráll
1419 Rift, DZ: the Dalvík Zone. Other abbreviations are RR: Reykjanes Ridge, KR: Kolbeinsey Ridge,
1420 RPR: Reykjanes Peninsula Rift Zone (also known as the Reykjanes Peninsula extensional transform
1421 zone), WVZ: Western Volcanic Zone, SISZ: South Iceland Seismic Zone, EVZ: Eastern Volcanic
1422 Zone, CIVZ: Central Iceland Volcanic Zone, NVZ: Northern Volcanic Zone, SIVZ: South Iceland
1423 Volcanic Zone, Kr, Ka, H and L: the central volcanoes Krafla, Katla, Hengill and Langjökull, V: the
1424 Vestmannaeyjar archipelago.

1425

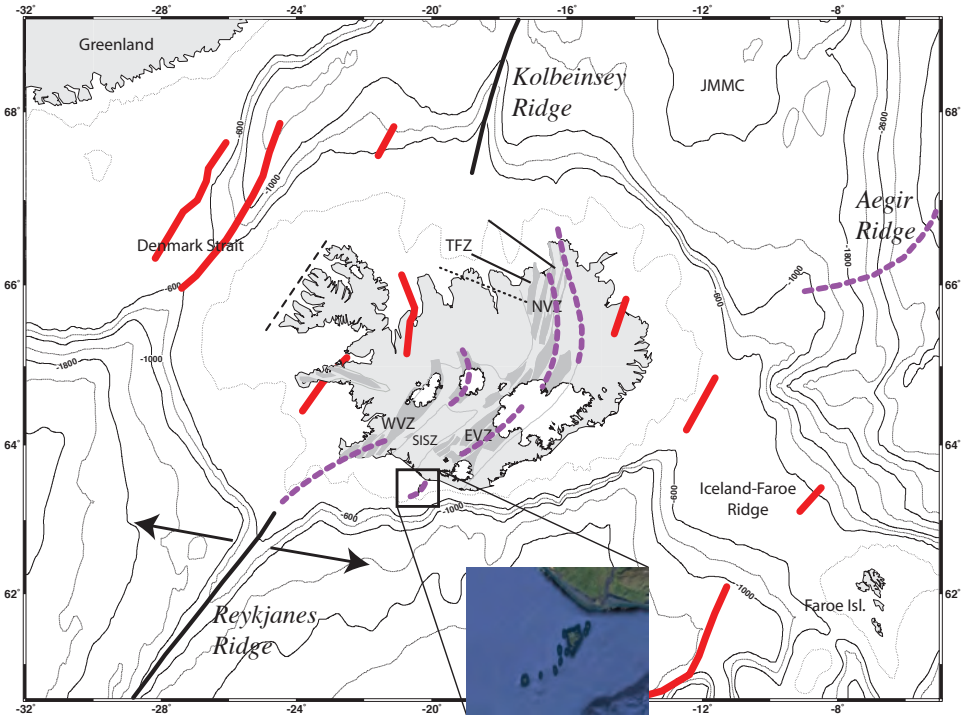

Figure 16: Similar to Figure 8 but showing additionally lines of curved sections of plate boundary that resemble curving, approaching crack tips (dashed magenta lines). Inset: expanded view of Vestmannaeyjar archipelago. Bold arrows: current direction of regional plate motion. For other details and abbreviations see caption of Figure 8.

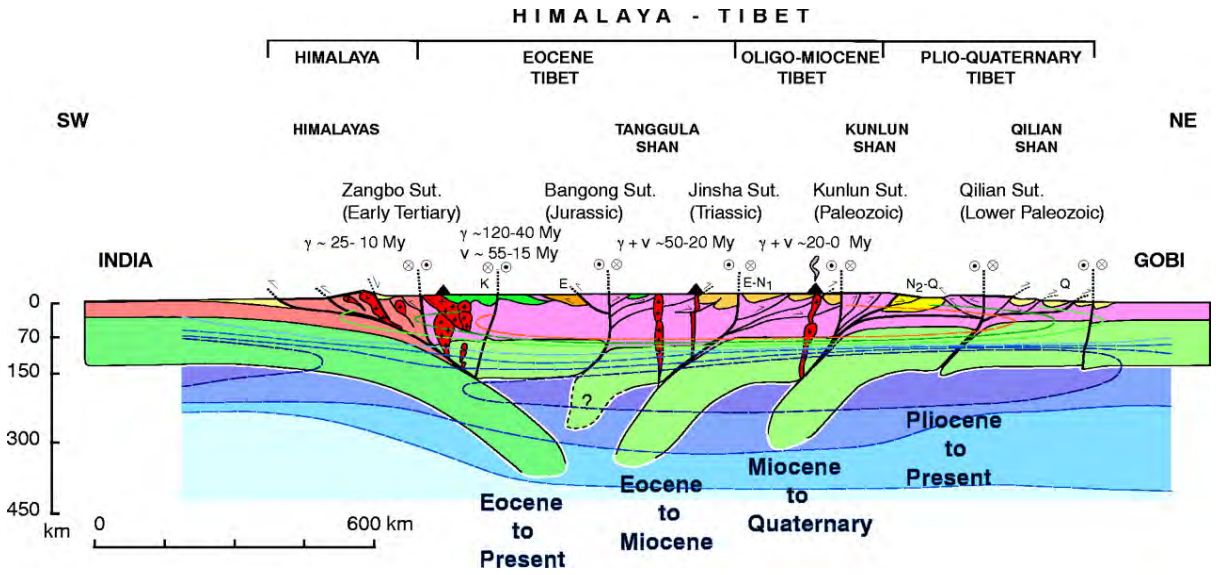

Figure 17: Schematic figure of the lithospheric structure of a well-studied, currently intact orogen—the Himalaya-Tibet orogen. Green: lithospheric mantle, red and pink: crust or intrusives, yellow and dark green: sedimentary basins. The orogen is underlain by an array of trapped fossil slabs that thicken the crust locally. Deeper parts of the slabs are in the dense eclogite facies and negatively buoyant [from Tapponnier *et al.*, 2001].

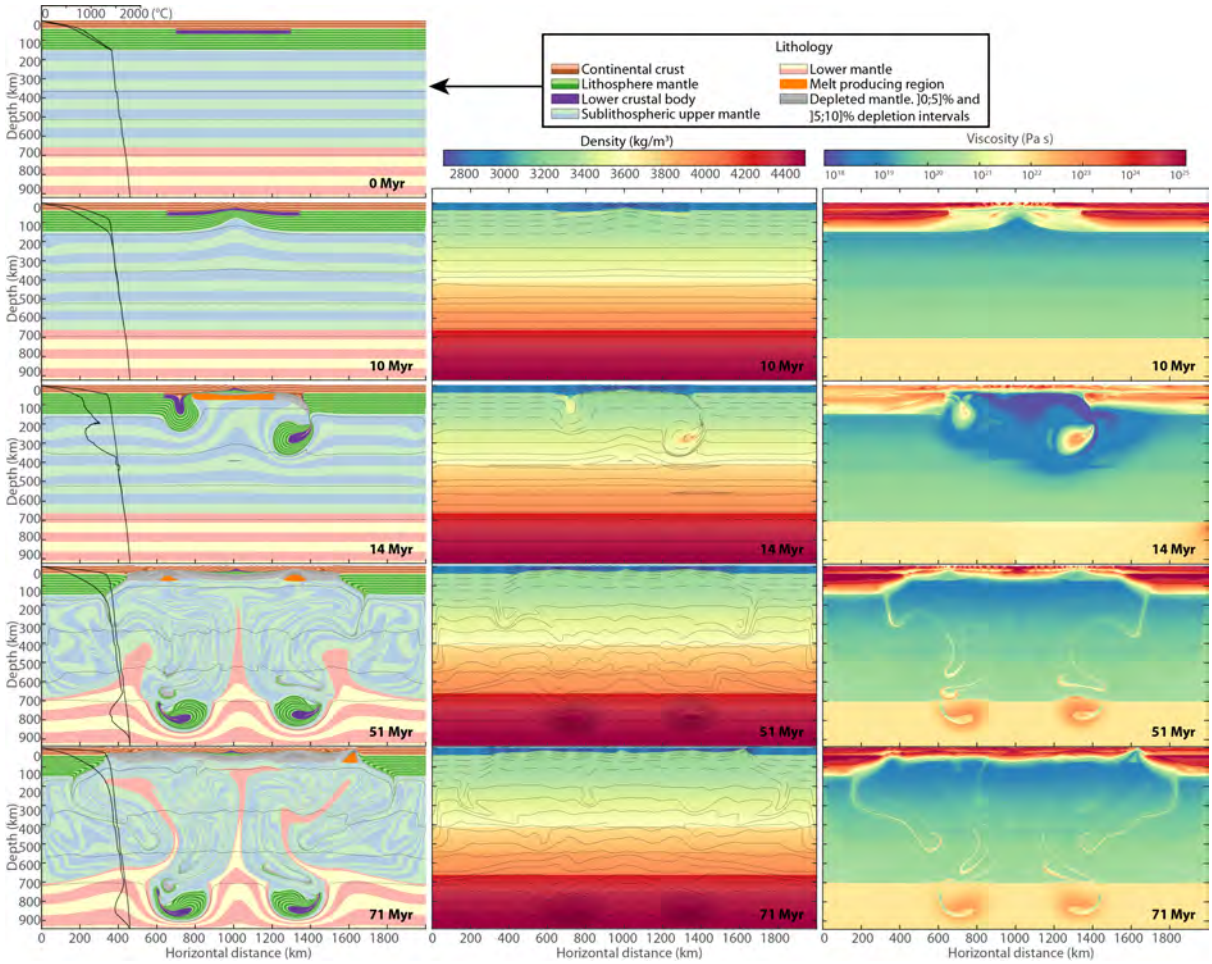

Figure 18: Simplified thermo-mechanical model of Cenozoic extension of the western frontal thrust of the Caledonian suture. Left panels: Lithology at selected times, thick black lines: minimum/maximum temperature profiles as a function of depth, thin black lines: isotherms from 1400˚C with 100˚C intervals. Upper left panel: initial model configuration. Central panels: density evolution, dashed black lines: isotherms from 0˚C to 1400˚C at 200˚C intervals, full black lines: isotherms from 1450˚C at 25˚C intervals. Right panels: effective viscosity evolution.

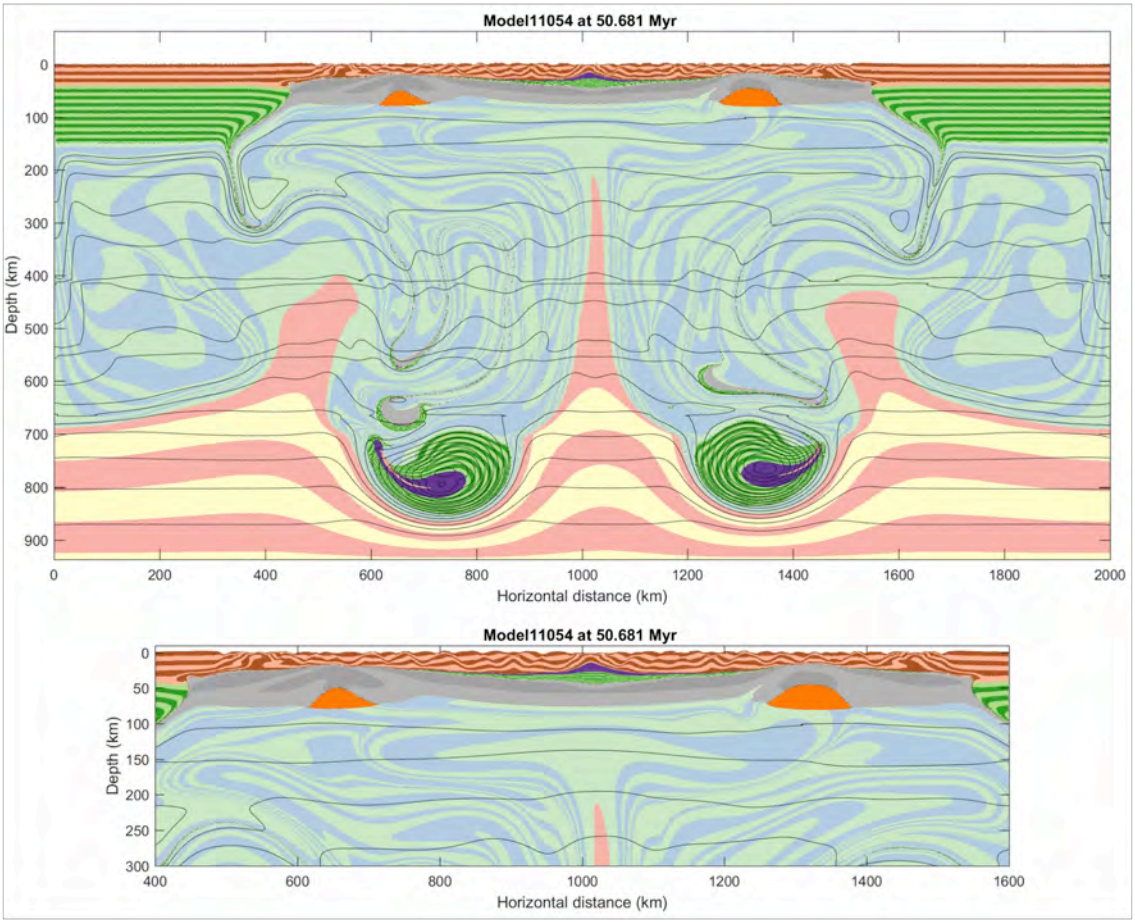

Figure 19: Expanded view of the lithology panel for 50.6 Myr, from Figure 18. See that Figure for details.

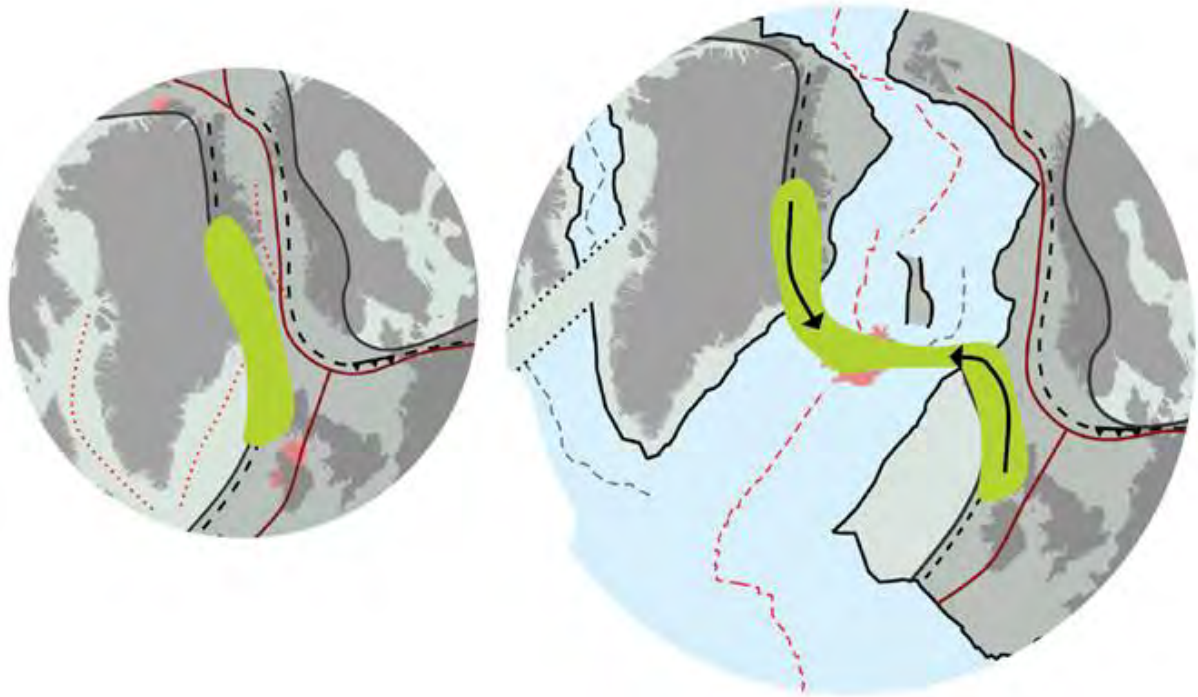

Figure 20: Map view sketch of our model. Green: the Caledonian frontal thrust zone where the crust is relatively thick prior to breakup, arrows: lateral inflow of weak lower crust into the extending, thinning zone. The persistence of continental crust beneath the GIFR maintains a warm, weak lithosphere and encourages distributed deformation and lateral rift jumps to persist.

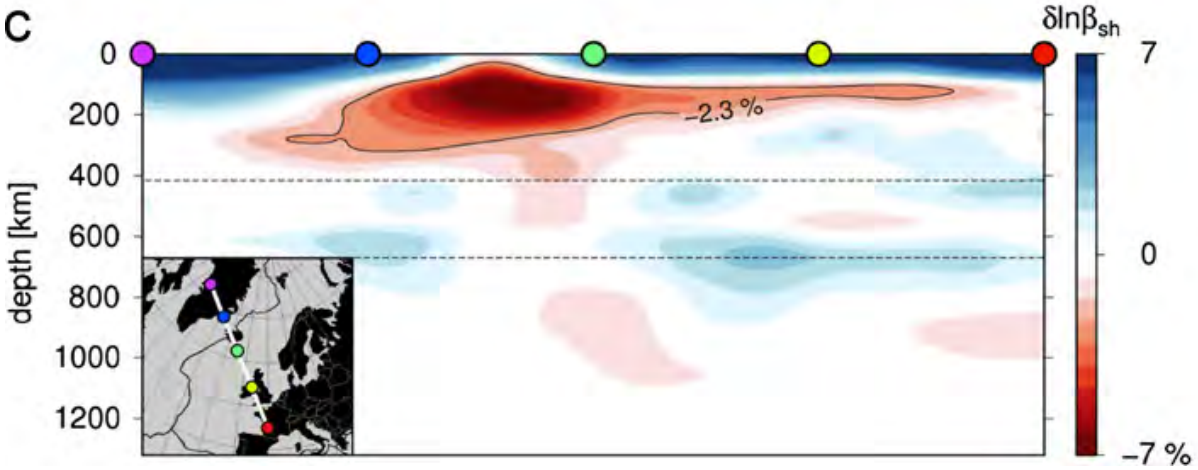

Figure 21: Cross section through the full-waveform inversion tomographic model of Rickers *et al.* [2013]. Colored dots are spaced at intervals of 1000 km. Compare with lower left panel of Figure 18.

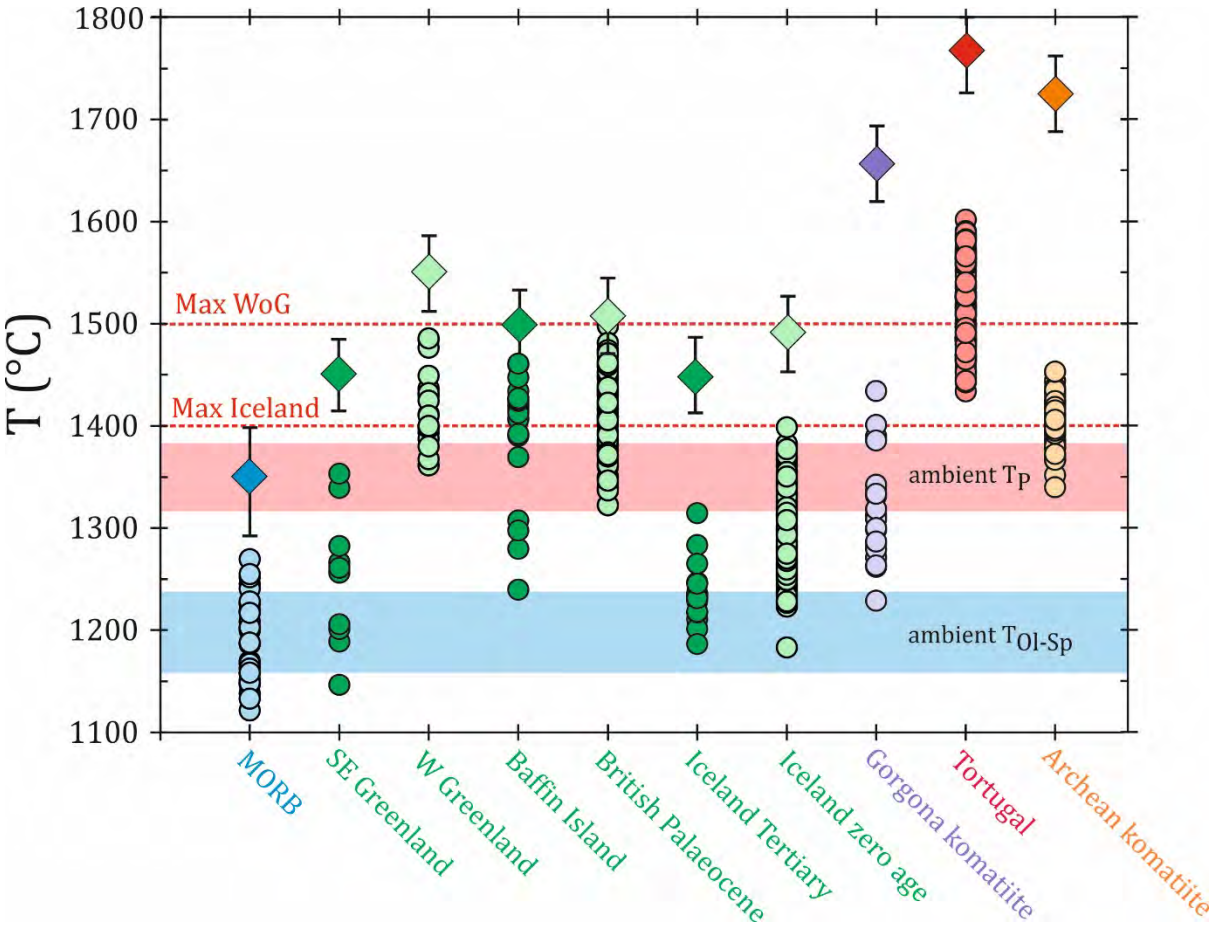

Figure 22: Summary of global maximum petrological estimates of T_P (diamonds ± 40˚C; Herzberg & Asimow [2015]) and olivine-spinel equilibrium crystallization temperatures (T_{Ol-Sp}) for magnesian olivine (dots). The lower light-blue shaded region represents the range of T_{Ol} for olivine which crystallized from near-primary magmas formed at ambient T_P ~1350 ± 40˚C (upper pink-shaded region). The horizontal dashed lines represent the maximum estimated T_P for Iceland and West of Greenland (WoG; Disko Island, Baffin Island) from Hole and Natland [this volume]. Data sources for T_{Ol-Sp}: MORB, Gorgona komatiite and Archean komatiite: Coogan *et al.* [2014], British Palaeocene, Baffin Island, West Greenland (Disko Island): Coogan *et al.* [2014], Spice *et al.* [2016], Iceland: Matthews *et al.* [2016], Spice *et al.* [2016], Tortugal: Trela *et al.* (2017). Petrological estimates from Herzberg and Asimow [2008; 2015], Hole [2015], Hole and Millett [2016] and Trela *et al.* [2017].

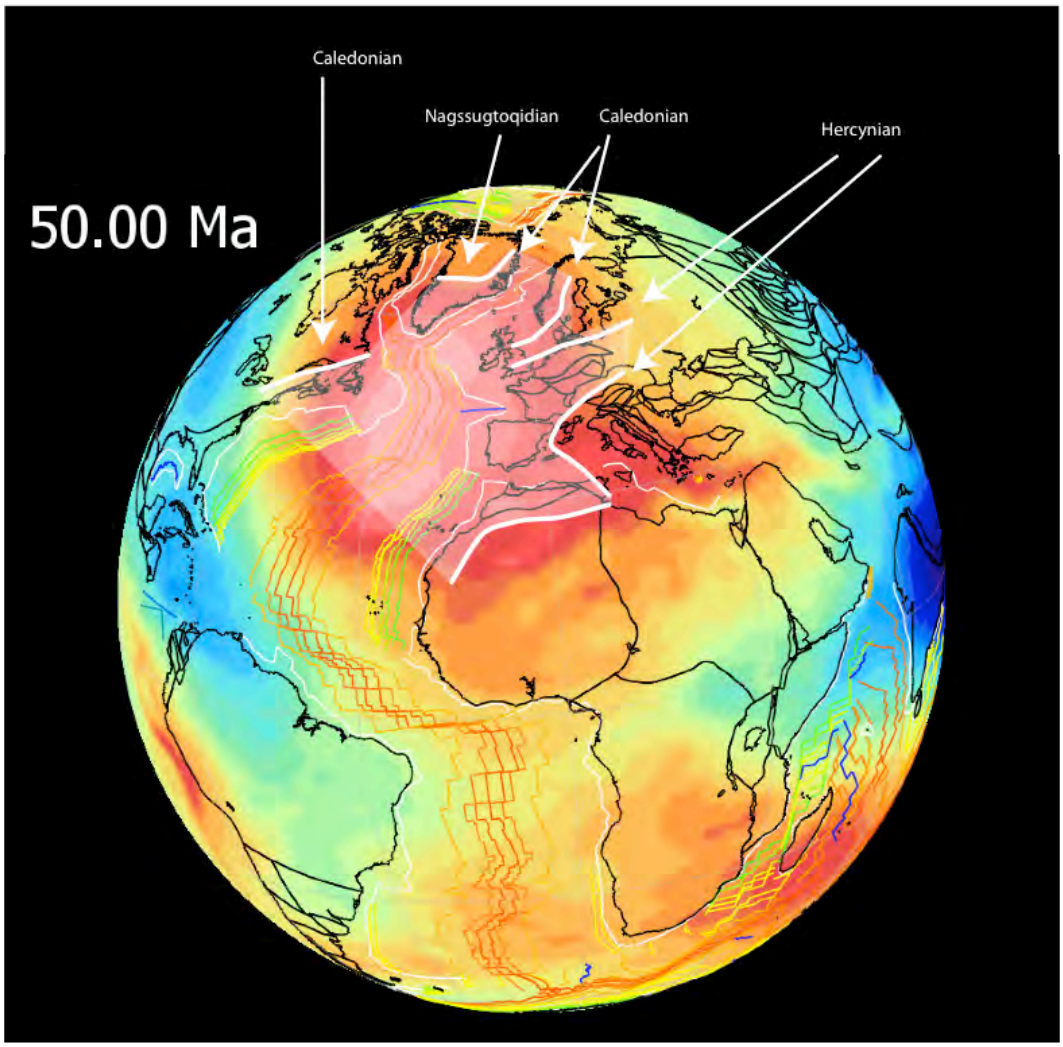

Figure 23: Continents reassembled to 50 Ma with the location of the future NE Atlantic centered over the present-day geoid high (red area). Thick white lines outline the Caledonian, Nagssugtoqidian, and Hercynian orogens. The area encompassed by these orogens is shaded and corresponds to the majority of the region of the geoid high.

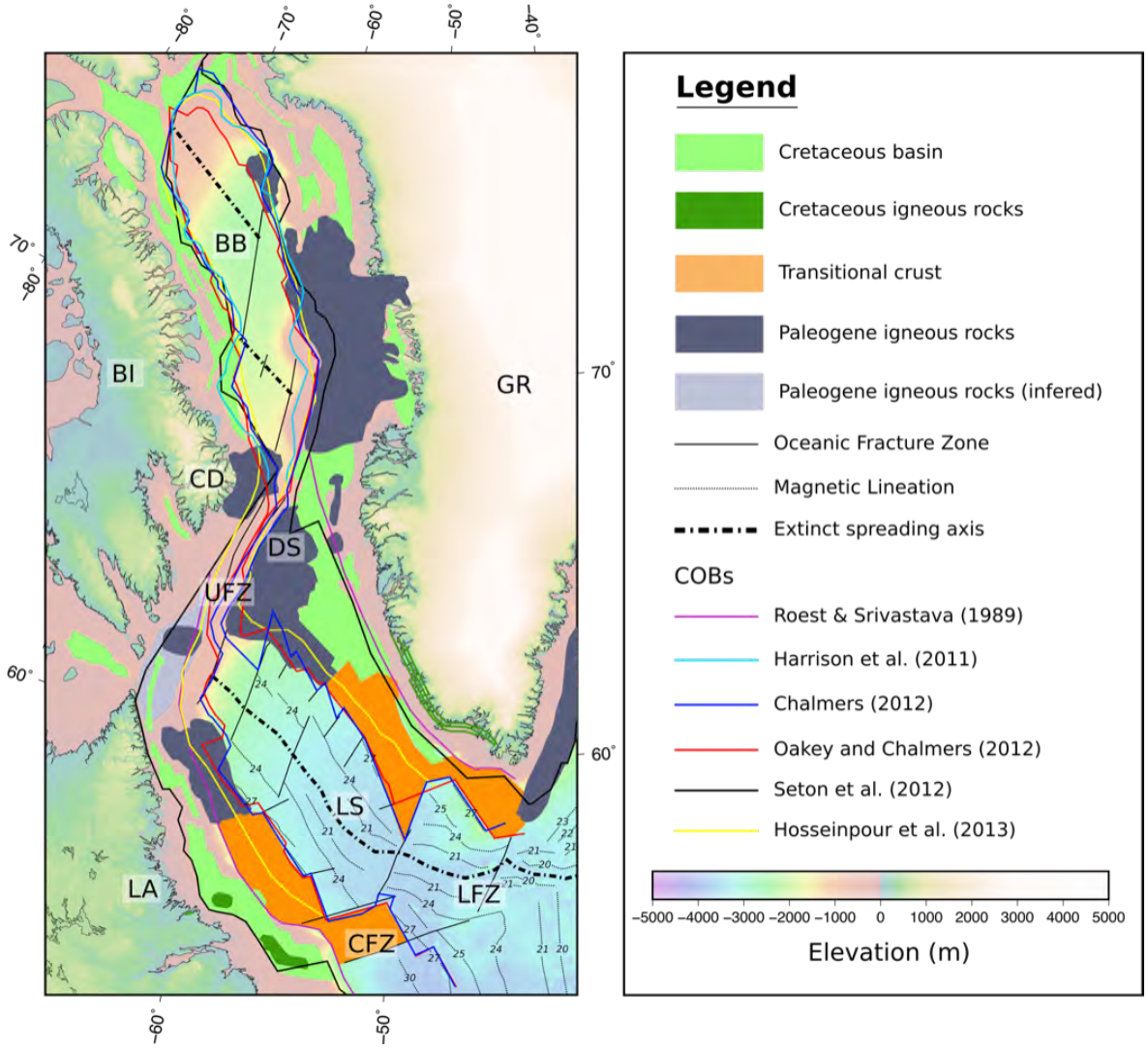

Figure 24: Structural map of the oceanic region west of Greenland showing Cretaceous basins and the extent of Paleogene volcanics, including inferred continuation as shown in Abdelmalak *et al.* [2018]. Different proposed continent-ocean boundaries are also shown. The magnetic lineations and fracture zones are reproduced from Chalmers [2012]. BB: Baffin Bay, BI: Baffin Island, CFZ: Cartwright Fracture Zone, DS: Davis Strait, GR: Greenland, LFZ: Leif Fracture Zone, LS: Labrador Sea, UFZ: Ungava Fault Zone, LA: Labrador. Elevation data are from Smith and Sandwell [1997].

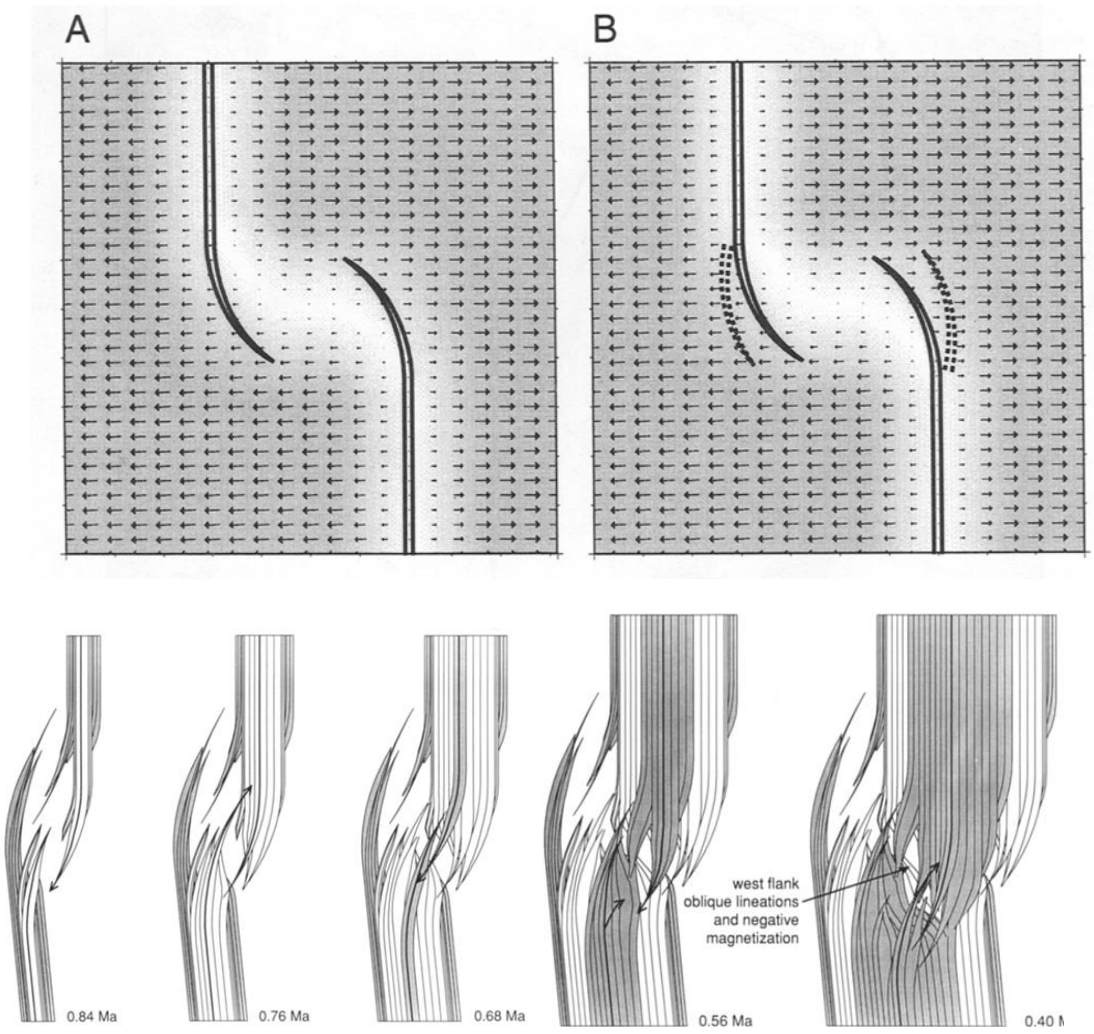

Figure 25: Schematic diagrams showing models of spreading ridge evolution observed on the East Pacific Rise. Top panels: ridges in the region 26˚S - 32˚S between the Easter and Juan Fernandez microplates. Parallel, solid lines: active ridges, parallel dashed lines: extinct ridges. The structure is modeled as a brittle layer overlying and weakly coupled with an underlying ductile layer. Deformation in this layer is shown by shading with gray indicating uniform motion and white indicating little or no motion. Arrows show displacement. Extension occurs in the overlap zone on curved, overlapping ridges that progressively migrate outward, are removed from the magma supply, become extinct, and are replaced by new ridges. Distributed bookshelf faulting occurs in the overlap zone [from Martínez *et al.*, 1997]. Bottom panels: Model for the evolution of the East Pacific Rise at 20˚40'S showing a possible origin of rotated blocks. Shading indicates magnetization polarities. The ridge tips alternate between propagation and retreat, leading to the term "dueling propagators" [from Perram *et al.*, 1993].

References

Á Horni, J., J. R. Hopper, and e. al. (2016), Regional distribution of volcanism within the North Atlantic Igneous Province, *in* The North-East Atlantic Region: A Reappraisal of Crustal Structure, Tectono-Stratigraphy and Magmatic Evolution, edited by G. Péron-Pinvidic, J. Hopper, M. S. Stoker, C. Gaina, H. Doornenbal, T. Funck and U. Árting, Geological Society, London, Special Publications.

Abdelmalak, M. M., J. I. Faleide, S. Planke, L. Gernigon, D. Zastrozhnov, G. E. Shephard, and R. Myklebust (2017), The T-Reflection and the Deep Crustal Structure of the Vøring Margin, Offshore mid-Norway, Tectonics, 36, 2497-2523.

Abdelmalak, M. M., S. Planke, S. Polteau, E. H. Hartz, J. I. Faleide, C. Tegner, D. A. Jerram, J. M. Millett, and R. Myklebust (2018), Breakup volcanism and plate tectonics in the NW Atlantic, Tectonophysics.

Acton, G. D., S. Stein, and J. F. Engeln (1991), Block rotation and continental extension in Afar: A comparison to oceanic microplate systems, Tectonics, 10, 501-526.

Ady, B. E., and R. C. Whittaker (2018), Examining the influence of tectonic inheritance on the evolution of the North Atlantic using a palinspastic deformable plate reconstruction, Geological Society, London, Special Publications, 470, SP470.479.

Amundsen, H. E. F., U. Schaltegger, B. Jamtveit, W. L. Griffin, Y. Y. Podladchikov, T. Torsvik, and K. Gronvold (2002), Reading the LIPs of Iceland and Mauritius, Proceedings of the 15th Kongsberg Seminar, Kongsberg, Norway.

Andersen, M. S., T. Nielsen, A. B. Sørensen, L. O. Boldreel, and A. Kuijpers (2000), Cenozoic sediment distribution and tectonic movements in the Faroe region, Global and Planetary Change, 24, 239-259.

Anderson, D. L. (2000a), The statistics of helium isotopes along the global spreading ridge system and the Central Limit Theorem, Geophys. Res. Lett., 27, 2401-2404.

Anderson, D. L. (2000b), The statistics and distribution of helium in the mantle, Int. Geol. Rev., 42, 289-311.

Anderson, D. L. (2001), A statistical test of the two reservoir model for helium, Earth planet. Sci. Lett., 193, 77-82.

Anderson, D. L., G. R. Foulger, and A. Meibom (2006), Helium: Fundamental models, edited, G. R. Foulger, http://www.mantleplumes.org/.

Angenheister, G., H. Gebrande, H. Miller, P. Goldflam, W. Weigel, W. R. Jacoby, G. Palmason, S. Bjornsson, P. Einarsson, N. I. Pavlenkova, S. M. Zverev, I. V. Litvinenko, B. Loncarevic, and S. C. Solomon (1980), Reykjanes ridge Iceland seismic experiment (RRISP 77), J. Geophys., 47, 228-238.

Artemieva, I. M., and H. Thybo (2013), EUNAseis: A seismic model for Moho and crustal structure in Europe, Greenland, and the North Atlantic region, Tectonophysics, 609, 97-153.

Atwater, T., and J. Severinghaus (1989), Tectonic maps of the northeast Pacific, *in* The Eastern Pacific Ocean and Hawaii, edited by E. L. Winterer, D. M. Hussong and R. W. Decker, pp. 15-20, Geological Society of America, Boulder, Colorado.

Barnett-Moore, N., D. R. Müller, S. Williams, J. Skogseid, and M. Seton (2018), A reconstruction of the North Atlantic since the earliest Jurassic, Basin Research, 30, 160-185.

Bauer, K., S. Neben, B. Schreckenberger, R. Emmermann, K. Hinz, N. Fechner, K. Gohl, A. Schulze, R. B. Trumbull, and K. Weber (2000), Deep structure of the Namibia continental margin as derived from integrated geophysical studies, J. Geophys. Res., 105, 25829–25853.

Beblo, M., and A. Bjornsson (1978), Magnetotelluric investigation of the lower crust and upper mantle beneath Iceland, J. Geophys., 45, 1-16.

Beblo, M., and A. Bjornsson (1980), Model of Electrical-Resistivity beneath Ne Iceland, Correlation with Temperature, Journal of Geophysics-Zeitschrift Fur Geophysik, 47, 184-190.

Beblo, M., A. Bjornsson, K. Arnason, B. Stein, and P. Wolfgram (1983), Electrical conductivity beneath Iceland - Constraints imposed by magnetotelluric results on temperature, partial melt, crust and mantle structure, J. Geophys., 53, 16-23.

1583 Benediktsdóttir, Á., R. Hey, F. Martinez, and Á. Höskuldsson (2012), Detailed tectonic evolution of
1584 the Reykjanes Ridge during the past 15 Ma, Geochem. Geophys. Geosys., 13.
1585 Benson, R. N. (2003), Age Estimates of the Seaward-Dipping Volcanic Wedge, Earliest Oceanic
1586 Crust, and Earliest Drift-Stage Sediments Along the North American Atlantic Continental
1587 Margin, *in* The Central Atlantic Magmatic Province: Insights from Fragments of Pangea, edited
1588 by W. Hames, J. Mchone, P. Renne and C. Ruppel, pp. 61–75, American Geophysical Union.
1589 Bergerat, F., and J. Angelier (2000), The South Iceland Seismic Zone: tectonic and sismotectonic
1590 analyses revealing the evolution from rifting to transform motion, J. Geodyn., 29, 211-231.
1591 Berzin, R., O. Oncken, J. H. Knapp, A. Pérez-Estaún, T. Hismatulin, N. Yunusov, and A. Lipilin
1592 (1996), Orogenic Evolution of the Ural Mountains: Results from an Integrated Seismic
1593 Experiment, Science, 274, 220.
1594 Bingen, B., and G. Viola (2018), The early-Sveconorwegian orogeny in southern Norway: Tectonic
1595 model involving delamination of the sub-continental lithospheric mantle, Precamb. Res., 313,
1596 170-204.
1597 Bjarnason, I. T., W. Menke, O. G. Flovenz, and D. Caress (1993), Tomographic image of the mid-
1598 Atlantic plate boundary in south-western Iceland, J. Geophys. Res., 98, 6607-6622.
1599 Bjornsson, A., G. Johnsen, S. Sigurdsson, G. Thorbergsson, and E. Tryggvason (1979), Rifting of the
1600 Plate Boundary in North Iceland 1975-1978, J. Geophys. Res., 84, 3029-3038.
1601 Björnsson, A., H. Eysteinsson, and M. Beblo (2005), Crustal formation and magma genesis beneath
1602 Iceland: magnetotelluric constraints, *in* Plates, Plumes, and Paradigms, edited by G. R. Foulger,
1603 J.H. Natland, D.C. Presnall and D.L. Anderson, pp. 665-686, Geological Society of America.
1604 Blischke, A., C. Gaina, J. R. Hopper, G. Peron-Pinvidic, B. Brandsdottir, P. Guarnieri, O. Erlendsson,
1605 and K. Gunnarsson (2017), The Jan Mayen microcontinent: an update of its architecture,
1606 structural development and role during the transition from the Ægir Ridge to the mid-oceanic
1607 Kolbeinsey Ridge, *in* The NE Atlantic Region: A Reappraisal of Crustal Structure,
1608 Tectonostratigraphy and Magmatic Evolution, edited by G. Peron-Pinvidic, J. R. Hopper, M. S.
1609 Stoker, C. Gaina, J. C. Doornenbal, T. Funck and U. E. Arting, pp. 299-337, Geological Society,
1610 London, Special Publications.
1611 Bohnhoff, M., and J. Makris (2004), Crustal structure of the southeastern Iceland-Faeroe Ridge (IFR)
1612 from wide aperture seismic data, J. Geodyn., 37, 233-252.
1613 Bonatti, E. (1985), Punctiform initiation of seafloor spreading in the Red Sea during transition from a
1614 continental to an oceanic rift, Nature, 316, 33.
1615 Bott, M. H. P. (1974), Deep structure, evolution and origin of the Icelandic transverse ridge, *in*
1616 Geodynamics of Iceland and the North Atlantic Area, edited by L. Kristjansson, pp. 33-48, D.
1617 Reidel Publishing Company, Dordrecht.
1618 Bott, M. H. P. (1985), Plate tectonic evolution of the Icelandic transverse ridge and adjacent regions,
1619 JGR, 90, 9953-9960.
1620 Bott, M. H. P., J. Sunderland, P. J. Smith, U. Casten, and S. Saxov (1974), Evidence for continental
1621 crust beneath the Faeroe Islands, Nature, 248, 202.
1622 Bourgeois, O., O. Dauteuil, and E. Hallot (2005), Rifting above a mantle plume: structure and
1623 development of the Iceland Plateau, Geodinamica Acta, 18, 59-80.
1624 Brandsdóttir, B., E. E. E. Hooft, R. Mjelde, and Y. Murai (2015), Origin and evolution of the
1625 Kolbeinsey Ridge and Iceland Plateau, N-Atlantic, Geochem. Geophys. Geosys., 16, 612–634.
1626 Breddam, K. (2002), Kistufell: Primitive melt from the Iceland mantle plume, J. Pet., 43, 345-373.
1627 Breivik, A. J., R. Mjelde, J. I. Faleide, and Y. Murai (2006), Rates of continental breakup magmatism
1628 and seafloor spreading in the Norway Basin–Iceland plume interaction, Journal of Geophysical
1629 Research: Solid Earth, 111.
1630 Breivik, A. J., R. Mjelde, J. I. Faleide, and Y. Murai (2012), The eastern Jan Mayen microcontinent
1631 volcanic margin, Geophys. J. Int., 188, 798-818.
1632 Bronner, A., D. Sauter, G. Manatschal, G. Péron-Pinvidic, and M. Munschy (2011), Magmatic
1633 breakup as an explanation for magnetic anomalies at magma-poor rifted margins, Nature
1634 Geoscience, 4, 549.
1635 Brooks, C. K. (2011), The East Greenland rifted volcanic margin, Geological Survey of Denmark and
1636 Greenland Bulletin, 24, 1-96.

1637 Brune, S., C. Heine, M. Pérez-Gussinyé, and S. V. Sobolev (2014), Rift migration explains
1638 continental margin asymmetry and crustal hyper-extension, Nature Communications, 5.
1639 Buck, R. W. (1986), Small-scale convection induced by passive rifting: the cause for uplift of rift
1640 shoulders, Earth planet. Sci. Lett., 77, 362–372.
1641 Buck, W. R. (1991), Modes of continental lithospheric extension, Journal of Geophysical Research:
1642 Solid Earth, 96, 20161-20178.
1643 Buiter, S. J. H., and T. H. Torsvik (2014), A review of Wilson Cycle plate margins: A role for mantle
1644 plumes in continental break-up along sutures?, Gondwana Research, 26, 627-653.
1645 Carminati, E., and C. Doglioni (2010), North Atlantic geoid high, volcanism and glaciations,
1646 Geophys. Res. Lett., 37.
1647 Chalmers, J. A. (2012), Labrador Sea, Davis Strait, and Baffin Bay, *in* Regional Geology and
1648 Tectonics: Phanerozoic Passive Margins, Cratonic Basins and Global Tectonic Maps, edited by
1649 D. G. Roberts and A. W. Bally, pp. 384-435, Elsevier, Boston.
1650 Chalmers, J. A., and K. H. Laursen (1995), Labrador Sea: The extent of continental and oceanic crust
1651 and the timing of the onset of seafloor spreading, Marine and Petroleum Geology, 12, 205–217.
1652 Chalmers, J. A., and T. C. R. Pulvertaft (2001), Development of the continental margins of the
1653 Labrador Sea: a review, Geological Society, London, Special Publications, 187, 77.
1654 Chauvel, C., and C. Hemond (2000), Melting of a complete section of recycled oceanic crust: Trace
1655 element and Pb isotopic evidence from Iceland, Geochem. Geophys. Geosys., 1, 1999GC000002.
1656 Chauvet, F., L. Geoffroy, H. Guillou, R. Maury, B. Le Gall, A. Agranier, and A. Viana (2019),
1657 Eocene continental breakup in Baffin Bay 757.
1658 Cheng, H., H. Zhou, Q. Yang, L. Zhang, F. Ji, and H. Dick (2016), Jurassic zircons from the
1659 Southwest Indian Ridge, Scientific Reports, 6, 26260.
1660 Chenin, P., G. Manatschal, L. L. Lavier, and D. Erratt (2015), Assessing the impact of orogenic
1661 inheritance on the architecture, timing and magmatic budget of the North Atlantic rift system: a
1662 mapping approach, Journal of the Geological Society, 172, 711.
1663 Christensen, N. I. (2004), Serpentinites, Peridotites, and Seismology, Int. Geol. Rev., 46, 795-816.
1664 Čížková, H., A. P. van den Berg, W. Spakman, and C. Matyska (2012), The viscosity of Earth's lower
1665 mantle inferred from sinking speed of subducted lithosphere, Phys. Earth Planet. Int., 200-201,
1666 56-62.
1667 Clarke, D. B., and E. K. Beutel (2019), Davis Strait Paleocene Picrites: Products of a Plume or
1668 Plates?, Earth-Science Reviews, this volume.
1669 Clerc, C., L. Jolivet, and J.-C. Ringenbach (2015), Ductile extensional shear zones in the lower crust
1670 of a passive margin, Earth planet. Sci. Lett., 431, 1-7.
1671 Connelly, J. N., K. Thrane, A. W. Krawiec, and A. A. Garde (2006), Linking the Palaeoproterozoic
1672 Nagssugtoqidian and Rinkian orogens through the Disko Bugt region of West Greenland, Journal
1673 of the Geological Society, 163, 319.
1674 Connolly, J. A. D. (2005), Computation of phase equilibria by linear programming: A tool for
1675 geodynamic modeling and its application to subduction zone decarbonation, Earth planet. Sci.
1676 Lett., 236, 524-541.
1677 Coogan, L. A., A. D. Saunders, and R. N. Wilson (2014), Aluminum-in-olivine thermometry of
1678 primitive basalts: Evidence of an anomalously hot mantle source for large igneous provinces,
1679 Chem. Geol., 368, 1-10.
1680 Craig, H., and J. E. Lupton (1976), Primordial neon, helium, and hydrogen in oceanic basalts, Earth
1681 planet. Sci. Lett., 31, 369-385.
1682 Dalhoff, F., L. M. Larsen, J. R. Ineson, S. Stouge, J. A. Bojesen-Koefoed, S. Lassen, A. Kuijpers, J.
1683 A. Rasmussen, and H. Nøhr-Hansen (2006), Continental crust in the Davis Strait: new evidence
1684 from seabed sampling, Geological Survey of Denmark and Greenland Bulletin, 10, 33–36.
1685 Dannowski, A., I. Grevemeyer, J. Phipps Morgan, C. R. Ranero, M. Maia, and G. Klein (2011),
1686 Crustal structure of the propagating TAMMAR ridge segment on the Mid-Atlantic Ridge,
1687 21.5°N, Geochemistry, Geophysics, Geosystems, 12.
1688 Darbyshire, F. A., I. T. Bjarnason, R. S. White, and O. G. Flovenz (1998a), Crustal structure above
1689 the Iceland mantle plume imaged by the ICEMELT refraction profile, Geophys. J. Int., 135,
1690 1131-1149.

1691 Darbyshire, F. A., I. T. Bjarnason, R. S. White, and I. G. Flovenz (1998b), Crustal structure above the
1692 Iceland mantle plume imaged by the ICEMELT refraction profile, Geophys. J. Int., 135, 1131-
1693 1149.
1694 Darbyshire, F. A., T. Dahl-Jensen, T. B. Larsen, P. H. Voss, and G. Joyal (2018), Crust and
1695 uppermost-mantle structure of Greenland and the Northwest Atlantic from Rayleigh wave group
1696 velocity tomography, Geophys. J. Int., 212, 1546-1569.
1697 Dean, K., K. McLachlan, and A. Chambers (1999), Rifting and the development of the Faeroe-
1698 Shetland Basin, Proceedings of the 5th Conference Petroleum Geology of Northwest Europe,
1699 London, pp. 533–544.
1700 Deemer, S., C. A. Hurich, and J. Hall (2010), Post-rift flood-basalt-like volcanism on the
1701 Newfoundland Basin nonvolcanic margin: The U event mapped with spectral decomposition
1702 494, 1-16 pp.
1703 Denk, T., F. Grímsson, R. Zetter, and L. A. Símonarson (2011), The Biogeographic History of Iceland
1704 – The North Atlantic Land Bridge Revisited, *in* Late Cainozoic Floras of Iceland, edited, pp.
1705 647-668, Springer Science+Business Media B.V.
1706 Detrick, R. S., J. G. Sclater, and J. Thiede (1977), The subsidence of aseismic ridges, Earth planet.
1707 Sci. Lett., 34, 185-196.
1708 Dewey, J. F., and R. A. Strachan (2003), Changing Silurian–Devonian relative plate motion in the
1709 Caledonides: sinistral transpression to sinistral transtension, Journal of the Geological Society,
1710 160, 219.
1711 Dick, H. J. B. (2015), The Southwest Indian Ridge: Remelting the Gondwanan Mantle, Acta
1712 Geologica Sinica - English Edition, 89, 27-27.
1713 Doré, A. G., E. R. Lundin, C. Fichler, and O. Olesen (1997), Patterns of basement structure and
1714 reactivation along the NE Atlantic margin, J. geol. Soc. Lon., 154, 85–92.
1715 Downes, H., B. G. J. Upton, A. D. J. Connolly, and J.-L. Bodinier (2007), Petrology and
1716 geochemistry of a cumulate xenolith suite from Bute: evidence for late Palaeozoic crustal
1717 underplating beneath SW Scotland, Journal of the Geological Society, London, 164, 1217–1231.
1718 Du, Z., and G. R. Foulger (1999), The crustal structure beneath the Northwest Fjords, Iceland, from
1719 receiver functions and surface waves, Geophys. J. Int., 139, 419-432.
1720 Du, Z., G. R. Foulger, B. R. Julian, R. M. Allen, G. Nolet, W. J. Morgan, B. H. Bergsson, P.
1721 Erlendsson, S. Jakobsdottir, S. Ragnarsson, R. Stefansson, and K. Vogfjord (2002), Crustal
1722 structure beneath western and eastern Iceland from surface waves and receiver functions,
1723 Geophys. J. Int., 149, 349-363.
1724 Du, Z. J., and G. R. Foulger (2001), Variation in the crustal structure across central Iceland, Geophys.
1725 J. Int., 145, 246-264.
1726 Dunbar, J. A., and D. S. Sawyer (1988), Continental rifting at pre-existing lithospheric weaknesses,
1727 Nature, 333, 450.
1728 Dunn, R., and F. Martinez (2011), Contrasting crustal production and rapid mantle transitions beneath
1729 backarc ridges, Nature, 469, 198–202.
1730 Eagles, G., L. Pérez-Díaz, and N. Scarselli (2015), Getting over continent ocean boundaries, Earth-
1731 Science Reviews, 151, 244-265.
1732 Ebbing, J., E. Lundin, O. Olesen, and E. K. Hansen (2006), The mid-Norwegian margin: a discussion
1733 of crustal lineaments, mafic intrusions, and remnants of the Caledonian root by 3D density
1734 modelling and structural interpretation, Journal of the Geological Society, 163, 47.
1735 Ebbing, J., R. W. England, T. Korja, T. Lauritsen, O. Olesen, W. Stratford, and C. Weidle (2012),
1736 Structure of the Scandes lithosphere from surface to depth, Tectonophysics, 536-537, 1-24.
1737 Ebdon, C. C., P. J. Granger, H. D. Johnson, and A. M. Evans (1995), Early Tertiary evolution and
1738 sequence stratigraphy of the Faeroe-Shetland Basin: implications for hydrocarbon prospectivity,
1739 *in* The Tectonics, Sedimentation and Palaeoceanography of the North Atlantic Region, edited by
1740 R. A. Scrutton, M. S. Stoker, G. B. Shimmield and A. W. Tudhope, pp. 51–69, Geological
1741 Society, London, Special Publications, London.
1742 Einarsson, P. (1988), The South Iceland Seismic Zone, Episodes, 11, 34-35.
1743 Einarsson, P. (1991), Earthquakes and present-day tectonism in Iceland, Tectonophysics, 189, 261-
1744 279.

1745 Einarsson, P. (2008), Plate boundaries, rifts and transforms in Iceland, Jökull, 58, 35-58.
1746 Eldholm, O., and K. Grue (1994a), North Atlantic volcanic margins: Dimensions and production
1747 rates, J. Geophys. Res., 99, 2955–2968.
1748 Eldholm, O., and K. Grue (1994b), North Atlantic volcanic margins: Dimensions and production
1749 rates, Journal of Geophysical Research: Solid Earth, 99, 2955-2968.
1750 Eldholm, O., J. Thiede, and E. Taylor (1989), Evolution of the Vøring Volcanic Margin, Proceedings
1751 of the ODP, Scientific Results, pp 1033-1065 104.
1752 Elliott, G. M., and L. M. Parson (2008), Influence of margin segmentation upon the break-up of the
1753 Hatton Bank rifted margin, NE Atlantic, Tectonophysics, 457, 161-176.
1754 Ellis, D., and M. S. Stoker (2014), The Faroe–Shetland Basin: a regional perspective from the
1755 Paleocene to the present day and its relationship to the opening of the North Atlantic Ocean, *in*
1756 Hydrocarbon Exploration to Exploitation West of Shetlands, edited by S. J. C. Cannon and D.
1757 Ellis, Geological Society, London, London.
1758 Engeln, J. F., S. Stein, J. Werner, and R. G. Gordon (1988), Microplate and shear zone models for
1759 oceanic spreading center reorganizations, Journal of Geophysical Research: Solid Earth, 93,
1760 2839-2856.
1761 Escartin, J., G. Hirth, and B. Evans (2001), Strength of slightly serpentinized peridotites: Implications
1762 for the tectonics of oceanic lithosphere, Geology, 29, 1023-1026.
1763 Eysteinsson, H., and J. Hermance (1985), Magnetotelluric measurements across the eastern
1764 neovolcanic zone in south Iceland, JGR, 90, 10,093-010,103.
1765 Fichler, C., T. Odinsen, H. Rueslåtten, O. Olesen, J. E. Vindstad, and S. Wienecke (2011), Crustal
1766 inhomogeneities in the Northern North Sea from potential field modeling: Inherited structure and
1767 serpentinites?, Tectonophysics, 510, 172-185.
1768 Flovenz, O. G. (1980), Seismic structure of the Icelandic crust above layer three and the relation
1769 between body wave velocity and the alteration of the basaltic crust, J. Geophys., 47, 211-220.
1770 Forsyth, D. W., N. Harmon, D. S. Scheirer, and R. A. Duncan (2006), Distribution of recent
1771 volcanism and the morphology of seamounts and ridges in the GLIMPSE study area:
1772 Implications for the lithospheric cracking hypothesis for the origin of intraplate, non-hot spot
1773 volcanic chains, J. Geophys. Res., 111, B11407.
1774 Fossen, H. (2010), Extensional tectonics in the North Atlantic Caledonides: a regional view,
1775 Geological Society, London, Special Publications, 335, 767.
1776 Foulger, G. R. (2006), Older crust underlies Iceland, Geophys. J. Int., 165, 672-676.
1777 Foulger, G. R. (2010), Plates vs Plumes: A Geological Controversy, Wiley-Blackwell, Chichester,
1778 U.K., xii+328 pp.
1779 Foulger, G. R. (2012), Are 'hot spots' hot spots?, J. Geodyn., 58, 1-28.
1780 Foulger, G. R. (2018), Origin of the South Atlantic igneous province, J. Volc. Geotherm. Res., 355, 2-
1781 20.
1782 Foulger, G. R., and D. G. Pearson (2001), Is Iceland underlain by a plume in the lower mantle?
1783 Seismology and helium isotopes, Geophys. J. Int., 145, F1-F5.
1784 Foulger, G. R., and D. L. Anderson (2005), A cool model for the Iceland hot spot, J. Volc. Geotherm.
1785 Res., 141, 1-22.
1786 Foulger, G. R., Z. Du, and B. R. Julian (2003), Icelandic-type crust, Geophys. J. Int., 155, 567-590.
1787 Foulger, G. R., J. H. Natland, and D. L. Anderson (2005), A source for Icelandic magmas in remelted
1788 Iapetus crust, J. Volc. Geotherm. Res., 141, 23-44.
1789 Foulger, G. R., C. H. Jahn, G. Seeber, P. Einarsson, B. R. Julian, and K. Heki (1992), Post-rifting
1790 stress relaxation at the divergent plate boundary in Northeast Iceland, Nature, 358, 488-490.
1791 Foulger, G. R., G. F. Panza, I. M. Artemieva, I. D. Bastow, F. Cammarano, J. R. Evans, W. B.
1792 Hamilton, B. R. Julian, M. Lustrino, H. Thybo, and T. B. Yanovskaya (2013), Caveats on
1793 tomographic images, Terra Nova, 25, 259-281.
1794 Fountain, D. M., T. M. Boundy, H. Austrheim, and P. Rey (1994), Eclogite-facies shear zones—deep
1795 crustal reflectors?, Tectonophysics, 232, 411-424.
1796 Funck, T., H. R. Jackson, S. A. Dehler, and I. D. Reid (2006), A refraction seismic transect from
1797 Greenland to Ellesmere Island, Canada: The crustal structure in southern Nares Strait,
1798 Polarforschung, 74, 94–112.

1799 Funck, T., H. R. Jackson, K. E. Louden, and F. Klingelhoefer (2007), Seismic study of the transform-
1800 rifted margin in Davis Strait between Baffin Island (Canada) and Greenland: What happens when
1801 a plume meets a transform, J. Geophys. Res., 112, B04402.
1802 Funck, T., M. S. Andersen, J. Keser Neish, and T. Dahl-Jensen (2008), A refraction seismic transect
1803 from the Faroe Islands to the Hatton-Rockall Basin, Journal of Geophysical Research: Solid
1804 Earth, 113.
1805 Funck, T., K. Gohl, V. Damm, and I. Heyde (2012), Tectonic evolution of southern Baffin Bay and
1806 Davis Strait: Results from a seismic refraction transect between Canada and Greenland, J.
1807 Geophys. Res., 117, B04107.
1808 Funck, T., W. H. Geissler, G. S. Kimbell, S. Gradmann, O. Erlendsson, K. McDermott, and U. K.
1809 Petersen (2016), Moho and basement depth in the NE Atlantic Ocean based on seismic refraction
1810 data and receiver functions, *in* The NE Atlantic Region: A Reappraisal of Crustal Structure,
1811 Tectonostratigraphy and Magmatic Evolution, edited by G. Peron-Pinvidic, J. R. Hopper, M. S.
1812 Stoker, C. Gaina, J. C. Doornenbal, T. Funck and U. E. Arting, pp. 207 - 231, Geological
1813 Society, London, Special Publications, London.
1814 Funck, T., W. H. Geissler, G. S. Kimbell, S. Gradmann, Ö. Erlendsson, K. McDermott, and U. K.
1815 Petersen (2017), Moho and basement depth in the NE Atlantic Ocean based on seismic refraction
1816 data and receiver functions, Geological Society, London, Special Publications, 447, 207.
1817 Gaina, C., L. Gernigon, and P. Ball (2009), Palaeocene–Recent plate boundaries in the NE Atlantic
1818 and the formation of the Jan Mayen microcontinent, Journal of the Geological Society, London,
1819 166, 1–16.
1820 Gaina, C., A. Nasuti, G. S. Kimbell, and A. Blischke (2017), Break-up and seafloor spreading
1821 domains in the NE Atlantic, Geological Society, London, Special Publications, 447, 393-417.
1822 Gans, P. B. (1987), An open-system, two-layer crustal stretching model for the Eastern Great Basin,
1823 Tectonics, 6, 1-12.
1824 Gao, C., H. J. B. Dick, Y. Liu, and H. Zhou (2016), Melt extraction and mantle source at a Southwest
1825 Indian Ridge Dragon Bone amagmatic segment on the Marion Rise, Lithos, 246-247, 48-60.
1826 Garde, A. A., M. A. Hamilton, B. Chadwick, J. Grocott, and K. J. McCaffrey (2002), The Ketilidian
1827 orogen of South Greenland: geochronology, tectonics, magmatism, and fore-arc accretion during
1828 Palaeoproterozoic oblique convergence, Canadian Journal of Earth Sciences, 39, 765-793.
1829 Gasser, D. (2014), The Caledonides of Greenland, Svalbard and other Arctic areas: status of research
1830 and open questions, Geological Society, London, Special Publications, 390, 93.
1831 Gebrande, H., H. Miller, and P. Einarsson (1980), Seismic structure of Iceland along RRISP-Profile I,
1832 J. Geophys., 47, 239-249.
1833 Gee, D. G., H. Fossen, N. Henriksen, and A. K. Higgins (2008a), From the Early Paleozoic Platforms
1834 of Baltica and Laurentia to the Caledonide Orogen of Scandinavia and Greenland, Episodes, 31,
1835 44-51.
1836 Gee, D. G., H. Fossen, N. Henriksen, and K. Higgins (2008b), From the early Paleozoic platforms of
1837 Baltica and Laurentia to the Caledonide orogen of Scandinavia and Greenland, Episodes, 44–51.
1838 Gee, J. (2015), Caledonides of Scandinavia, Greenland, and Svalbard, *in* Reference Module in Earth
1839 Systems and Environmental Sciences, edited by S. A. Elias, Elsevier.
1840 Geoffroy, L. (2005), Volcanic passive margins, Comptes Rendus Geoscience, 337, 1395-1408.
1841 Geoffroy, L., E. B. Burov, and P. Werner (2015), Volcanic passive margins: another way to break up
1842 continents, Scientific Reports, 5, 14828.
1843 Geoffroy, L., C. Aubourg, J.-P. Callot, and J.-A. Barrat (2007), Mechanisms of crustal growth in large
1844 igneous provinces: The north Atlantic province as a case study, *in* Plates, Plumes, and Planetary
1845 Processes, edited by G. R. Foulger and D. M. Jurdy, pp. 747-774, Geological Society of
1846 America, Boulder, CO.
1847 Geoffroy, L., H. Guan, L. Gernigon, G. R. Foulger, and P. Werner (submitted), C-Blocks and the
1848 extent of continental material in oceans: the Laxmi Basin case study, Geophys. J. Int.
1849 Gernigon, L., J.-C. Ringenbach, S. Planke, and B. L. Gall (2004), Deep structures and breakup along
1850 volcanic rifted margins: insights from integrated studies along the outer Vøring Basin (Norway),
1851 Marine and Petroleum Geology, 21, 363–372.

1852 Gernigon, L., A. Blischke, A. Nasuti, and M. Sand (2015), Conjugate volcanic rifted margins,
1853 seafloor spreading, and microcontinent: Insights from new high-resolution aeromagnetic surveys
1854 in the Norway Basin, Tectonics, 34.
1855 Gernigon, L., F. Lucazeau, F. Brigaud, e.-C. Ringenbach, S. Planke, and B. L. Gall (2006), A
1856 moderate melting model for the Vøring margin (Norway) based on structural observations and a
1857 thermo-kinematical modelling: Implication for the meaning of the lower crustal bodies,
1858 Tectonophysics, 412, 255-278.
1859 Gernigon, L., C. Gaina, O. Olesen, P. J. Ball, G. Péron-Pinvidic, and T. Yamasaki (2012), The
1860 Norway Basin revisited: From continental breakup to spreading ridge extinction, Marine and
1861 Petroleum Geology, 35, 1-19.
1862 Gernigon, L., D. Franke, L. Geoffroy, C. Schiffer, G. R. Foulger, M. Stoker, and e. al. (this volume),
1863 Crustal fragmentation, magmatism, and the diachronous breakup of the Norwegian-Greenland
1864 Sea, Earth-Science Reviews.
1865 Gernigon, L., O. Olesen, J. Ebbing, S. Wienecke, C. Gaina, J. O. Mogaard, M. Sand, and R.
1866 Myklebust (2009), Geophysical insights and early spreading history in the vicinity of the Jan
1867 Mayen Fracture Zone, Norwegian–Greenland Sea, Tectonophysics, 468, 185–205.
1868 Gerya, T. (2011), Origin and models of oceanic transform faults, Tectonophysics.
1869 Gillard, M., D. Sauter, J. Tugend, S. Tomasi, M.-E. Epin, and G. Manatschal (2017), Birth of an
1870 oceanic spreading center at a magma-poor rift system, Scientific Reports, 7, 15072.
1871 Goodwin, T., D. Cox, and J. Trueman (2009), Paleocene sedimentary models in the sub-basalt around
1872 the Munkagrunnur–East Faroes Ridge, Proceedings of the Faroe Islands Exploration Conference,
1873 2nd Conference, pp. 267–285.
1874 Graça, M. C., N. Kusznir, and N. S. Gomes Stanton (2019), Crustal thickness mapping of the central
1875 South Atlantic and the geodynamic development of the Rio Grande Rise and Walvis Ridge,
1876 Marine and Petroleum Geology, 101, 230-242.
1877 Gradstein, F. M., J. G. Ogg, M. D. Schmitz, and G. M. Ogg (2012), The Geologic Time Scale 2012,
1878 Elsevier, Amsterdam.
1879 Greenhalgh, E. E., and N. J. Kusznir (2007), Evidence for thin oceanic crust on the extinct Aegir
1880 Ridge, Norwegian Basin, NE Atlantic derived from satellite gravity inversion, Geophys. Res.
1881 Lett., 34, L06305.
1882 Grocott, J., and K. J. W. McCaffrey (2017), Basin evolution and destruction in an Early Proterozoic
1883 continental margin: the Rinkian fold–thrust belt of central West Greenland, Journal of the
1884 Geological Society.
1885 Guan, H., L. Geoffroy, L. Gernigon, F. Chauvet, C. Grigné, and P. Werner (2019), Magmatic ocean-
1886 continent transitions, Marine and Petroleum Geology, 104, 438-450.
1887 Guarnieri, P. (2015), Pre-break-up palaeostress state along the East Greenland margin, J. geol. Soc.
1888 Lon., 172, 727–739.
1889 Gudlaugsson, S. T., K. Gunnarsson, M. Sand, and J. Skogseid (1988), Tectonic and volcanic events at
1890 the Jan Mayen Ridge microcontinent, *in* Early Tertiary Volcanism and the Opening of the NE
1891 Atlantic, edited by A. C. Morton and L. M. Parson, pp. 85-93, Geological Society Special
1892 Publications.
1893 Gudmundsson, O. (2003), The dense root of the Iceland crust, Earth planet. Sci. Lett., 206, 427-440.
1894 Haller, J. (1971), Geology of the East Greenland Caledonides, Interscience, New York.
1895 Hansen, J., D. A. Jerram, K. McCaffrey, and S. R. Passey (2009), The onset of the North Atlantic
1896 Igneous Province in a rifting perspective, Geological Magazine, 146, 309-325.
1897 Harry, D. L., D. S. Sawyer, and W. P. Leeman (1993), The mechanics of continental extension in
1898 western North America: implications for the magmatic and structural evolution of the Great
1899 Basin, Earth planet. Sci. Lett., 117, 59-71.
1900 Heki, K., G. R. Foulger, B. R. Julian, and C.-H. Jahn (1993), Plate dynamics near divergent
1901 boundaries: Geophysical implications of postrifting crustal deformation in NE Iceland, J.
1902 Geophys. Res., 98, 14279-14297.
1903 Henriksen, N. (1999), Conclusion of the 1:500 000 mapping project in the Caledonian fold belt in
1904 North-East Greenland, Geology of Greenland Survey Bulletin, 183, 10-22.

1905 Henriksen, N., and A. K. Higgins (1976), East Greenland Caledonian fold belt, *in* Geology of
1906 Greenland, edited by A. Escher and W. S. Watt, pp. 182–246, Geological Survey of Greenland,
1907 Copenhagen.
1908 Hermance, J. F., and L. R. Grillot (1974), Constraints on temperatures beneath Iceland from
1909 magnetotelluric data, Phys. Earth Planet. Int., 8, 1-12.
1910 Heron, P., A. Peace, K. McCaffrey, J. K. Welford, R. Wilson, and R. N. Pysklywec (2019),
1911 Segmentation of rifts through structural inheritance: Creation of the Davis Strait, Tectonics, in
1912 press.
1913 Herzberg, C., and P. D. Asimow (2008), Petrology of some oceanic island basalts: PRIMELT2.XLS
1914 software for primary magma calculation, Geochemistry, Geophysics, Geosystems, 9.
1915 Herzberg, C., and P. D. Asimow (2015), PRIMELT3 MEGA.XLSM software for primary magma
1916 calculation: Peridotite primary magma MgO contents from the liquidus to the solidus,
1917 Geochemistry, Geophysics, Geosystems, 16, 563-578.
1918 Hey, R., F. Martinez, Á. Höskuldsson, and Á. Benediktsdóttir (2008), Propagating Rift Origin of the
1919 V-Shaped Ridges South of Iceland, paper presented at IAVCEI 2008 General assembly, 17-22
1920 August, 2008.
1921 Hey, R., F. Martinez, A. Höskuldsson, and A. Benediktsdóttir (2010), Propagating rift model for the
1922 V-shaped ridges south of Iceland, Geochem. Geophys. Geosys., 11.
1923 Hey, R., F. Martinez, Á. Höskuldsson, D. E. Eason, J. Sleeper, S. Thordarson, Á. Benediktsdóttir, and
1924 S. Merkuryev (2016), Multibeam investigation of the active North Atlantic plate boundary
1925 reorganization tip, Earth planet. Sci. Lett., 435, 115-123.
1926 Hey, R. N., and D. S. Wilson (1982), Propagating rift explanation for the tectonic evolution of the
1927 northeast Pacific–the pseudomovie, Earth planet. Sci. Lett., 58, 167-188.
1928 Hjartarson, A., O. Erlendsson, and A. Blischke (2017), The Greenland–Iceland–Faroe Ridge
1929 Complex, *in* The NE Atlantic Region: A Reappraisal of Crustal Structure, Tectonostratigraphy
1930 and Magmatic Evolution, edited by G. Peron-Pinvidic, J. R. Hopper, M. S. Stoker, C. Gaina, J.
1931 C. Doornenbal, T. Funck and U. E. Arting, pp. 127-148, Geological Society, London, Special
1932 Publications.
1933 Hofton, M. A., and G. R. Foulger (1996a), Post-rifting anelastic deformation around the spreading
1934 plate boundary, north Iceland, 2: Implications of the model derived from the 1987-1992
1935 deformation field, J. Geophys. Res., 101, 25,423 - 425,436.
1936 Hofton, M. A., and G. R. Foulger (1996b), Post-rifting anelastic deformation around the spreading
1937 plate boundary, north Iceland, 1: Modeling of the 1987-1992 deformation field using a
1938 viscoelastic Earth structure, JGR, 101, 25,403 - 425,421.
1939 Holbrook, W. S., H. C. Larsen, J. Korenaga, T. Dahl-Jensen, I. D. Reid, P. B. Kelemen, J. R. Hopper,
1940 G. M. Kent, D. Lizarralde, S. Bernstein, and R. S. Detrick (2001), Mantle thermal structure and
1941 active upwelling during continental breakup in the north Atlantic, Earth planet. Sci. Lett., 190,
1942 251-266.
1943 Holdsworth, R. E., A. Morton, D. Frei, A. Gerdes, R. A. Strachan, E. Dempsey, C. Warren, and A.
1944 Whitham (2018), The nature and significance of the Faroe-Shetland Terrane: linking Archaean
1945 basement blocks across the North Atlantic, Precamb. Res., in press.
1946 Hole, M. J. (2015), The generation of continental flood basalts by decompression melting of internally
1947 heated mantle, Geology, 43, 311-314.
1948 Hole, M. J., and J. M. Millett (2016), Controls of mantle potential temperature and lithospheric
1949 thickness on magmatism in the North Atlantic Igneous Province, J. Pet., 57, 417-436.
1950 Hole, M. J., and J. H. Natland (this volume), Magmatism in the North Atlantic Igneous Province;
1951 mantle temperatures, rifting and geodynamics, Earth-Science Reviews.
1952 Hole, M. J., R. M. Ellam, D. I. M. Macdonald, and S. P. Kelley (2015), Gondwana break-up related
1953 magmatism in the Falkland Islands, J. geol. Soc. Lon., 173, 108–126.
1954 Hopper, J. R., T. Dahl-Jensen, W. S. Holbrook, H. C. Larsen, D. Lizarralde, J. Korenaga, G. M. Kent,
1955 and P. B. Kelemen (2003), Structure of the SE Greenland margin from seismic reflection and
1956 refraction data: Implications for nascent spreading center subsidence and asymmetric crustal
1957 accretion during North Atlantic opening, Journal of Geophysical Research: Solid Earth, 108.

1958 Huismans, R., and C. Beaumont (2011), Depth-dependent extension, two-stage breakup and cratonic
1959 underplating at rifted margins, Nature, 473, 74.
1960 Huismans, R. S., and C. Beaumont (2014), Rifted continental margins: The case for depth-dependent
1961 extension, Earth planet. Sci. Lett., 407, 148-162.
1962 Jamtveit, B., R. Brooker, K. Brooks, L. M. Larsen, and T. Pedersen (2001), The water content of
1963 olivines from the North Atlantic Volcanic Province, Earth planet. Sci. Lett., 186, 401-415.
1964 Johannesson, H., and K. Saemundsson (1998), Geological Map of Iceland at 1/500 000, Geological
1965 Map of Iceland, 1:500 000. Bedrock Geology.
1966 Johnson, H., J. D. Ritchie, K. Hitchen, D. B. McInroy, and G. S. Kimbell (2005), Aspects of the
1967 Cenozoic deformational history of the northeast Faroe-Shetland Basin, Wyville-Thomson Ridge
1968 and Hatton Bank areas, Proceedings of the Petroleum Geology: NW Europe and Global
1969 Perspectives, 6th Conference, pp. 993–1007.
1970 Jones, E. J. W., R. Siddall, M. F. Thirlwall, P. N. Chroston, and A. J. Lloyd (1994), Anton Dohrn
1971 Seamount and the evolution of the Rockall Trough, Oceanologica Acta, 17, 237-247.
1972 Jones, S. M. (2003), Test of a ridge–plume interaction model using oceanic crustal structure around
1973 Iceland, Earth planet. Sci. Lett., 208, 205-218.
1974 Jones, S. M., N. White, and J. Maclennan (2002), V-shaped ridges around Iceland; implications for
1975 spatial and temporal patterns of mantle convection, Geochem. Geophys. Geosys., 3,
1976 2002GC000361.
1977 Kandilarov, A., R. Mjelde, E. Flueh, and R. B. Pedersen (2015), Vp/Vs-ratios and anisotropy on the
1978 northern Jan Mayen Ridge, North Atlantic, determined from ocean bottom seismic data, Polar
1979 Science, 9, 293-310.
1980 Karato, S.-i., and P. Wu (1993), Rheology of the Upper Mantle: A Synthesis, Science, 260, 771.
1981 Keen, C. E., and R. R. Boutilier (1995), Lithosphere-asthenosphere interactions below rifts, Rifted
1982 Ocean-Continent Boundaries, 17-30.
1983 Keen, C. E., L. T. Dafoe, and K. Dickie (2014), A volcanic province near the western termination of
1984 the Charlie-Gibbs Fracture Zone at the rifted margin, offshore northeast Newfoundland,
1985 Tectonics, 33, 1133–1153.
1986 Keen, C. E., K. Dickie, and L. T. Dafoe (2018), Structural characteristics of the ocean-continent
1987 transition along the rifted continental margin, offshore central Labrador, Marine and Petroleum
1988 Geology, 89, 443-463.
1989 King, S. D. (2005), North Atlantic topographic and geoid anomalies: the result of a narrow ocean
1990 basin and cratonic roots?, *in* Plates, Plumes, and Paradigms, edited by G. R. Foulger, J.H.
1991 Natland, D.C. Presnall and D.L. Anderson, pp. 653-664, Geological Society of America,
1992 Boulder, CO.
1993 Klein, E. M., and C. H. Langmuir (1987), Global correlations of ocean ridge basalt chemistry with
1994 axial depth and crustal thickness, J. Geophys. Res., 92, 8089-8115.
1995 Kodaira, S., R. Mjelde, K. Gunnarsson, H. Shiobara, and H. Shimamura (1998), Structure of the Jan
1996 Mayen microcontinent and implications for its evolution, Geophys. J. Int., 132, 383-400.
1997 Korenaga, J. (2004), Mantle mixing and continental breakup magmatism, Earth planet. Sci. Lett., 218,
1998 463-473.
1999 Korenaga, J., and P. B. Kelemen (2000), Major element heterogeneity in the mantle source of the
2000 north Atlantic igneous province, Earth planet. Sci. Lett., 184, 251-268.
2001 Korenaga, J., and W. W. Sager (2012), Seismic tomography of Shatsky Rise by adaptive importance
2002 sampling, Journal of Geophysical Research: Solid Earth, 117.
2003 Korenaga, J., P. B. Kelemen, and W. S. Holbrook (2002), Methods for resolving the origin of large
2004 igneous provinces from crustal seismology, J. Geophys. Res., 107, 2178,
2005 doi:2110.1029/2001JB001030.
2006 Krabbendam, M. (2001), When the Wilson Cycle breaks down: how orogens can produce strong
2007 lithosphere and inhibit their future reworking, Geological Society, London, Special Publications,
2008 184, 57.
2009 Kumar, P., R. Kind, K. Priestley, and T. Dahl-Jensen (2007), Crustal structure of Iceland and
2010 Greenland from receiver function studies, Journal of Geophysical Research: Solid Earth, 112.

2011 Kurashimo, E., M. Shinohara, K. Suyehiro, J. Kasahara, and N. Hirata (1996), Seismic evidence for
2012 stretched continental crust in the Japan Sea, Geophys. Res. Lett., 23, 3067-3070.
2013 Kusznir, N., and e. al. (2018), Intra-ocean Ridge Jumps, Oceanic Plateaus & Upper Mantle
2014 Inheritance, Earth Science Reviews, submitted.
2015 Kusznir, N. J., and G. D. Karner (2007), Continental lithospheric thinning and breakup in response to
2016 upwelling divergent mantle flow: application to the Woodlark, Newfoundland and Iberia
2017 margins, *in* Imaging, Mapping and Modelling Continental Lithosphere Extension and Breakup,
2018 edited by G. D. Karner, G. Manatschal and L. M. Pinheiro, pp. 389-419, Geological Society of
2019 London, Special Publications.
2020 Lamers, E., and S. M. M. Carmichael (1999), The Paleocene deepwater sandstone play West of
2021 Shetland, Proceedings of the Petroleum Geology of Northwest Europe, 5th Conference, pp. 645–
2022 659.
2023 Larsen, L. M., R. Waagstein, A. K. Pedersen, and M. Storey (1999), Trans-Atlantic correlation of the
2024 Palaeogene volcanic successions in the Faeroe Islands and East Greenland, Journal of the
2025 Geological Society, 156, 1081-1095.
2026 Larsen, L. M., L. M. Heaman, R. A. Creaser, R. A. Duncan, R. Frei, and M. Hutchinson (2009),
2027 Tectonomagnetic events during stretching and basin formation in the Labrador Sea and the Davis
2028 Strait: evidence from age and composition of Mesozoic to Palaeogene dyke swarms in West
2029 Greenland, Journal of the Geological Society, London, 166, 999–1012.
2030 Lundin, E., and T. Doré (2005), The fixity of the Iceland "hotspot" on the Mid-Atlantic Ridge:
2031 observational evidence, mechanisms and implications for Atlantic volcanic margins, *in* Plates,
2032 Plumes, and Paradigms, edited by G. R. Foulger, J.H. Natland, D.C. Presnall and D.L. Anderson,
2033 pp. 627-652, Geological Society of America.
2034 Lundin, E. R., and A. G. Doré (2011), Hyperextension, serpentinization, and weakening: A new
2035 paradigm for rifted margin compressional deformation, Geology, 39, 347-350.
2036 Lundin, E. R., and A. G. Doré (2018), Non-Wilsonian break-up predisposed by transforms: examples
2037 from the North Atlantic and Arctic, *in* Fifty Years of the Wilson Cycle Concept in Plate
2038 Tectonics, edited by R. W. Wilson, G. A. Houseman, K. J. W. Mccaffrey, A. G. Doré and S. J.
2039 H. Buiter, Geological Society, London, Special Publications.
2040 Lundin, E. R., A. G. Doré, and T. F. Redfield (2018), Magmatism and extension rates at rifted
2041 margins, Petroleum Geoscience.
2042 Manton, B., S. Planke, D. Zastrozhnov, M. M. Abdelmalak, J. Millett, D. Maharjan, S. Polteau, J. I.
2043 Faleide, L. Gernigon, and R. Myklebust (2018), Pre-Cretaceous Prospectivity of the Outer Møre
2044 and Vøring Basins Constrained by New 3D Seismic Data, paper presented at 80th EAGE
2045 Conference and Exhibition.
2046 Marquart, G. (1991), Interpretations of Geoid Anomalies around the Iceland Hotspot, Geophys. J. Int.,
2047 106, 149-160.
2048 Martinez, F., and R. N. Hey (this volume), Reykjanes Ridge evolution by plate kinematics and
2049 propagating small-scale mantle convection within a regional upper mantle anomaly, Earth-
2050 Science Reviews.
2051 Martinez, F., R. J. Stern, K. A. Kelley, Y. Ohara, J. D. Sleeper, J. M. Ribeiro, and M. Brounce (2018),
2052 Diffuse extension of the southern Mariana margin, J. Geophys. Res., 123, 892–916.
2053 Martínez, F., R. N. Hey, and P. D. Johnson (1997), The East ridge system 28.5–32°S East Pacific rise:
2054 Implications for overlapping spreading center development, Earth planet. Sci. Lett., 151, 13-31.
2055 Mason, A. J., R. R. Parrish, and T. S. Brewer (2004), U–Pb geochronology of Lewisian orthogneisses
2056 in the Outer Hebrides, Scotland: implications for the tectonic setting and correlation of the South
2057 Harris Complex, Journal of the Geological Society, 161, 45.
2058 Matthews, S., O. Shorttle, and J. Maclennan (2016), The temperature of the Icelandic mantle from
2059 olivine-spinel aluminum exchange thermometry, Geochemistry, Geophysics, Geosystems, 17,
2060 4725-4752.
2061 McKenzie, D., and J. Jackson (2002), Conditions for flow in the continental crust, Tectonics, 21, 5-1-
2062 5-7.
2063 Meissner, R. (1999), Terrane accumulation and collapse in central Europe: seismic and rheological
2064 constraints, Tectonophysics, 305, 93-107.

2065 Menke, W. (1999), Crustal isostasy indicates anomalous densities beneath Iceland, Geophys. Res.
2066 Lett., 26, 1215-1218.
2067 Menke, W., and V. Levin (1994), Cold crust in a hot spot, Geophys. Res. Lett., 21, 1967-1970.
2068 Menke, W., V. Levin, and R. Sethi (1995), Seismic attenuation in the crust at the mid-Atlantic plate
2069 boundary in south-west Iceland, Geophys. J. Int., 122, 175-182.
2070 Meyer, R., J. G. H. Hertogen, R. B. Pedersen, L. Viereck-Götte, and M. Abratis (2009), Elements and
2071 isotopic measurements of magmatic rock samples from ODP Hole 104-642E, in Supplement to:
2072 Meyer, R. et al. (2009): Interaction of mantle derived melts with crust during the emplacement of
2073 the Vöring Plateau, N.E. Atlantic. Marine Geology, 261(1-4), 3-16, edited, PANGAEA.
2074 Mjelde, R., A. Goncharov, and R. D. Müller (2013), The Moho: Boundary above upper mantle
2075 peridotites or lower crustal eclogites? A global review and new interpretations for passive
2076 margins, Tectonophysics, 609, 636-650.
2077 Mjelde, R., S. Kodaira, H. Shimamura, T. Kanazawa, H. Shiobara, E. W. Berg, and O. Riise (1997),
2078 Crustal structure of the central part of the Vøring Basin, mid-Norway margin, from ocean bottom
2079 seismographs, Tectonophysics, 277, 235-257.
2080 Mjelde, R., R. Aurvåg, S. Kodaira, H. Shimamura, K. Gunnarsson, A. Nakanishi, and H. Shiobara
2081 (2002), Vp/Vs-ratios from the central Kolbeinsey Ridge to the Jan Mayen Basin, North Atlantic;
2082 implications for lithology, porosity and present-day stress field, Mar. Geophys. Res., 23, 123-
2083 145.
2084 Mjelde, R., P. Digranes, H. Shimamura, H. Shiobara, S. Kodaira, H. Brekke, T. Egebjerg, N. Sørenes,
2085 and S. Thorbjørnsen (1998), Crustal structure of the northern part of the Vøring Basin, mid-
2086 Norway margin, from wide-angle seismic and gravity data, Tectonophysics, 293, 175-205.
2087 Mjelde, R., P. Digranes, M. Van Schaack, H. Simamura, H. Shiobara, S. Kodaira, O. Naess, N.
2088 Sørenes, and E. Vagnes (2001), Crustal structure of the outer Voring Plateau, offshore Norway,
2089 from ocean bottom seismic and gravity data, J. Geophys. Res., 106, 6769-6791.
2090 Mudge, D. C. (2015), Regional controls on Lower Tertiary sandstone distribution in the North Sea
2091 and NE Atlantic margin basins, *in* Tertiary Deep-Marine Reservoirs of the North Sea Region,
2092 edited by T. McKie, P. T. S. Rose, A. J. Hartley, D. W. Jones and T. L. Armstrong, pp. 17–42,
2093 Geological Society, London, Special Publications.
2094 Müller, R. D., M. Seton, S. Zahirovic, S. E. Williams, K. J. Matthews, N. M. Wright, G. E. Shephard,
2095 K. T. Maloney, N. Barnett-Moore, M. Hosseinpour, D. J. Bower, and J. Cannon (2016), Ocean
2096 basin evolution and global-scale plate reorganization events since Pangea breakup, Ann. Rev.
2097 Earth Planet. Sci., 44, 107.
2098 Muñoz, G., A. Mateus, J. Pous, W. Heise, F. Monteiro Santos, and E. Almeida (2008), Unraveling
2099 middle-crust conductive layers in Paleozoic Orogens through 3D modeling of magnetotelluric
2100 data: The Ossa-Morena Zone case study (SW Iberian Variscides), Journal of Geophysical
2101 Research: Solid Earth, 113.
2102 Müntener, O., G. Manatschal, L. Desmurs, and T. Pettke (2010), Plagioclase Peridotites in Ocean–
2103 Continent Transitions: Refertilized Mantle Domains Generated by Melt Stagnation in the
2104 Shallow Mantle Lithosphere, J. Pet., 51, 255-294.
2105 Mutter, J. C., and C. M. Zehnder (1988), Deep crustal structure and magmatic processes; the inception
2106 of seafloor spreading in the Norwegian-Greenland Sea, *in* Early Tertiary volcanism and the
2107 opening of the NE Atlantic, edited by A. C. Morton and L. M. Parson, pp. 35-48.
2108 Natland, J. H. (2003), Capture of helium and other volatiles during the growth of olivine phenocrysts
2109 in picritic basalts from the Juan Fernandez Islands, J. Pet., 44, 421-456.
2110 Nemčok, M., and S. Rybár (2017), Rift–drift transition in a magma-rich system: the Gop Rift–Laxmi
2111 Basin case study, West India, Geological Society, London, Special Publications, 445, 95.
2112 Nichols, A. R. L., M. R. Carroll, and A. Hoskuldsson (2002), Is the Iceland hot spot also wet?
2113 Evidence from the water contents of undegassed submarine and subglacial pillow basalts, Earth
2114 planet. Sci. Lett., 202, 77-87.
2115 Nirrengarten, M., G. Manatschal, J. Tugend, N. Kusznir, and D. Sauter (2018), Kinematic Evolution
2116 of the Southern North Atlantic: Implications for the Formation of Hyperextended Rift Systems,
2117 Tectonics, 37, 89-118.

2118 O'Reilly, B. M., F. Hauser, A. W. B. Jacob, and P. M. Shannon (1996), The lithosphere below the
2119 Rockall Trough: wide-angle seismic evidence for extensive serpentinisation, Tectonophysics,
2120 255, 1-23.
2121 Oakey, G. N., and J. A. Chalmers (2012), A new model for the Paleogene motion of Greenland
2122 relative to North America: Plate reconstructions of the Davis Strait and Nares Strait regions
2123 between Canada and Greenland, Journal of Geophysical Research: Solid Earth, 117.
2124 Ólavsdóttir, J., L. O. Boldreel, and M. S. Andersen (2010), Development of a shelf-margin delta due
2125 to uplift of Munkagrunnut Ridge at the margin of Faroe-Shetland Basin: a seismic sequence
2126 stratigraphic study, Petroleum Geoscience, 16, 91-103.
2127 Ólavsdóttir, J., M. S. Andersen, and L. O. Boldreel (2013a), Seismic stratigraphic analysis of the
2128 Cenozoic sediments in the NW Faroe–Shetland Basin Implications for inherited structural
2129 control of sediment distribution, Marine and Petroleum Geology, 46, 19–35.
2130 Ólavsdóttir, J., M. S. Andersen, and L. O. Boldreel (2013b), Seismic stratigraphic analysis of the
2131 Cenozoic sediments in the NW Faroe Shetland Basin–Implications for inherited structural
2132 control of sediment distribution, Marine and Petroleum Geology, 46, 19-35.
2133 Ólavsdóttir, J., Ó. R. Eidesgaard, and M. S. Stoker (2017), The stratigraphy and structure of the
2134 Faroese continental margin, *in* The NE Atlantic Region: A Reappraisal of Crustal Structure,
2135 Tectonostratigraphy and Magmatic Evolution, edited by G. Péron-Pinvidic, J. R. Hopper, M. S.
2136 Stoker, C. Gaina, J. C. Doornenbal, T. Funck and U. E. Árting, pp. 339–356, Geological Society,
2137 London, Special Publications, London.
2138 Palmason, G. (1971), Crustal structure of Iceland from explosion seismology, Soc. Sci. Isl. Greinar V,
2139 187 pp., Reykjavik.
2140 Paquette, J., O. Sigmarsson, and M. Tiepolo (2006), Continental basement under Iceland revealed by
2141 old zircons, paper presented at American Geophysical Union, Fall Meeting.
2142 Parman, S. W., Kurz, M.D. , S. R. Hart, and T. L. Grove (2005), Helium solubility in olivine and
2143 implications for high $^{3}He/^{4}He$ in ocean island basalts, Nature, 437, 1140-1143.
2144 Passey, S. R., and D. W. Jolley (2009), A revised lithostratigraphic nomenclature for the Palaeogene
2145 Faroe Islands basalt Group, NE Atlantic ocean, Earth and Environmental Science Transaction of
2146 the Royal Society of Edinburgh, 99, 127-158.
2147 Peace, A., K. McCaffrey, J. Imber, J. Hunen, R. Hobbs, and R. Wilson (2018), The role of pre-
2148 existing structures during rifting, continental breakup and transform system development,
2149 offshore West Greenland, Basin Research, 30, 373-394.
2150 Peace, A., K. McCaffrey, J. Imber, J. Phethean, G. Nowell, K. Gerdes, and E. Dempsey (2016), An
2151 evaluation of Mesozoic rift-related magmatism on the margins of the Labrador Sea: Implications
2152 for rifting and passive margin asymmetry, Geosphere, 12.
2153 Peace, A. J., D. Franke, A. Doré, G. R. Foulger, N. Kusznir, J. G. McHone, J. Phethean, S. Rocchi, S.
2154 Schiffer, M. Schnabel, and J. K. Welford (this volume), Pangea dispersal and Large Igneous
2155 Provinces – in search for causative mechanisms, Earth-Science Reviews.
2156 Peace, A. L., G. R. Foulger, C. Schiffer, and K. J. W. McCaffrey (2017), Evolution of Labrador Sea-
2157 Baffin Bay: Plate or plume processes?, Geoscience Canada, 44, 91-102.
2158 Peace, A. L., E. D. Dempsey, C. Schiffer, J. K. Welford, and J. W. Ken (submitted), Evidence for
2159 basement reactivation during the opening of the Labrador Sea from the Makkovik Province,
2160 Labrador, Canada: Insights from field-data and numerical models, Geosciences.
2161 Perlt, J., M. Heinert, and W. Niemeier (2008), The continental margin in Iceland — A snapshot
2162 derived from combined GPS networks, Tectonophysics, 447, 155-166.
2163 Peron-Pinvidic, G., and G. Manatschal (2010), From microcontinents to extensional allochthons:
2164 witnesses of how continents rift and break apart?, Petroleum Geoscience, 16, 1-10.
2165 Peron-Pinvidic, G., G. Manatschal, and P. T. Osmundsen (2013), Structural comparison of archetypal
2166 Atlantic rifted margins: A review of observations and concepts, Marine and Petroleum Geology,
2167 43, 21-47.
2168 Peron-Pinvidic, G., L. Gernigon, C. Gaina, and P. Ball (2012), Insights from the Jan Mayen system in
2169 the Norwegian–Greenland sea—I. Mapping of a microcontinent, Geophys. J. Int., 191, 385-412.

2170 Perram, L. J., M.-H. Cormier, and K. C. Macdonald (1993), Magnetic and tectonic studies of the
2171 dueling propagating spreading centers at 20°40′S on the East Pacific Rise: Evidence for crustal
2172 rotations, Journal of Geophysical Research: Solid Earth, 98, 13835-13850.
2173 Petersen, K., J. Armitage, S. Nielsen, and H. Thybo (2015), Mantle temperature as a control on the
2174 time scale of thermal evolution of extensional basins. , Earth planet. Sci. Lett., 409, 61–70.
2175 Petersen, K. D., and C. Schiffer (2016), Wilson Cycle Passive Margins: Control of orogenic
2176 inheritance on continental breakup, Gondwana Research, 39, 131-144.
2177 Petersen, K. D., C. Schiffer, and T. Nagel (2018), LIP formation and protracted lower mantle
2178 upwelling induced by rifting and delamination, Scientific Reports, 8, 16578.
2179 Pharaoh, T. C. (1999), Palaeozoic terranes and their lithospheric boundaries within the Trans-
2180 European Suture Zone (TESZ): a review, Tectonophysics, 314, 17-41.
2181 Planke, S., P. A. Symonds, E. Alvestad, and J. Skogseid (2000), Seismic volcanostratigraphy of large-
2182 volume basaltic extrusive complexes on rifted margins, Journal of Geophysical Research: Solid
2183 Earth, 105, 19335-19351.
2184 Pollitz, F. F., and I. S. Sacks (1996), Viscosity structure beneath northeast Iceland, JGR, 101, 17,771-
2185 717,793.
2186 Presnall, D., and G. Gudfinnsson (2011), Oceanic volcanism from the low-velocity zone – without
2187 mantle plumes, J. Pet., 52, 1533-1546.
2188 Presnall, D. C., and G. Gudfinnsson (2007), Global Na8-Fe8 Systematics of MORBs: Implications for
2189 Mantle Heterogeneity, Temperature, and Plumes, paper presented at European Geophysical
2190 Union General Assembly, 15-20 April, 2007.
2191 Prestvik, T., S. Goldberg, H. Karlsson, and K. Gronvold (2001), Anomalous strontium and lead
2192 isotope signatures in the off-rift Oraefajokull central volcano in south-east Iceland. Evidence for
2193 enriched endmember(s) of the Iceland mantle plume?, Earth planet. Sci. Lett., 190, 211-220.
2194 Putirka, K. D. (2008), Excess temperatures at ocean islands: Implications for mantle layering and
2195 convection, Geology, 36, 283-286.
2196 Quick, J. E., S. Sinigoi, and A. Mayer (1995), Emplacement of mantle peridotite in the lower
2197 continental crust, Ivrea-Verbano zone, northwest Italy, Geology, 23, 739-742.
2198 Ranalli, G. (1995), Rheology of the Earth, Springer.
2199 Reston, T. J., J. Pennell, A. Stubenrauch, I. Walker, and M. Pérez-Gussinyé (2001), Detachment
2200 faulting, mantle serpentinization, and serpentinite- mud volcanism beneath the Porcupine Basin,
2201 southwest of Ireland, Geology, 29, 587-590.
2202 Reynisson, R. F., J. Ebbing, E. Lundin, and P. T. Osmundsen (2011), Properties and distribution of
2203 lower crustal bodies on the mid-Norwegian margin, edited, pp. 843-854, Geological Society,
2204 London.
2205 Ribe, N. M., U. R. Christensen, and J. Theissing (1995), The dynamics of plume-ridge interaction, 1:
2206 Ridge-centered plumes, Earth planet. Sci. Lett., 134, 155-168.
2207 Richard, K. R., R. S. White, R. W. England, and J. Fruehn (1999), Crustal structure east of the Faroe
2208 Islands; mapping sub-basalt sediments using wide-angle seismic data, Petroleum Geoscience, 5,
2209 161-172.
2210 Rickers, F., A. Fichtner, and J. Trampert (2013), The Iceland–Jan Mayen plume system and its impact
2211 on mantle dynamics in the North Atlantic region: Evidence from full-waveform inversion, Earth
2212 planet. Sci. Lett., 367, 39-51.
2213 Ritchie, J. D., H. D. Johnson, M. F. Quinn, and R. W. Gatliff (2008), Cenozoic compressional
2214 deformation within the Faroe-Shetland Basin and adjacent areas, *in* The Nature and Origin of
2215 Compression in Passive Margins, edited by H. D. Johnson, A. G. Doré, R. E. Holdsworth, R. W.
2216 Gatliff, E. R. Lundin and J. D. Ritchie, pp. 121–136, Geological Society, London, Special
2217 Publications.
2218 Roberts, D. (2003), The Scandinavian Caledonides: event chronology, palaeogeographic settings and
2219 likely, modern analogues, Tectonophysics, 365, 283-299.
2220 Roberts, D. G., M. Thompson, B. Mitchener, J. Hossack, S. Carmichael, and H. M. Bjornseth (1999),
2221 Palaeozoic to Tertiary rift and basin dynamics: mid-Norway to the Bay of Biscay – a new context
2222 for hydrocarbon prospectivity in the deep water frontier, Proceedings of the 5th Conference of
2223 the Petroleum Geology of Northwest Europe, London, pp. 7-40.

2224 Roest, W. R., and S. P. Srivastava (1989), Sea-floor spreading in the Labrador Sea: a new
2225 reconstruction, Geology, 17, 1000–1003.
2226 Rognvaldsson, S. T., A. Gudmundsson, and R. Slunga (1998), Seismotectonic analysis of the Tjornes
2227 Fracture Zone, an active transform fault in north Iceland, Journal of Geophysical Research-Solid
2228 Earth, 103, 30117-30129.
2229 Royden, L. (1996), Coupling and decoupling of crust and mantle in convergent orogens: Implications
2230 for strain partitioning in the crust, Journal of Geophysical Research: Solid Earth, 101, 17679-
2231 17705.
2232 Rudnick, R. L., and D. M. Fountain (1995), Nature and composition of the continental crust: A lower
2233 crustal perspective, Rev. Geophys., 33, 267-309.
2234 Rutter, E. H., K. H. Brodie, and P. J. Evans (1993), Structural geometry, lower crustal magmatic
2235 underplating and lithospheric stretching in the Ivrea-Verbano zone, northern Italy, J. Str. Geol.,
2236 15, 647-662.
2237 Sallares, V., and P. Charvis (2003), Crustal thickness constraints on the geodynamic evolution of hte
2238 Galápagos volcanic province, Earth planet. Sci. Lett., 214, 545-559.
2239 Sandwell, D. T., R. D. Müller, W. H. F. Smith, E. Garcia, and R. Francis (2014), New global marine
2240 gravity model from CryoSat-2 and Jason-1 reveals buried tectonic structure, Science, 346, 65.
2241 Santos Ventura, R., C. E. Ganade, C. M. Lacasse, I. S. L. Costa, I. Pessanha, E. P. Frazão, E. L.
2242 Dantas, and J. A. Cavalcante (2019), Dating Gondwanan continental crust at the Rio Grande
2243 Rise, South Atlantic, Terra Nova, 0.
2244 Sarafian, E., G. A. Gaetani, E. H. Hauri, and A. R. Sarafian (2017), Experimental constraints on the
2245 damp peridotite solidus and oceanic mantle potential temperature, Science, 355, 942-945.
2246 Sato, H., I. S. Sacks, T. Murase, G. Muncill, and H. Fukuyama (1989), Qp-melting temperature
2247 relation in peridotite at high pressure and temperature: Attenuation mechanism and implications
2248 for the mechanical properties of the upper mantle, J. Geophys. Res., 94, 10647-10661.
2249 Schaltegger, U., H. E. F. Amundsen, B. Jamtveit, M. Frank, W. L. Griffin, K. Gronvold, R. G.
2250 Tronnes, and T. Torsvik (2002), Contamination of OIB by underlying ancient continental
2251 lithosphere: U-Pb and Hf isotopes in zircons question EM1 and EM2 mantle components,
2252 Geochim. Cosmochim. Acta, 66, A673.
2253 Schiffer, C., N. Balling, B. H. Jacobsen, R. A. Stephenson, and S. B. (2014), Seismological evidence
2254 for a fossil subduction zone in the East Greenland Caledonides, Geology, 42, 311-314.
2255 Schiffer, C., N. Balling, J. Ebbing, B. H. Jacobsen, and S. B. Nielsen (2016), Geophysical-
2256 petrological modelling of the East Greenland Caledonides - Isostatic support from crust and
2257 upper mantle, Tectonophysics, 692, 44-57.
2258 Schiffer, C., C. Tegner, A. J. Schaeffer, V. Pease, and S. B. Nielsen (2017), High Arctic geopotential
2259 stress field and implications for geodynamic evolution, Geological Society, London, Special
2260 Publications, 460.
2261 Schiffer, C., R. A. Stephenson, K. D. Petersen, S. B. Nielsen, B. H. Jacobsen, N. Balling, and D. I. M.
2262 Macdonald (2015), A sub-crustal piercing point for North Atlantic reconstructions and tectonic
2263 implications, Geology, 43, 1087-1090.
2264 Schiffer, C., A. Peace, J. Phethean, K. McCaffrey, L. Gernigon, K. D. Petersen, and G. Foulger
2265 (2018), The Jan Mayen Microplate Complex and the Wilson Cycle, *in* Tectonic Evolution: 50
2266 Years of the Wilson Cycle Concept, edited by G. Houseman, Geological Society of London
2267 Schiffer, C., A. G. Doré, G. R. Foulger, D. Franke, L. Geoffroy, L. Gernigon, B. Holdsworth, N.
2268 Kusznir, E. Lundin, K. McCaffrey, A. Peace, K. D. Petersen, R. Stephenson, M. S. Stoker, and
2269 K. Welford (this volume), The role of tectonic inheritance in the evolution of the North Atlantic,
2270 Earth-Science Reviews.
2271 Schlindwein, V., and W. Jokat (2000), Post-collisional extension of the East Greenland Caledonides:
2272 a geophysical perspective, Geophys. J. Int., 140, 550-567.
2273 Schmidt-Aursch, M. C., and W. Jokat (2005), The crustal structure of central East Greenland—II:
2274 From the Precambrian shield to the recent mid-oceanic ridges, Geophys. J. Int., 160, 753-760.
2275 Shen, F., L. H. Royden, and B. C. Burchfiel (2001), Large-scale crustal deformation of the Tibetan
2276 Plateau, Journal of Geophysical Research: Solid Earth, 106, 6793-6816.

2277 Shih, J., and P. Molnar (1975), Analysis and implications of the sequence of ridge jumps that
2278 eliminated the Surveyor Transform Fault, J. Geophys. Res., 80, 4815-4822.
2279 Shorttle, O., J. Maclennan, and A. M. Piotrowski (2013), Geochemical provincialism in the Iceland
2280 plume, Geochim. Cosmochim. Acta, 122, 363-397.
2281 Sigmundsson, F. (1991), Post-glacial rebound and asthenosphere viscosity in Iceland, Geophys. Res.
2282 Lett., 18, 1131-1134.
2283 Simon, K., R. S. Huismans, and C. Beaumont (2009), Dynamical modelling of lithospheric extension
2284 and small-scale convection: implications for magmatism during the formation of volcanic rifted
2285 margins, Geophys. J. Int., 176, 327–350.
2286 Skogseid, J., S. Planke, J. I. Faleide, T. Pedersen, O. Eldholm, and F. Neverdal (2000), NE Atlantic
2287 continental rifting and volcanic margin formation, *in* Dynamics of the Norwegian Margin, edited
2288 by A. Nottvedt, pp. 295-326.
2289 Slagstad, T., Y. Maystrenko, V. Maupin, and S. Gradmann (2017), An extinct, Late Mesoproterozoic,
2290 Sveconorwegian mantle wedge beneath SW Fennoscandia, reflected in seismic tomography and
2291 assessed by thermal modelling, Terra Nova, 30, 72-77.
2292 Smith, W. H. F., and D. T. Sandwell (1997), Global Sea Floor Topography from Satellite Altimetry
2293 and Ship Depth Soundings, Science, 277, 1956.
2294 Smythe, D. K., A. Dobinson, R. McQuillin, J. A. Brewer, D. H. Matthews, D. J. Blundell, and B.
2295 Kelk (1982), Deep structure of the Scottish Caledonides revealed by the MOIST reflection
2296 profile, Nature, 299, 338-340.
2297 Soper, N. J., R. A. Strachan, R. E. Holdsworth, R. A. Gayer, and R. O. Greilung (1992), Sinistral
2298 transpression and the Silurian closure of Iapetus, Journal - Geological Society (London), 149,
2299 871-880.
2300 Spice, H. E., J. G. Fitton, and L. A. Kirstein (2016), Temperature fluctuation of the Iceland mantle
2301 plume through time, Geochemistry, Geophysics, Geosystems, 17, 243-254.
2302 Srivastava, S., B. MacLean, R. Macnab, H. Jackson, A. Embry, and H. Balkwill (1982), Davis Strait:
2303 structure and evolution as obtained from a systematic geophysical survey, Proceedings of the
2304 Third International Symposium on Arctic Geology, Calgary, Alberta, pp. 267-278.
2305 Srivastava, S. P. (1978), Evolution of the Labrador Sea and its bearing on the early evolution of the
2306 North Atlantic, Geophys. J. Int., 52, 313-357.
2307 St-Onge, M. R., J. A. M. V. Gool, A. A. Garde, and D. J. Scott (2009), Correlation of Archaean and
2308 Palaeoproterozoic units between northeastern Canada and western Greenland: constraining the
2309 pre-collisional upper plate accretionary history of the Trans-Hudson orogen, *in* Earth
2310 Accretionary Systems in Space and Time, edited by P. A. Cawood and A. Kröner, pp. 193-235,
2311 Geological Society of London.
2312 Staples, R. K., R. S. White, B. Brandsdottir, W. Menke, P. K. H. Maguire, and J. H. McBride (1997),
2313 Faeroe-Iceland ridge experiment 1. Crustal structure of northeastern Iceland, JGR, 102, 7849-
2314 7866.
2315 Starkey, N. A., F. M. Stuart, R. M. Ellam, J. G. Fitton, S. Basu, and L. M. Larsen (2009), Helium
2316 isotopes in early Iceland plume picrites: constraints on the composition of high 3He/4He mantle,
2317 Earth planet. Sci. Lett., 277, 91–100.
2318 Steffen, R., G. Strykowski, and B. Lund (2017), High-resolution Moho model for Greenland from
2319 EIGEN-6C4 gravity data, Tectonophysics, 706-707, 206-220.
2320 Stixrude, L., and C. Lithgow-Bertelloni (2011), Thermodynamics of mantle minerals – II. Phase
2321 equilibria, Geophys. J. Int., 184, 1180-1213.
2322 Stoker, M. S., A. B. Leslie, and K. Smith (2013), A record of Eocene (Stronsay Group) sedimentation
2323 in BGS borehole 99/3, offshore NW Britain: implications for early post-rift development of the
2324 Faroe-Shetland Basin, Scottish Journal of Geology, 49, 133–148.
2325 Stoker, M. S., S. P. Holford, and R. R. Hillis (2018), A rift-to-drift record of vertical crustal motions
2326 in the Faroe–Shetland Basin, NW European margin: establishing constraints on NE Atlantic
2327 evolution, Journal of the Geological Society, 175, 263-274.
2328 Stoker, M. S., G. S. Kimbell, D. B. McInroy, and A. C. Morton (2012), Eocene post-rift
2329 tectonostratigraphy of the Rockall Plateau, Atlantic margin of NW Britain: Linking early
2330 spreading tectonics and passive margin response, Marine and Petroleum Geology, 30, 98–125.

2331 Stoker, M. S., D. Praeg, J. S. Hjelstuen, J. S. Laberg, T. Nielsen, and P. M. Shannon (2005a),
2332 Neogene stratigraphy and the sedimentary and oceanographic development of the NW European
2333 Atlantic margin, Marine and Petroleum Geology, 22, 977–1005.
2334 Stoker, M. S., D. Praeg, P. M. Shannon, B. O. Hjelstuen, J. S. Laberg, T. Nielsen, T. C. E. van
2335 Weering, H. P. Sejrup, and D. Evans (2005b), Neogene evolution of the Atlantic continental
2336 margin of NW Europe (Lofoten Islands to SW Ireland): anything but passive, *in* Petroleum
2337 Geology: North-West Europe and Global Perspectives–Proceedings of the 6th Petroleum
2338 Geology Conference, edited by A. G. Doré and B. A. Vining, pp. 1057-1076, Geological Society,
2339 London.
2340 Stoker, M. S., R. J. Hoult, T. Nielsen, J. S. Hjelstuen, J. S. Laberg, P. M. Shannon, D. Praeg, A.
2341 Mathiesen, T. C. E. van Weering, and A. M. McDonnell (2005c), Sedimentary and
2342 oceanographic responses to early Neogene compression on the NW European margin, Marine
2343 and Petroleum Geology, 22, 1031–1044.
2344 Stoker, M. S., M. A. Stewart, P. M. Shannon, M. Bjerager, T. Nielsen, A. Blischke, B. O. Hjelstuen,
2345 C. Gaina, K. McDermott, and J. Ólavsdóttir (2017), An overview of the Upper Palaeozoic-
2346 Mesozoic stratigraphy of the NE Atlantic margin, *in* The NE Atlantic Region: A Reappraisal of
2347 Crustal Structure, Tectonostratigraphy and Magmatic Evolution, edited by G. Péron-Pinvidic , J.
2348 R. Hopper, M. S. Stoker, C. Gaina, J. C. Doornenbal, T. Funck and U. E. Árting, pp. 11-68,
2349 Geological Society, London, Special Publications.
2350 Stuart, F. M., S. Lass-Evans, J. G. Fitton, and R. M. Ellam (2003), High 3He/4He ratios in picritic
2351 basalts from Baffin Island and the role of a mixed reservoir in mantle plumes, Nature, 424, 57-
2352 59.
2353 Suckro, S. K., K. Gohl, T. Funck, I. Heyde, B. Schreckenberger, J. Gerlings, and V. Damm (2013),
2354 The Davis Strait crust—a transform margin between two oceanic basins, Geophys. J. Int., 193,
2355 78-97.
2356 Suckro, S. K., K. Gohl, T. Funck, I. Heyde, A. Ehrhardt, B. Schreckenberger, J. Gerlings, V. Damm,
2357 and W. Jokat (2012), The crustal structure of southern Baffin Bay: implications from a seismic
2358 refraction experiment, Geophys. J. Int., 190, 37-58.
2359 Talwani, M., and O. Eldholm (1977), Evolution of the Norwegian-Greenland Sea, GSA Bull., 88,
2360 969-999.
2361 Tapponnier, P., X. Zhiqin, F. Roger, B. Meyer, N. Arnaud, G. Wittlinger, and Y. Jingsui (2001),
2362 Oblique Stepwise Rise and Growth of the Tibet Plateau, Science, 294, 1671-1677.
2363 Taylor, B., K. Crook, and J. Sinton (1994), Extensional transform zones and oblique spreading
2364 centers, Journal of Geophysical Research: Solid Earth, 99, 19707-19718.
2365 Theissen-Krah, S., D. Zastrozhnov, M. M. Abdelmalak, D. W. Schmid, J. I. Faleide, and L. Gernigon
2366 (2017), Tectonic evolution and extension at the Møre Margin – Offshore mid-Norway,
2367 Tectonophysics, 721, 227-238.
2368 Thorbergsson, G., I. T. Magnusson, and G. Palmason (1990), Gravity data and gravity map of
2369 IcelandOS-90001/JHD-01, National Energy Authority Reykjavik.
2370 Thybo, H., and I. M. Artemieva (2013), Moho and magmatic underplating in continental lithosphere,
2371 Tectonophysics, 609, 605-619.
2372 Trela, J., E. Gazel, A. V. Sobolev, L. Moore, M. Bizimis, B. Jicha, and V. G. Batanova (2017), The
2373 hottest lavas of the Phanerozoic and the survival of deep Archaean reservoirs, Nature
2374 Geoscience, 10, 451.
2375 Tryggvason, E. (1962), Crustal structure of the Iceland region from dispersion of surface waves, Bull.
2376 seismol. Soc. Am., 52, 359-388.
2377 Tuttle, O. F., and N. L. Bowen (1958), Origin of granite in the light of experimental studies in the
2378 system NaAlSi3O8–KAlSi3O8–SiO2–H2O, *in* Origin of Granite in the Light of Experimental
2379 Studies in the System NaAlSi3O8–KAlSi3O8–SiO2–H2O, edited by O. F. Tuttle and N. L.
2380 Bowen, Geological Society of America.
2381 Ulmer, P., and V. Trommsdorff (1995), Serpentine Stability to Mantle Depths and Subduction-
2382 Related Magmatism, Science, 268, 858.

2383 van Gool, J. A. M., J. N. Connelly, M. Marker, and F. C. Mengel (2002), The Nagssugtoqidian
2384 Orogen of West Greenland: tectonic evolution and regional correlations from a West Greenland
2385 perspective, Canadian Journal of Earth Sciences, 39, 665-686.
2386 Vauchez, A., G. Barruol, and A. Tommasi (1997), Why do continents break-up parallel to ancient
2387 orogenic belts?, Terra Nova, 9, 62-66.
2388 Vogt, P. R. (1971), Asthenosphere motion recorded by the ocean floor south of Iceland, Earth planet.
2389 Sci. Lett., 13, 153-160.
2390 Vogt, P. R., G. L. Johnson, and L. Kristjansson (1980), Morphology and magnetic anomalies north of
2391 Iceland, Journal of Geophysics-Zeitschrift Fur Geophysik, 47, 67-80.
2392 Voppel, D., S. R. Srivastava, and U. Fleischer (1979), Detailed magnetic measurements south of the
2393 Iceland-Faroe Ridge, Deutsche Hydrographische Zeitschrift, 32, 154-172.
2394 Walker, R. J., R. E. Holdsworth, J. Imber, and D. Ellis (2011), Onshore evidence for progressive
2395 changes in rifting directions during continental break-up in the NE Atlantic, Journal of the
2396 Geological Society, 168, 27.
2397 Wegener, A. (1915), Die Entstehung der Kontinente und Ozeane, Friedrich Vieweg und Sohn,
2398 Braunschweig.
2399 Welford, J. K., A. L. Peace, M. Geng, S. A. Dehler, and K. Dickie (2018), Crustal structure of Baffin
2400 Bay from constrained 3-D gravity inversion and deformable plate tectonic models, Geophys. J.
2401 Int., 214, 1281–1300.
2402 Wilkinson, C. M., M. Ganerød, B. W. H. Hendriks, and E. A. Eide (2017), Compilation and appraisal
2403 of geochronological data from the North Atlantic Igneous Province (NAIP), Geological Society,
2404 London, Special Publications, 447, 69.
2405 Zastrozhnov, D., L. Gernigon, I. Gogin, M. M. Abdelmalak, S. Planke, J. I. Faleide, S. Eide, and R.
2406 Myklebust (2018), Cretaceous-Paleocene evolution and crustal structure of the northern Vøring
2407 Margin (offshore Mid-Norway): results from integrated geological and geophysical study,
2408 Tectonics, 37.
2409 Zhang, J., and H. W. Green (2007), Experimental Investigation of Eclogite Rheology and Its Fabrics
2410 at High Temperature and Pressure, Journal of Metamorphic Geology, 25, 97-115.
2411 Zhou, H., and H. J. B. Dick (2013), Thin crust as evidence for depleted mantle supporting the Marion
2412 Rise, Nature, 494, 195–200.
2413